

CAPITAL UNIVERSITY OF SCIENCE AND  
TECHNOLOGY, ISLAMABAD



# Fixed Frequency Sliding Mode Control for Power Electronic Converters

by

Abdul Rehman Yasin

A thesis submitted in partial fulfillment for the  
degree of Doctor of Philosophy

in the

Faculty of Engineering

Department of Electrical Engineering

2019

# Fixed Frequency Sliding Mode Control for Power Electronic Converters

By

Abdul Rehman Yasin

(PE 133002)

Dr. Adrian Traian Plesca, Professor

Gheorghe Asachi Technical University of Iasi, Romania

(Foreign Evaluator 1)

Dr. Keum-Shik Hong, Professor

Pusan National University (South) Korea

(Foreign Evaluator 2)

Dr. Muhammad Ashraf

(Thesis Supervisor)

Dr. Aamer Iqbal Bhatti

(Thesis Co-Supervisor)

Dr. Noor Muhammad Khan

(Head, Department of Electrical Engineering)

Dr. Imtiaz Ahmed Taj

(Dean, Faculty of Engineering)

DEPARTMENT OF ELECTRICAL ENGINEERING  
CAPITAL UNIVERSITY OF SCIENCE AND TECHNOLOGY  
ISLAMABAD

2019

Copyright © 2019 by Abdul Rehman Yasin

All rights reserved. No part of this thesis may be reproduced, distributed, or transmitted in any form or by any means, including photocopying, recording, or other electronic or mechanical methods, by any information storage and retrieval system without the prior written permission of the author.

To my beloved parents.





**CAPITAL UNIVERSITY OF SCIENCE & TECHNOLOGY  
ISLAMABAD**

Expressway, Kahuta Road, Zone-V, Islamabad  
Phone: +92-51-111-555-666 Fax: +92-51-4486705  
Email: [info@cust.edu.pk](mailto:info@cust.edu.pk) Website: <https://www.cust.edu.pk>

**CERTIFICATE OF APPROVAL**

This is to certify that the research work presented in the thesis, entitled “**Fixed Frequency Sliding Mode Control for Power Electronic Converters**” was conducted under the supervision of **Dr. Muhammad Ashraf**. No part of this thesis has been submitted anywhere else for any other degree. This thesis is submitted to the **Department of Electrical Engineering, Capital University of Science and Technology** in partial fulfillment of the requirements for the degree of Doctor in Philosophy in the field of **Electrical Engineering**. The open defence of the thesis was conducted on **September 26, 2019**.

Student Name: Mr. Abdul Rehman Yasin (PE133002)

  
26/Sept/19

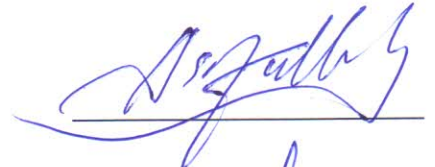
The Examining Committee unanimously agrees to award PhD degree in the mentioned field.

**Examination Committee :**

(a) External Examiner 1: Dr. Nisar Ahmed,  
Professor  
GIKI, Topi, Swabi



(b) External Examiner 2: Dr. Asifullah Khan,  
Professor,  
PIEAS, Islamabad



(c) Internal Examiner : Dr. Raza Samar  
Professor  
CUST, Islamabad



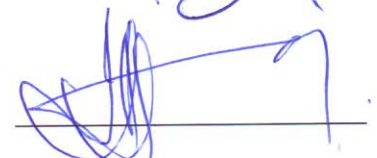
**Supervisor Name :** Dr. Muhammad Ashraf  
Professor  
CUST, Islamabad



**Name of HoD :** Dr. Noor Muhammad Khan  
Professor  
CUST, Islamabad



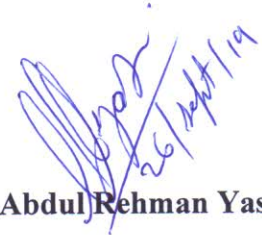
**Name of Dean :** Dr. Imtiaz Ahmad Taj  
Professor  
CUST, Islamabad



## AUTHOR'S DECLARATION

I, **Mr. Abdul Rehman Yasin** (Registration No. PE-133002), hereby state that my PhD thesis titled, '**Fixed Frequency Sliding Mode Control for Power Electronic Converters**' is my own work and has not been submitted previously by me for taking any degree from Capital University of Science and Technology, Islamabad or anywhere else in the country/ world.

At any time, if my statement is found to be incorrect even after my graduation, the University has the right to withdraw my PhD Degree.



(**Mr. Abdul Rehman Yasin**)

Dated: 26 September, 2019

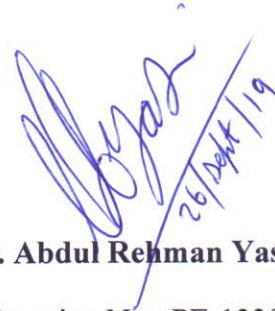
Registration No : PE-133002

## PLAGIARISM UNDERTAKING

I solemnly declare that research work presented in the thesis titled “**Fixed Frequency Sliding Mode Control for Power Electronic Converters**” is solely my research work with no significant contribution from any other person. Small contribution/ help wherever taken has been duly acknowledged and that complete thesis has been written by me.

I understand the zero tolerance policy of the HEC and Capital University of Science and Technology towards plagiarism. Therefore, I as an author of the above titled thesis declare that no portion of my thesis has been plagiarized and any material used as reference is properly referred/ cited.

I undertake that if I am found guilty of any formal plagiarism in the above titled thesis even after award of PhD Degree, the University reserves the right to withdraw/ revoke my PhD degree and that HEC and the University have the right to publish my name on the HEC/ University Website on which names of students are placed who submitted plagiarized thesis.



(Mr. Abdul Rehman Yasin)

Registration No : PE-133002

Dated:

26 September, 2019

---

## *List of Publications*

It is certified that following publication(s) have been made out of the research work that has been carried out for this thesis:-

1. **A.R. Yasin**, M. Ashraf, and A. I. Bhatti, “A Novel Filter Extracted Equivalent Control Based Fixed Frequency Sliding Mode Approach for Power,” *Energies*, vol. 12(5), pp. 853, 2019. IF = 2.707
2. **A.R. Yasin**, M. Ashraf, and A. I. Bhatti, “Fixed Frequency Sliding Mode Control of Power Converters for Improved Dynamic Response in DC Micro-Grids,” *Energies*, vol. 11(10), pp. 2799, 2018. IF = 2.707
3. **A.R. Yasin**, M. Ashraf, A. I. Bhatti and A. A. Uppal,, “Fixed Frequency Sliding Mode Control of Renewable Energy Resources in DC Micro Grid,” *Asian Journal of Control*, 2019. IF = 2.005

**Abdul Rehman Yasin**

(Registration No.PE133002)

## *Acknowledgements*

In the name of Almighty Allah, The Most Beneficent and The Most Merciful.

Doubtlessly it is a present obligation to express my sincere gratitude towards my supervisor Dr. Muhammad Ashraf for his continuous support, consistent guidance and encouragement during the research period. Without his support and guidance, it was not possible for me to complete this research.

Failures are a part of life and mistakes are the basic ingredient of discovering new ways. This is why Albert Einstein once said, “A person who never made a mistake never tried anything new.” I am particularly thankful to to my co-supervisor, Prof. Dr. Aamer Iqbal Bhatti for his encouraging soft words that helped me to muster up my courage whenever we got unsatisfactory results. I would also like to thank him for not only developing my interest in the field of sliding mode control but also for his continuous guidance through out my PhD progress.

I would like to thank all the members of CASPR research group especially Dr. Ali Arshad, Dr. Imran Khan and Dr. Yasir Awais Butt. I would like to thank them all for the group discussions and the talks that were full of knowledge and wisdom.

I would like to thank my parents, brothers, wife, daughters and my son Ibrahim Yasin. Special thanks to my sister Dr. Misbah Yasin for the financial assistance and above all, her moral support.

Towards the end, I would like to thank all of my teachers and friends who helped me achieve my ambitions.

# *Abstract*

In the modern era of industrialization, power electronic converters have gained key importance due to their wide range of applications such as; use in arc furnaces, induction heating systems, variable speed drives of motors, power supplies of various electronic systems, fluorescent lamps, elevators and cooling systems. Furthermore, the low-cost proliferation of power electronic devices due to the technological developments in the semiconductor industry has made them an attractive choice for integrating renewable energy resources. They are the essential and integral part of the systems providing solutions to issues like voltage sag, swell, frequency regulation, current sharing among different renewable energy resources, power factor correction and voltage regulation in different types of micro-grids.

In all the above-mentioned applications, the robustness of the system under different load and line conditions depend upon the control algorithm of the power electronic converters. This is why the research in the field of power electronics has been focused on the control of power converters during the last decade. Among different types of control techniques, Sliding Mode Control (SMC) is renowned for its disturbance rejection and parameter invariant nature which makes it an irresistible choice for controlling such systems. However due to physical constraints of the switching components, ideal condition of infinite frequency cannot be satisfied. This causes the system to operate at finite but time varying switching frequency which is a serious issue for power electronic converters as they consist of passive components whose size and value depends upon the switching frequency. Moreover, the time varying switching frequency degrades the power quality and causes electromagnetic interference (EMI) issues in case of grid connected power converters.

In the first phase of this research, a fixed frequency sliding mode controller utilizing an integral sliding manifold is designed to improve the dynamic response of the power converter regulating the grid voltage, in the presence of unknown

load condition and uncertain network parameter of the micro-grid. A special-purpose test rig is designed to experimentally validate the results in comparison with conventional PI controllers.

In the second phase of the research, the power quality issues regarding DC micro-grids are addressed. Power quality issues have been widely discussed regarding AC power systems but discussion regarding DC power quality in micro-grids is rare in research community because in past power transmission was carried out using AC systems only. However, in the recent years DC grids and transmission has emerged as an attractive solution to integrate renewable energy resources. Hence, to enhance the power quality, a fixed frequency SMC is proposed with harmonic cancellation and chattering reduction, using a PI type sliding manifold. Experimental results are presented to validate the theoretical derivations using the test rig.

Finally, a new method based upon filter extraction of the equivalent control is proposed to fix the switching frequency in power converters controlled by SMC. The technique is implemented on a boost converter and the results are presented in comparison with PWM-SMC. Rigorous mathematical analysis is provided along with experimental results to validate the proposed technique.

# Contents

<b>Author's Declaration</b>	<b>v</b>
<b>Plagiarism Undertaking</b>	<b>vi</b>
<b>List of Publications</b>	<b>vii</b>
<b>Acknowledgements</b>	<b>viii</b>
<b>Abstract</b>	<b>ix</b>
<b>List of Figures</b>	<b>xiv</b>
<b>List of Tables</b>	<b>xvi</b>
<b>Abbreviations</b>	<b>xvii</b>
<b>Symbols</b>	<b>xviii</b>
<b>1 Introduction</b>	<b>1</b>
1.1 Parameters Influencing Control . . . . .	2
1.1.1 Switching Frequency . . . . .	2
1.1.2 Passive Energy Storing Components . . . . .	3
1.1.3 Control Gains . . . . .	3
1.2 Common Control Techniques . . . . .	4
1.2.1 Hysteresis Voltage Controllers . . . . .	4
1.2.2 Linear Controllers . . . . .	4
1.2.2.1 Voltage Mode Control . . . . .	5
1.2.2.2 Current Mode Control . . . . .	5
1.3 Problem in Using Small Signal Model . . . . .	6
1.4 Advanced Control Techniques . . . . .	7
1.4.1 Fuzzy Logic Control . . . . .	7
1.4.2 Adaptive Control . . . . .	7
1.4.3 Artificial Neural Networks . . . . .	8
1.4.4 Sliding Mode Control . . . . .	8
1.5 Motivation . . . . .	9



---

1.6	Research Gap Analysis . . . . .	10
1.7	Thesis Contributions . . . . .	11
1.8	Thesis Structure . . . . .	14
1.9	Summary . . . . .	15
<b>2</b>	<b>DC Micro-Grids and Standards</b>	<b>16</b>
2.1	Motivation to use DC Micro-Grids . . . . .	16
2.2	DC Systems and Standards . . . . .	17
2.3	Power Converters in DC Micro-grids . . . . .	18
2.4	Motivation and Challenges in Deploying Boost Converter for Micro-grid Operation . . . . .	19
2.4.1	Control Problem . . . . .	20
2.5	Performance Attributes . . . . .	20
2.6	Power Quality . . . . .	21
2.7	Experimental Setup . . . . .	22
2.8	Motivation for a New Fixed Frequency SMC . . . . .	22
2.9	Summary . . . . .	23
<b>3</b>	<b>Power Converter for Micro-grid Operation</b>	<b>24</b>
3.1	Introduction . . . . .	24
3.2	Mathematical Modeling . . . . .	26
3.3	Controller Design . . . . .	28
3.4	Stability of Sliding Mode Control . . . . .	32
3.4.1	Existence of Sliding Mode Control . . . . .	32
3.4.2	Finite Time Convergence to the Sliding Manifold . . . . .	34
3.5	Sliding Surface and Parametrization of the Controller . . . . .	35
3.6	Results and Discussion . . . . .	39
3.6.1	Open Loop Response . . . . .	40
3.6.2	Performance of Proposed Controller in Comparison with PI-Controller . . . . .	41
3.6.2.1	Dynamic Response . . . . .	41
3.6.2.2	Robustness of the Controller . . . . .	43
3.6.3	Grid Testing for Fault Condition . . . . .	44
3.7	Summary . . . . .	45
<b>4</b>	<b>Power Quality Improvement</b>	<b>47</b>
4.1	Introduction . . . . .	47
4.2	Design of Fixed Frequency SMC using PI- Type Sliding Manifold . . . . .	48
4.2.1	Stability of the Controller . . . . .	51
4.2.2	Selection of Sliding Constants . . . . .	52
4.2.3	Parameterization of Controller . . . . .	53
4.3	Hardware Description . . . . .	55
4.4	Experimental Setup and Results . . . . .	57
4.4.1	Pulse Width Modulation Circuit . . . . .	57
4.4.2	Step Response of the Closed Loop System . . . . .	59

---

4.4.3	Robustness to Load and Line Variations . . . . .	59
4.4.4	Grid Operation . . . . .	63
4.5	Summary . . . . .	64
<b>5</b>	<b>A Novel Filter Extracted Equivalent Control Based SMC</b>	<b>65</b>
5.1	Introduction . . . . .	65
5.2	Issue in SMC Implementation . . . . .	65
5.3	Fixed Frequency SMC . . . . .	66
5.4	Proposed Technique . . . . .	68
5.5	PWM-SMC with Double Integral Type Sliding Surface . . . . .	74
5.5.1	Stability of Inner Loop . . . . .	76
5.6	Experimental Results and Discussion . . . . .	77
5.6.1	Experimental Setup . . . . .	78
5.6.2	Steady State Error . . . . .	79
5.6.3	Transient Response . . . . .	79
5.6.4	Robustness to Load Variations . . . . .	79
5.7	Summary . . . . .	80
<b>6</b>	<b>Conclusion and Future Work</b>	<b>82</b>
6.1	Conclusion . . . . .	82
6.2	Future Work . . . . .	84
	<b>Bibliography</b>	<b>86</b>

# List of Figures

2.1	Connection of distributed energy resources to a Direct Current (DC) micro-grid. . . . .	19
3.1	Basic architecture of DC micro-grid. . . . .	25
3.2	Simplified scheme for the voltage and current control using DC-DC boost converter. . . . .	28
3.3	State space trajectories under Sliding Mode Control (SMC). (a) reaching phase; (b) sliding phase. . . . .	29
3.4	Experimental set-up for the proposed technique. (a) 24 V setup; (b) 110 V setup. . . . .	38
3.5	Schematic diagram of the proposed technique for voltage regulation in a single source using boost converter. . . . .	39
3.6	Output voltage of the boost converter in an open loop during rated load and full load. . . . .	40
3.7	Step response of the system. (a) conventional current-mode controller; (b) fixed frequency Double Integral Sliding Mode Control (DI-SMC). . . . .	41
3.8	Fixed frequency operation of the converter. (a) switching signal; (b) drain voltage and inductor current. . . . .	42
3.9	Performance of the DI-SMC during large power application. (a) inductor current; (b) step response. . . . .	43
3.10	Experiment waveform of the output voltage when an additional load of $47 \Omega$ is connected in parallel to $82 \Omega$ load. (a) conventional current-mode controller; (b) fixed frequency DI-SMC. . . . .	44
3.11	Grid operation of DI-SMC. (a) output current of Source-1; (b) output current of Source-2; (c) output current of Source-3. (d) Load voltage during fault condition. . . . .	45
4.1	Structure of control loops in DC micro-grid using boost converter. . . . .	48
4.2	Block diagram showing parallel operation of power converter in a DC micro-grid. . . . .	49
4.3	Schematic of the proposed technique for voltage regulation in a single renewable energy resource. . . . .	54
4.4	The CH. 1 shows chattering along with low frequency oscillations for $R_x = 10 k\Omega$ while CH. 2 shows the generated gating sequence as a consequence of improper selection of $R_x$ . . . . .	56
4.5	Output of comparator IC LM311 showing oscillations at crossover (a) For $R_x = 1 k\Omega$ and $V_{cc} = 9 \text{ V}$ (b) For $R_x = 333 \Omega$ and $V_{cc} = 9 \text{ V}$ . . . . .	57

---

4.6	Steady state response of the closed loop system. . . . .	60
4.7	Complete response of the system with step change in input voltage from 0 V to $V_{in}$ . . . . .	60
4.8	The CH. 1 shows the ripple/chattering in the output voltage at 82 $\Omega$ load resistor while CH. 2 shows the gating signal at the output of MC34152. . . . .	61
4.9	The CH. 1 shows the inductor current at steady state when operating at 82 $\Omega$ load resistor while CH. 2 shows the gating signal observed at the output of LM311. . . . .	61
4.10	Hardware setup for the closed loop system. . . . .	62
4.11	Response of the system to step change in load from 82 $\Omega$ to 29.83 $\Omega$	62
4.12	Current sharing of the two sources using proposed controller. . . . .	63
4.13	Harmonic cancellation of chattering in the output (a) Chattering due to single source. (b) Chattering in the output when the harmonics in chattering signal of Source 2 cancels the harmonics from Source 1. . . . .	64
5.1	Block digram of the proposed filter extracted equivalent control based sliding mode control (FEEC-SMC) for voltage regulation in boost converter. . . . .	69
5.2	Complete circuit diagram of the proposed FEEC-SMC. . . . .	70
5.3	Experimental waveforms of the closed loop system with PWM-SMC. (a) Step response of the closed loop system. (b) Output voltage when load is shifted from 82 $\Omega$ to 29.88 $\Omega$ (c) Inductor current and gating signal at output of LM311 during steady state operation. (d) Chattering in the output voltage. . . . .	74
5.4	Experimental waveforms of the closed loop system with FEEC-SMC. (a) Step response of the closed loop system. (b) Output voltage when load is shifted from 82 $\Omega$ to 29.88 $\Omega$ indicating robustness of the closed loop system. (c) Inductor current and gating signal at output of LM311 during steady state operation. (d) Chattering in the output voltage. . . . .	75
5.5	Experimental setup to evaluate the performance of the controllers. . . . .	80

# List of Tables

3.1	Parameters of power converter. . . . .	42
3.2	Output voltages for variations in input. . . . .	43
4.1	Voltage regulation at different input source voltages. . . . .	57
5.1	Parameters of Buck Converter . . . . .	78

# Abbreviations

<b>AC</b>	Alternating Current
<b>BJT</b>	Bipolar Junction Transistor
<b>DC</b>	Direct Current
<b>DGU</b>	Distributed Generation Units
<b>DSP</b>	Digital Signal Processors
<b>EMI</b>	Electromagnetic Interference
<b>FPGA</b>	Field-Programmable Gate Array
<b>FEEC</b>	Filter Extracted Equivalent Control
<b>LED</b>	Light Emitting Diode
<b>Li-ion</b>	Lithium-ion
<b>MOSFET</b>	Metal Oxide Field-Effect Transistor
<b>Ni-Cd</b>	Nickel-Cadmium
<b>PID</b>	Proportional Integral Derivative
<b>PI</b>	Proportional Integral
<b>PWM</b>	Pulse Width Modulation
<b>PV</b>	Photo-Voltaic
<b>RER</b>	Renewable Energy Resources
<b>SMC</b>	Sliding Mode Control

# Symbols

$C$	Capacitance
$\gamma$	Attenuation Constant
$f_{bw}$	Bandwidth of the Converter
$u$	Control Input
$V_{con}$	Control Signal
$\zeta$	Damping Ratio
$\lambda$	Design Constants
$V_d$	Desired Output Voltage
$d$	Duty Ratio
$u_{eq}$	Equivalent Control
$e(t)$	Error Signal
$I_L$	Inductor Current
$L$	Inductor of coil
$V_{in}$	Input Voltage
$R_{load}$	Load Resistor
$V_{out}$	Output Voltage
$V_{Pramp}$	Peak Amplitude of Modulating Ramp
$I_{ref}$	Reference Current
$V_{ref}$	Reference Voltage
$\sigma$	Sliding Manifold

# Chapter 1

## Introduction

Electronic converters are the major component of modern power systems and their responsibilities include conversion of voltage, current and frequency from one level to another desired level. The conversion process is managed by a closed loop control system which is designed to achieve desired performance with minimum power losses. Electronic converters that convert DC voltages and currents to another DC level are termed as DC-DC converters. There are two basic types of DC-DC converters namely, buck and boost converter. All other types of converter can be constructed by the combination of above mentioned types.

Buck converters are designed to convert the input voltage to a lower level of voltage, hence acts as a step down converter. Therefore, its input voltage is always greater than its output voltage. Boost converters can only step-up the input voltage while the buck-boost converters can perform both operations. It is important to mention that all these converters are controlled by a binary input by turning the semiconductor switch ON or OFF.

It shall be emphasized that the energy transfer to both inductor and capacitor, in a buck converter, takes place when the switch is ON. Whereas in case of boost converters, the inductor is energized when switch is ON while the energy transfer to the capacitor occurs only when the switch is OFF. This phenomena causes its



transfer function to have a Right Handed Zero (RHZ) in the s-plane which is also termed as non-minimum phase property.

## 1.1 Parameters Influencing Control

In this section, the parameters effecting the control of power electronic converters are discussed. Primarily these parameters are:

1. The switching frequency.
2. The size of the passive energy storing elements.
3. The gain of the controller.

### 1.1.1 Switching Frequency

A DC-DC converter can give a perfect DC output only when operating at infinite switching frequency. However, due to the physical limitations like turning on and off times of the semi-conductor devices, the converters operates at finite switching frequency. As a result ripples are observed in the output voltage of the converters.

High switching frequencies are not appreciated by the power electronic engineers as they increase the switching losses. Moreover, power loss due to skin effect and eddy current occurring in the magnetic material of the inductor core also increase with increase in the switching frequency. Furthermore, the electromagnetic noise emitted by the converter is directly proportional to the increase in switching frequency.

Therefore, considering all the above mentioned factors, it may be concluded that there is a trade off between the power quality (output ripples) and the power efficiency of the converter when selecting the switching frequency.

### 1.1.2 Passive Energy Storing Components

All the DC-DC converters consists of two major types of passive energy storing components, namely the inductor and the capacitor. Large values of these components reduce the output voltage ripples, however at the same time they increase the inertia of the system and thus the converter requires large time to react to the change in the output voltage, if perturbed by some external disturbance. For smaller values of the inductor and capacitor the ability of the converter to respond to a voltage change is improved but at the cost of increased output voltage ripples.

It is important to mention that different control strategies result in different dynamic response for the same converter because of the different time constants associated with the feedback systems. Hence, the dynamic response is determined by the control technique along with the size of the energy storing elements.

### 1.1.3 Control Gains

It is a well known fact in the control theory that increasing the control gains reduces the steady state error along with improvement of the dynamic response but at the cost of the system stability. In general, the stability of the feedback system controlled by and any technique, whether linear or non-linear, is adversely effected by the large control gains.

In conventional proportional integral derivative control (PID), increasing the proportional gain  $K_e$  reduces the steady state error but increases the percentage overshoot and a further increase in  $K_e$  may cause system instability. The integral gain  $K_i$  can be increased to reduce the time taken by the system to eliminate the steady state error but however, its high values cause instability of the feedback system. Increasing the derivative gain  $K_d$  reduces the system overshoot and has no effect on the steady state performance, however it amplifies the noise in the system and its high values may cause instability.

## 1.2 Common Control Techniques

This section deals with the discussion of commonly used control schemes for DC-DC converters and their brief critical analysis.

### 1.2.1 Hysteresis Voltage Controllers

Before the invention of Pulse width modulation technique, Hysteresis controllers were perhaps the most commonly used controller to control DC-DC converters. This controller consists of a hysteresis relay that compares the actual output of the converter with desired output voltage. If the output voltage goes low as compared to the desired output voltage, the switch is turned on. If the output voltage goes above the desired voltage, the switch is turned off. The controller works well for the buck type of converters but it fails for the boost and buck-boost converters. Problem with boost and buck - boost type of converters is the presence of a right hand side zero that causes the system to be non-minimum in phase. The right hand side zero results in a phase lag between the control input and the output voltage of the converter [1]. To control the converters with a right half plane zero, hysteresis current controllers are used.

Problem with this type of control is that both the turn on time and the turn off time of hysteresis controller depend on the load resistance, input voltage and the upon the values of inductor and capacitor used. Thus if the input voltage changes or the output load resistance change, the frequency of operation of the converter changes. This results in an unpredictable noise spectrum that makes the electromagnetic interference control quite difficult [2].

### 1.2.2 Linear Controllers

Voltage regulation of DC bus bar is conventionally achieved by using linear Proportional Integral (PI) controllers. The controllers act by increasing or decreasing the pulse width of the switching signal of the power converter. Due to fixed frequency

operation of these controllers, the filter design for electromagnetic compatibility becomes trivial. With proper shielding and grounding the fixed frequency operation makes the filter design easy which is the need for power supplies in this modern world of communication and computation [3]. Another reason of their popularity is the availability of linear controllers with PWM output in IC forms. However, PI controllers are based on the average model of the converter which is linearized at a specific operating point to get the transfer function. Because of this constraint, their performance is degraded under large disturbance and load changes [4]. Moreover, under varying load conditions the PI gains need rapid tuning. Auto tuning methods are proposed in [5, 6] for PI, PD and PID controllers. But the schemes are rather complex than conventional PI controllers. These controllers can also be divided into two categories.

1. Voltage Mode Control
2. Current Mode Control

### 1.2.2.1 Voltage Mode Control

This is a single loop controller where scaled output voltage is feedback to close the control loop. The feedback voltage is subtracted from the reference signal to generate an error signal. The error signal is then passed through a compensating network  $Z_f$  which creates a control signal. The compensated control signal is then compared with a ramp function to generate a pulse width modulated signal (PWM) which is used for switching. One of the main disadvantage of this scheme is its susceptibility to noise from the input voltage side [2].

### 1.2.2.2 Current Mode Control

Current mode control is a two loop control scheme with series compensated networks. The inner loop uses inductor current while the outer loop is the voltage feedback loop. Current mode control is usually applied to boost and buck-boost

converters because of their non-minimum phase. The inner loop that uses current feedback actually introduces a non linear term in the feedback and differs from Voltage mode control in this aspect which is totally linear. Current mode control can be divided into further two categories. Peak current mode control and average current mode control.

In peak current mode control the idea is to use the inductor current as reference signal instead of a ramp signal. The inductor current is triangular in wave shape and can be used instead of ramp signal to generate PWM waveform. The major disadvantage of this scheme is the instability of the controller for duty cycle greater than 0.5. The other disadvantage of this scheme is that it is extremely susceptible to noise since the inductor current contains a sufficient amount of high frequency noise due to turn on and off of the power electronic switch [7].

In the average current mode control, the compensated output voltage of the converter is subtracted from the triangular shaped inductor current to generate a compensated current error. This compensated current error is then compared with an externally generated saw tooth waveform to give pulse width modulated output. The advantage of having two compensation networks in series is that this controller is stable for duty cycles greater than 0.5. However solving and analyzing two compensation networks in series is non-trivial. This is a major reason for not adopting this method [2].

### 1.3 Problem in Using Small Signal Model

In general all the above mentioned techniques to generate PWM output are based on linear and time-invariant model of the power converters. But actually a DC-DC converter is a non-linear with time varying characteristics. This places a strict constraint on the operating conditions of the converter while using the linearized mathematical model. Larger changes in the operating conditions, such as load variations or the input voltage change to large extend, will cause the controller to deviate from the desired outputs or may even cause instability. Therefore,

the industrial applications like the control of micro-grids require advanced control techniques that are robust to input voltage variations as well as invariant to changes in the system parameters.

## 1.4 Advanced Control Techniques

To cope with the above mentioned drawback of linear controllers, the researchers have proposed the use of advanced non-linear controllers which are summarized as follows.

### 1.4.1 Fuzzy Logic Control

In this technique, the control algorithm is based upon the experience of the designer rather than being based upon a mathematical model of the plant [8]. In fact, fuzzy logic is a heuristic reasoning approach that relies upon the understanding of the designer about the system behavior, thus extending its abilities beyond the limits of linear control theory. This fact has motivated the researchers for its implementation in DC-DC converters [9–11], but however, they did not prove a distinguished improvement as compared to linear controllers [7]. Moreover, its implementation requirements like digital signal processors and EEPROM makes it less feasible as compared to analogue controllers.

### 1.4.2 Adaptive Control

In this control technique, the parameters of the control equation are adjusted automatically according to the operating conditions of the system [12]. Therefore, ideally this technique can provide optimal performance under all the operating conditions [13]. However, its practical realization requires instantaneous sensing of the operating points that adds additional cost to the design. This adaptation is achieved by deriving a mathematical equation based upon the model of the plant.

The digital implementation of such controllers is not cost effective because of instantaneous sensing and run-time adaptation calculations, while their analogue construction is very complex. This explains their unpopularity in the field of power electronics.

### 1.4.3 Artificial Neural Networks

Artificial Neural Networks (ANN) is a type of control scheme where different layers of artificial neurons are connected together and are trained to achieve a desired relationship between the input and the output. Inspired by the biological nerves system, this scheme can be used to implement highly non-linear control equations after using sufficient number of training samples. Each neuron has a specific weight which is self-tuned to an appropriate value during the training process [14].

The inherent capability of ANN to learn and produce a highly non-linear control function has motivated the researchers for its implementation in DC-DC converters [15, 16]. However, the major obstacles in its industrial use for power converters are its non-trivial implementation, time consuming training process and requirements of relatively high end digital signal processors as compared to other schemes.

### 1.4.4 Sliding Mode Control

Sliding mode control (SMC) is a good choice to achieve the objective, because they provide parametric invariance and robustness [17–21] against unknown disturbances. Moreover, as the power electronic switch in the converter operates in either on or off state. This makes SMC a natural choice to control such systems. Since SMC is a nonlinear control technique, it eliminates the need to obtain a linearized model of the power converter.

A major drawback in SM based controller is the varying switching frequency of the power converter. SM controllers do not provide a fixed switching frequency which causes the power electronic switch, in the converter, to operate under time varying

frequency. This degrades the power quality and makes it difficult to suppress the electromagnetic emissions (EME) resulting from high current switching [22]. These emissions are filtered out by designing passive filters, so that the emissions do not interfere with nearby electronic components. The filter design depends upon the switching frequency, while variations in frequency makes the filter design non-trivial. Details of electromagnetic interference (EMI) and its importance in power converters can be found in [23]. However, by achieving fixed switching frequency in SMC both the issues of namely, switching losses and EMI emissions can be addressed simultaneously. Two appropriate solutions in this regard are discussed in Chapter 3 and Chapter 4 of this thesis.

## 1.5 Motivation

The advancements in low cost and high power semiconductor fabrication has turned the power electronic converter into an essential component of industrial systems like arch furnaces, induction heating, motor drives, hybrid vehicles and power supplies of various electrical appliances. In modern era of increased power demand, they are essential part of systems controlling voltage, current, frequency and power flow in different types of micro-grids.

Conventionally power electronic converters are controlled using linear controllers with pulse width modulated (PWM) output. In this strategy, the control law is derived using small signal theory based on the assumption that the operating condition will not change significantly. If the system is forced to operate away from the set equilibrium point, then the linear controller will not be able to work properly [24]. This control technique works quite well in the situations where the load is fixed like the case of energy savers or light emitting diodes. But in scenarios such as micro-grids, where the output current and the load resistance are variable while network parameters are uncertain, linear controller fails because they are designed under the assumptions of small signal theory. For systems having



unknown load conditions and uncertain parameters, better results can be achieved by using non-linear controller techniques.

Among non-linear controllers, the robust nature of SMC and discrete nature of power electronic converters makes SMC an appropriate choice for controlling such circuits [25]. The SMC is ideally implemented using a discontinuous function that operates the switch at infinite frequency. Thus, forcing the state trajectories to slide along the designed manifold towards the origin. However, it is not possible to achieve infinite switching frequency in physical systems. The first realistic approach towards SMC implementation is presented in [26], where the discontinuous *sign* function is replaced by a hysteresis comparator which is tuned to limit the maximum switching frequency according to the physical limits of the system. The scheme results in finite, but time varying switching frequency [27]. As a result, finite magnitude oscillations, known as chattering, appear in the output of the system [28]. The chattering is acceptable within limits for a particular system. However, the problem of variable switching frequency becomes a serious issue for electronic converters. They need a fixed frequency operation [29–31] because they consist of passive energy storing components (inductors and capacitors) and their correct size primarily depends upon the switching frequency. Moreover, the varying switching frequency degrades the power quality and makes it non-trivial to suppress electromagnetic interference (EMI) [32]. Hence, there is a necessary need to fix the switching frequency of SMC controlled power converters, in order to benefit from its robust and parameter invariant nature along with reduced EMI issues.

## 1.6 Research Gap Analysis

Different methods to fix the switching frequency are proposed by the researchers [29, 31, 33–36], but however, they only address stand alone applications. Previously hysteresis band SMC has been applied on micro-grids [37, 38] but fixed frequency SMC and have not been tested on this position. Therefore, in the light

of previous discussion, a hypothesis for the research is build which stated that, “fixed frequency SMC may shows better performance than its counterpart in the phase of introduced disturbances.”

Moreover, the chattering and ripples appearing at the output of power electronic converters degrades the power quality and are a special concern in micro-grids. The power quality issues in AC micro-grids is widely discussed, but discussion regarding power quality issues in DC micro-grids are rare in research community because in past the power transmission network was only AC in nature. However, due to the advancement in the semiconductor manufacturing industry during the recent years, DC micro-grids have emerged as an attractive solution for the integration of renewable energy resources. Therefore there is a necessary need to address the problem of degraded power quality in position of DC micro-grids which utilizes electronic converters for power flow.

Finally, the study and literature review reviles that existing techniques to fix the switching frequency of SMC are either complex or they compromise robustness with in limits. A detailed literature review of above mentioned fixed frequency SMC techniques is presented in Chapter 5 of this thesis. Therefore, there is a need for a comprehensive and novel method to fix the switching frequency in stand alone applications which is simple to implement using commercial IC's and also exhibit robustness and disturbance rejection properties of SMC.

## 1.7 Thesis Contributions

Significance of mathematical modeling along with design of a robust and parameter invariant controller having fixed switching frequency are the highlights of the research activities conducted in the domain of power electronic converters. The major contributions of the thesis are summarized as under:

- **Improvement in dynamic response of power converters.** A double integral type sliding manifold is designed to achieve the desired performance

by controlling a boost converter that regulates the grid voltage and ensures proper current sharing in the presence of un-modeled dynamics caused by uncertain load and line variations without using observers, which add cost and complexity to the design. Major contributes lie in the following three dimensions:

1. Improving the dynamic response of the closed loop system and increasing the robustness against unknown load demands in a DC micro-grid, using fixed frequency SMC.
2. Designing a novel sliding manifold that results in stable operation of boost converter for wide range of gains, followed by a rigorous mathematical analysis for the stability condition.
3. Designing a special-purpose test rig with three sources, in order to validate the results in comparison with conventional PI controllers. Moreover, the technique is also tested for fault condition at one of the sources connected to the micro-grid.
4. An analogue design based on commercially available ICs is presented in order to avoid use of Digital Signal Processors (DSP) and Field-Programmable Gate Array (FPGA) boards which are less immune to Electromagnetic interference.

- **Power quality improvement in DC micro-grids.**

The presented research proposes a solution to the problem of degraded power quality due to the output voltage ripples by proposing a fixed frequency SMC along with harmonic cancellation of the chattering signal in a micro-grid by utilizing an intuitive PI-type sliding manifold. Major contributions lie in the following dimensions:

1. Designing a dual loop control structure, where the inner current loop is based on the proposed SMC technique with fixed switching frequency. The outer control loop is based upon a conventional PI controller which provides reference signal to the inner loop.

2. Achieving a wide range stable operation along with addressing the load sharing problem of parallel connected converters in a micro-grid.
  3. The objective of the research is not only to achieve required robustness and harmonic cancellation of chattering but also to outline the hardware design approach in accordance with mathematical calculations, while ensuring the stability of the system.
  4. Hardware design based on low cost commercially available IC's is presented in order to avoid use of discrete time signal processors which are more sensitive to electromagnetic interference.
- **Design of a novel filter extracted equivalent control based fixed frequency SMC.**

The existing techniques for fixing frequency in SMC are complex or they compromise one or the other properties of SMC. Consequently, there is a need for a comprehensive, fixed frequency SMC design which is simple to implement and also retains the inherent properties of SMC. This research addresses the problem by proposing a novel method for fixing the switching frequency in SMC. The major contributions of the research are as follows:

1. The actual equivalent control of the system is extracted from the discontinuous function by means of a low pass filter and is used to achieve fixed frequency SMC which has not been previously reported.
2. The technique is implemented on a boost converter and the results are compared with existing PWM-SMC having a double integral type sliding surface.
3. The experimental results demonstrate that the proposed technique achieves zero steady state error with improved dynamic response, and also exhibits better disturbance rejection properties as compared to PWM-SMC.
4. A complete hardware test bench is designed and used to validate the proposed technique.

## 1.8 Thesis Structure

An overview of all the chapters presented in the thesis is given below as:

**Chapter 1** is devoted to the introduction of power electronic converters, factors effecting their control and a brief introduction of various control techniques. The motivation and research gap are analyzed and the thesis contributions are discussed.

**Chapter 2** describes the advantages of DC micro-grids along with its basic architecture. The role of power electronic converter in micro-grids is discussed and the performance parameter are presented. The details of experimental test rig are presented along with highlighting the motivation for developing a new type of fixed frequency sliding mode controller.

**Chapter 3** presents the first contribution of the thesis. The mathematical model of a DC micro-grid from the control prospective is discussed. A double integral type sliding surface is proposed to achieve better dynamic response of a boost converter, responsible for delivering power from a renewable energy resource to a micro-grid. Rigorous mathematical analysis is presented to outline the stability conditions using Lyapunov theorem and experimental results are presented to validate the design.

**Chapter 4** presents the second contribution of the thesis. A PI-type sliding surface is proposed along with harmonic cancellation of the chattering signal to improve the power quality in a DC micro-grid. Mathematical constraints that apply to guarantee the closed loop behavior of the system are derived. Finally, experimental results are presented to validate the proposed technique.

**Chapter 5** presents the third contribution of the thesis. A novel methodology is proposed where a low pass filter based extraction of the equivalent control is used to fix the switching frequency of the sliding mode control. Mathematical constraints are derived that outline the necessary conditions for extraction of the equivalent control along with Lyapunov based stability conditions for the closed loop system.

A test rig is designed to validate the proposed technique and experimental results are presented in comparison with existing fixed frequency SMC technique.

**Chapter 6** concludes the thesis along with providing some directions for the future research.

## 1.9 Summary

In this chapter the fundamental concepts related to the control of power electronic converters are presented. A detailed discussion on conventional and advanced control schemes, highlighting their advantages and drawbacks is presented. In summary, the disturbance rejection, order reduction and the capability to handle systems with un-modeled dynamics are the key properties of Sliding Mode Control (SMC) that make it a good choice to control non-linear perturbed systems like micro-grids. The system under SMC becomes invariant to parametric changes and its performance is completely robust against matched disturbances. Due to these properties, SMC is most suitable for controlling power flow and voltage control in a micro-grid where load conditions are dynamically changing and network parameter are uncertain. Moreover the complexity of feedback control design is reduced by SMC because it decouples the system into reduced order dynamics.

The following chapter will highlight the motivation for using DC micro-grids, along with discussing the voltage standards and the performance parameters.

# Chapter 2

## DC Micro-Grids and Standards

### 2.1 Motivation to use DC Micro-Grids

Exponential increase in the energy demand due to massive industrial growth and urbanization has called for the installation of new generation units. To increase the reliability of the system and reduce the probability of complete black out, the researchers are focusing on the development and integration of Distributed power Generation Units (DGU) [39–42]. Moreover, the alarming momentum at which the conventional energy resources are being depleted to meet the power demand motivated the use of Renewable Energy Resources (RER). However, as several DGUs are connected together, issues like voltage regulation and current sharing arise along with protection problems. To address these issues for the large scale integration of RERs, the so-called concept of micro-grids has emerged in the field of power systems. The micro-grid is a power distribution network that consists of DGU clusters, different types of loads, energy storage units and energy conversion devices interconnected via power distribution lines.

Among different types of RERs, solar energy is the most abundant source and researchers are focusing on developing more efficient photo-voltaic cells to achieve the concept of green energy [43, 44]. Most of the renewable energy resources, like fuel cells and Photo-Voltaic (PV) cells, are Direct Current (DC) in nature. The

energy storage banks use super capacitors, Li-ion, lead-acid and Ni-Cd batteries, which can store energy only in DC form. Other renewable resources like wind mills and bio-gas installations are also DC friendly. On the consumer side, the variable speed drives of induction motors, LEDs and electronic circuitry operate at DC voltages.

Connecting RERs and energy storage banks to Alternating Current (AC) micro-grids requires multiple conversions (DC–AC and AC–DC) that result in unwanted power loss and reduced efficiency [45, 46]. To resolve this issue, DC micro-grids have attracted the attention of the researchers [47–51]. Furthermore, skin effect losses are not present in DC micro-grids and the control of DC micro-grids is less complex as compared to AC micro-grids, where issues of frequency regulation and synchronization, flow of reactive power, unwanted harmonics and unbalanced load are the key issues [52–56].

## 2.2 DC Systems and Standards

AC systems have a history of more than one hundred years while DC system could not be deployed earlier due to the difficulty in voltage conversion levels. AC could be easily stepped up and stepped down using transformers while maintaining more than 90% efficiency [57] while this facility was not available for DC system in those times. However, with the advancements in the fabrication of high power and low cost semi-conductor devices, in the last decade, it became possible to build cost effective power electronic converters capable of stepping up and stepping down DC voltages with required efficiency. It is important to mention that most of the daily life domestic loads are DC in nature. Since these loads do not draw a sinusoidal current from the source, they cause harmonic currents when connected to the AC distribution system. The loads including Computers using SMPS (switched-mode power supplies), lightings, modern washing machines, inverter air conditioners and refrigerators, variable frequency drives, induction furnaces, rectifiers, fans with dimmers and treadmills all require DC power. As a result, the harmonic



currents are increasing dramatically in all residential, commercial, and industrial installations as such loads are increasing rapidly over the past few years. De-rating of standard transformer is up to 50% if 60% of its loads consist of SMPS. Similarly de-rating of power cables, generators and motors also occurs due to non linear loads. Hence, the researchers are focusing to avail the benefits of the DC systems which also eliminate skin effect losses, reactive power flows and frequency synchronization issues.

The literature survey reveals that different standards for the DC bus bar voltages are deployed for various operations. For the domestic applications 24V and 48V standards are used. For a micro-grid application with short length bus bar, a 110/120V system is recommended while the data centers utilize 380-400V system [58–61].

The control techniques proposed in this thesis are suitable for 24V, 48V, 110/120V and 380-400V systems. The experimental results are presented for 24V and 110V systems. The proposed controller is easily scalable for other systems by simply changing the attenuation constants and feedback ratio, as discussed in Chapter 3.

## 2.3 Power Converters in DC Micro-grids

The major advantage of DC micro-grids over conventional AC transmission system is the absenteeism of losses due to skin effect and reactive power flow. Moreover, micro-grids are reliable, economical, efficient and easily manageable [47, 62, 63]. However, as DERs are connected to the same micro-grid, the power converters responsible for power flow from these DERs operate in parallel as shown in Figure 2.1. This creates challenges like voltage control of the grid, stability of parallel connected converters and load sharing among DERs [49, 64, 65]. These tasks are accomplished by either using a controlled buck or a boost converter.

The voltage of the DC grid is conventionally controlled by DC-DC converters [66, 67]. Buck converter has been proposed in [68] to control DC voltage in micro-grid. The output voltage of buck converters is always lower than the input voltage. However, for photo-voltaic (PV) cells based applications where energy is harvested from solar radiations, it is required to boost the input voltages to draw maximum power from the PV cells [69]. Transformer based converter can efficiently provide higher output to input voltage ratio. But requirements in renewable energy applications like size, weight and cost makes transformerless converters a more appropriate choice.

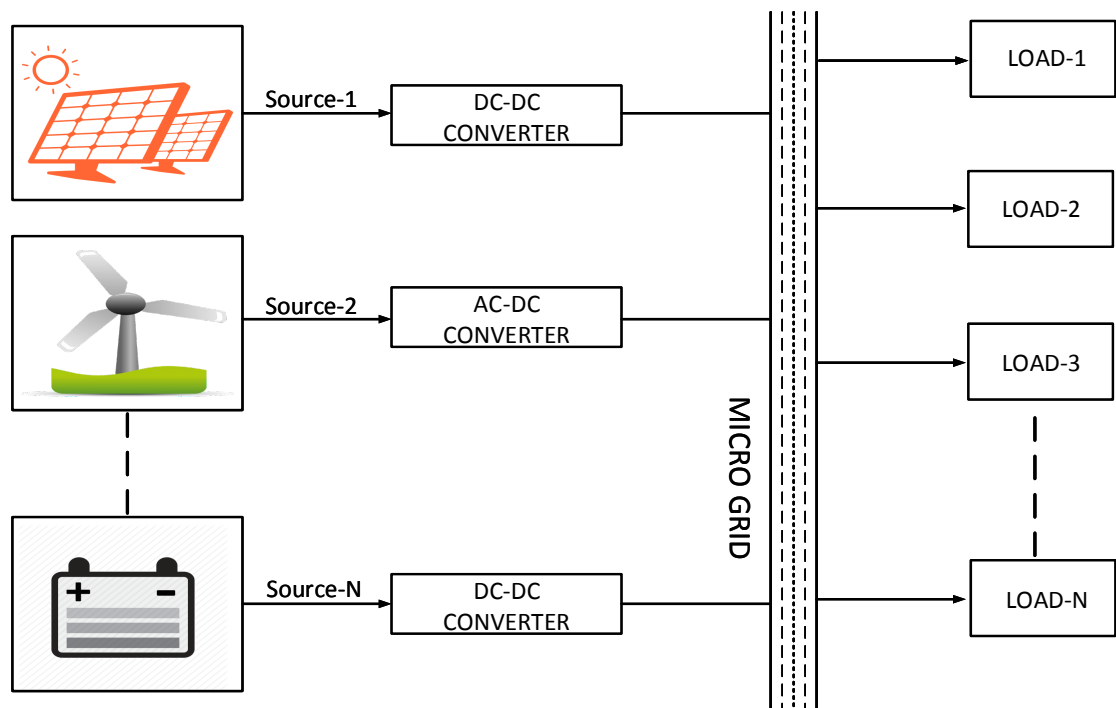


FIGURE 2.1: Connection of distributed energy resources to a Direct Current (DC) micro-grid.

## 2.4 Motivation and Challenges in Deploying Boost Converter for Micro-grid Operation

The capability of boost converter to supply output voltage more than the input voltage, makes it more feasible to be used in renewable energy applications

[70–72]. Most of the applications deploying solar cells to harvest energy require, boost converters to match the output voltage with the standard grid voltage while maintaining maximum power point tracking. Using a boost converter to control the voltage of a micro-grid is a challenging problem because of its bilinear nature [73]. Bilinear systems belong to the class of non-linear systems where the non-linearity arises because of the product of control input with the system states [74]. Moreover, the system is non-minimum in phase and its linearized model has a right handed zero. This causes the dynamics of inductor current to become unstable if feedback design is based on measuring only the output voltage [75–77]. This complicates the control problem and makes it difficult to control as compared to buck type of converters.

### 2.4.1 Control Problem

The issue of non-minimum phase can be avoided if the voltage regulation in boost converter is redefined as a current regulation problem [73, 78]. However, under uncertain load conditions a current regulator cannot keep its output voltage constant [79]. This makes the system extremely sensitive to load fluctuations. Fortunately, the current dynamics of boost converter are faster as compared to that of output voltage, therefore the issue can be resolved using a dual loop control structure. The inner current loop controls the power electronic switch based upon the reference signal provided by the outer voltage control loop [80]. Detailed discussion of controlling voltage in micro-grids using boost converter is presented in Chapters 3 and 4.

## 2.5 Performance Attributes

For a micro-grid case, it is common to have different type of loads being connected and disconnected from the grid. The step change of heavy loads on the bus bar

results in voltage sag or swell. The capability of the controller to compensate them depends upon the robustness and dynamic response of the feedback system. For a given micro-grid system, following two cases may occur.

### **Case 1:**

In case, the attached load is within the maximum power handling capability of the system then the time required to remove the voltage sag totally depends upon the robustness of the feedback system.

### **Case2:**

However, if the additional load exceeds the maximum limits then a supplementary source is connected to compensate the voltage sag. In this case, the dynamic response of the feedback system plays the most important role and a controller with better dynamic response will remove the voltage sag in less time. Discussion on improvement of both robustness and dynamic response of the feedback system is presented in Chapter 3 and 5.

## **2.6 Power Quality**

Power quality issues have been widely discussed regarding AC power systems but discussion regarding DC power quality in micro-grids is rare in research community because in past power transmission was carried out using AC systems only. However, in the recent years DC grids and transmission has emerged as an attractive solution to integrate renewable energy resources. Hence, to enhance the power quality, a fixed frequency SMC is proposed with harmonic cancellation and chattering reduction, using a PI type sliding manifold. Experimental results are presented in Chapter 4 to validate the theoretical derivations using the test rig.

## 2.7 Experimental Setup

In the experimentation, Matrix power supplies having precision to one decimal place are used to test the performance of the controller under varying input voltages and changing load conditions. The experimental results are obtained using a two channel Rigol oscilloscope having 70 MHz bandwidth and sampling rate of 1 GHz. To test the wide range operation of the boost converter, the outdoor experiment is performed using solar panels and measurements are taken with regular intervals.

The parameters of DC–DC converter are selected on the basis of 250 W output power. The inductance of the coil is 100  $\mu\text{H}$  and the output filter capacitor is of 1000  $\mu\text{F}$ . Power Metal-Oxide-Semiconductor Field-Effect Transistor (MOSFET) (IRF540) with on-resistance of 0.06  $\Omega$  and continuous drain current capability of 20 A is selected as an electronic switch. The efficiency of the converter at this frequency is experimentally observed to be greater than 90% when delivering 7 W to the load. It is observed that, in order to ensure the efficient switching, the resistance seen by the MOSFET at its drain shall be kept less than 47  $\Omega$  so as to keep the discharge interval of body diode capacitance of the MOSFET, less than its switching interval under SMC. A reference signal of 2.5 V is generated using adjustable shunt regulator TL431 with its reference pin connected to its cathode. Due to the uni-directional nature of inductor current, it is not possible to measure it using a current transformer (CT). To measure  $I_L$ , a resistor  $R_M$  is placed in its return path. As  $I_L$  flows, a voltage  $V_M$  is developed across  $R_M$  and we measure the inductor current as:

$$I_L = \frac{V_M}{R_M}. \quad (2.1)$$

## 2.8 Motivation for a New Fixed Frequency SMC

Different schemes to fix the switching frequency in SMC have been proposed and are discussed in detail in Section 5.3. The literature survey reveals that the existing techniques are either too complex or they compromise some of the intended

properties of SMC. Consequently, there is a need for a methodology that is easy and cost effective to implement while maintaining inherent properties of SMC. To address the above mentioned issue, a new technique to fix the switching frequency in power electronic converters using filter extracted equivalent control signal is proposed in Chapter 5.

## **2.9 Summary**

In this chapter, the motivation of using DC system is presented along with highlighting the different standards available in literature regarding DC bus bar voltages. The importance of robustness, improved dynamic response and better power quality on position of DC micro-grids is discussed. The following chapter will focus on the use of fixed frequency SMC by utilizing the non-linear model of the DC-DC converter for the improvement of its dynamic response, while regulating the voltage of DC micro-grids.

# Chapter 3

## Power Converter for Micro-grid Operation

### 3.1 Introduction

Micro-grids are renowned for their advantages like sustained energy generation and appropriate utilization of distributed energy resources (DER). These DERs like solar cells, wind turbines, bio-gas installations and fuel cells are not located at a single sight and are interconnected to micro-grids via controllable power electronic converters [69, 81]. These converters are scalable and show good conversion efficiencies and add flexibility in the control process. Micro-grids can be operated in grid connected or islanded mode [82, 83]. Numerous control strategies are implemented and developed for integrating DERs with central grid system [84–86].

Different energy generation units located at distributed locations are connected to DC micro-grid using DC–DC power electronic converters as shown in Figure 3.1. The major control problems in this scenario are the voltage regulation and the current sharing among different power sources. Voltage regulation is required for the proper functioning of the load devices, while current sharing is required to ensure that no source is overstressed. These objectives are achieved simultaneously by using a hierarchical control. [87–89]. Conventionally Proportional

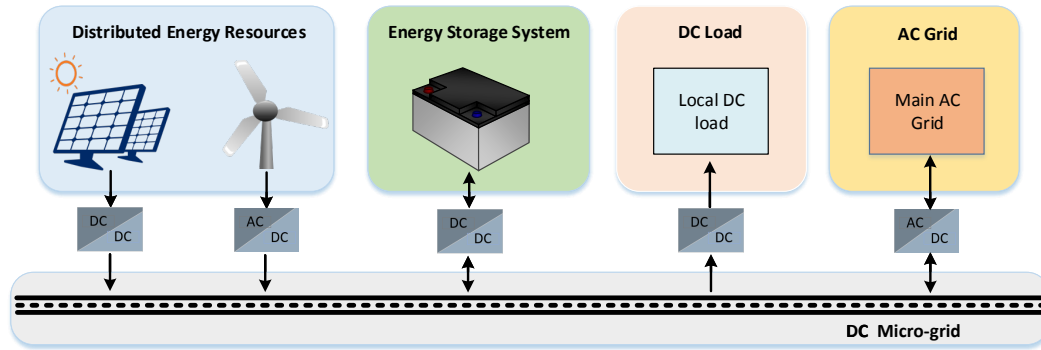


FIGURE 3.1: Basic architecture of DC micro-grid.

Integral Derivative (PID) controllers are used in the voltage and current control loops of these power electronic converters [90]. However, under uncertain load conditions, the gains of the PID controllers require periodic tuning to give the desired performance [4]. The researchers have proposed auto-tuning methods [91] and Fuzzy controllers [92, 93] to achieve better results. However, these methods are system dependent and add complexity to the design.

It is reported that the performance improvement is achieved by using boundary layer control [94–96], adaptive nonlinear control [97], model predictive control [98–100], and a time delayed based robust controller [101]. However, these techniques are not completely parameter independent and require some knowledge of the system specifications like inductance of the coil and capacitance of the filter stage. This calls for the need of a robust controller that can control the nonlinear dynamics of the power converter in order to tightly regulate the voltage in the presence of unknown load demands and uncertain grid parameters.

Indeed, the robustness and parameter invariance [102, 103] of Sliding Mode Control (SMC) is well known and makes it an attractive choice for voltage and current control in micro-grids, where load conditions are unknown and network parameters are subject to variations [104–110]. SMC based techniques result in better voltage regulation in the presence of parametric variations, modeling uncertainties and external disturbances [73, 111, 112]. However, the major drawback of SMC is its variable switching frequency. Power electronic converters require to operate at fixed switching frequency in order to minimize switching losses [113] and to



suppress Electro-Magnetic Interference (EMI) [23]. Hence, the researchers are motivated to combine the advantages of fixed frequency with the robust nature of SMC [29, 31, 33–36], thereby reducing EMI emissions and switching losses simultaneously. However, these techniques are implemented on a single DC–DC converter and its behavior has not been observed yet on the position of a micro-grid.

To fill the above-mentioned research gap, this chapter of the thesis is devoted to fixed frequency SMC based approach to track the reference voltage of each source connected to the micro-grid. The proposed technique achieves the desired performance by controlling a boost converter that regulates the grid voltage and ensures proper current sharing in the presence of un-modeled dynamics caused by uncertain load and line variations without using observers, which add cost and complexity to the design. It is important to mention that, in case of micro-grids, the electromagnetic interference (EMI) caused by the power lines and switching of the large inductor current, makes the environment less feasible for the use of Digital Signal Processors (DSP) and Field-Programmable Gate Array (FPGA) boards. Therefore, these boards are used in such applications along with specially designed electromagnetic shielding mechanisms to avoid interference from high frequency switching currents. Moreover, they need additional line filters to permit their interaction with the power lines. Due to these reasons, the proposed technique is demonstrated using low cost commercially available analogue Integrated Circuits (ICs), which present a workable industrial solution without involving A/D converters and DSP/FPGA boards which are less immune to EMI and also add additional cost to the design. Moreover, the analogue implementation gives a better picture of the controller design and its implementation procedure.

## 3.2 Mathematical Modeling

Each source in the DC micro grid comprises of a DC–DC converter as shown in Figure 3.2, where input voltage from the renewable energy source is denoted by  $V_{in}$ ,  $I_L$  is the instantaneous inductor current,  $V_{out}$  is the output voltage of the converter,

$R_{load}$  is the load resistance,  $C$  is the capacitance of the output filter capacitor while  $L$  is the inductance of the coil. By using circuit analysis techniques, the nonlinear dynamic model of the system is written as:

$$\begin{aligned}\dot{I}_L &= -(1-u)\frac{1}{L}V_{out} + \frac{(V_{in+\delta n})}{L}, \\ \dot{V}_{out} &= (1-u)\frac{1}{C}I_L - \frac{1}{(R_{load} + \Delta R_{esr})C}V_{out},\end{aligned}\quad (3.1)$$

where  $\delta n$  is an unknown but bounded time varying disturbance, which satisfies the condition  $|\delta n| < V_{in}$ ;  $\Delta R_{esr}$  represents the parameter uncertainty caused by Equivalent Series Resistance (ESR) of the capacitor. Since the power electronic switch can be either On or Off, thus mathematically the control signal  $u$  belongs to a discrete set:  $u \in \{1, 0\}$ . We define  $\tilde{u} = (1 - u)$ , where the control input  $u$  is defined with respect to the power electronic switch as:

$$u(t) = \begin{cases} 1, & \text{Switch is conducting,} \\ 0, & \text{Switch is open circuit.} \end{cases}\quad (3.2)$$

The boost converters are nonlinear and non-minimum in-phase with respect to output voltage [114, 115] and the dynamics of the inductor current are unstable if the output voltage is considered to be the only variable to be controlled [116]. However, the boost converter satisfies the motion separation principle derived from singular Perturbation Theory [117, 118]. It means that the dynamics of  $I_L$  are much faster as compared to the dynamics of  $V_{out}$  and the problem can be solved by designing a cascaded control structure with two control loops. The inner loop controls the inductor current while the outer loop controls the load voltage. The inner control loop is designed using fixed frequency SMC while the outer control loop having slower dynamics is designed using PI controller.

Since the controller is robust; therefore, throughout the article, we consider the simplified model with  $\delta n = 0$  and  $\Delta R_{esr} = 0$ . The section on experimental results and discussion where the input voltage is varied and sudden changes in load are deliberately applied is an exception in order to evaluate the performance of the

controller and verify its robustness. The steady state dynamics of the system are found by setting the time derivatives of system states to zero. Thus, as  $t \rightarrow \infty$ ,  $\dot{I}_L = \dot{V}_{out} = 0$  and  $V_{out} = V_d$ . Setting these values in Equation (3.1), the reference current in the inner loop is derived as:

$$I_{ref}^* = \frac{V_d^2}{R_{load}V_{in}}, \quad (3.3)$$

where  $I_{ref}^*$  is the reference current for the inner control loop at equilibrium and  $V_d$  is the desired output voltage of the converter.

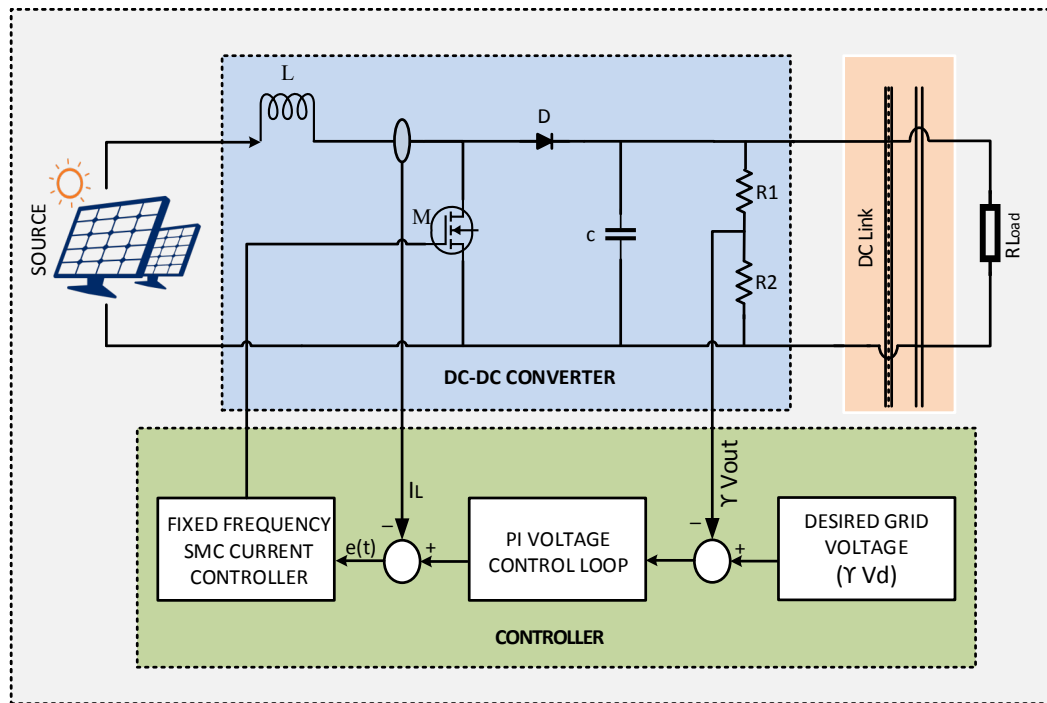


FIGURE 3.2: Simplified scheme for the voltage and current control using DC-DC boost converter.

### 3.3 Controller Design

The SMC design concept is based upon a discontinuous control law, which directs the system states towards a sliding manifold in the state space. Sliding manifold is designed to insure the finite time convergence of the state trajectories at the origin. The control process of SMC can be segregated into two phases, namely the

reaching phase and the sliding phase. During the reaching phase, the controller generates a series of switching commands such that the state trajectories hit the sliding manifold irrespective to their initial conditions as shown in Figure 3.3a. In the second phase, the controller executes its operation via switching commands, ensuring the trajectory to be in a small vicinity of the sliding manifold  $\sigma = 0$ , which in turn gets directed concurrently towards the desired reference at the origin 'O' as shown in Figure 3.3b. In short, the sliding mode operation can be explained such that the controller utilizes the sliding plane as a reference to perform its decisions in order to ensure the convergence of the state trajectories to the origin, where steady state operation is achieved. We select the control law based on the reaching law [21] as:

$$u = \frac{1}{2}(1 + \text{sign}(\sigma)). \quad (3.4)$$

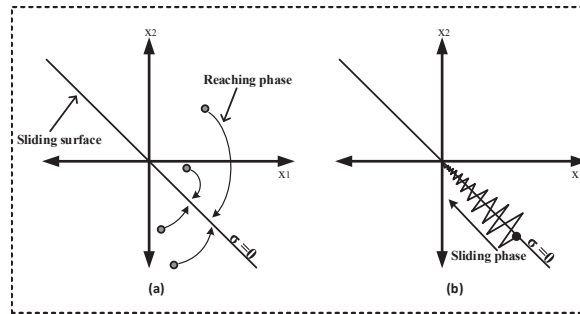


FIGURE 3.3: State space trajectories under Sliding Mode Control (SMC). (a) reaching phase; (b) sliding phase.

The reaching law ensures that the state trajectories are always directed towards the sliding manifold  $\sigma = 0$ , regardless of their initial conditions. It is shown in [119] that a double integral type sliding manifold performs better in terms of steady state error as compared to conventional PID type sliding manifold. Therefore, a double integral type sliding surface is selected as:

$$\sigma = \lambda_1 \iint e(t) dt dt + \lambda_2 \int e(t) dt + \lambda_3 e(t), \quad (3.5)$$

where

$$e(t) = I_{ref} - I_L \quad (3.6)$$

and  $\lambda_1$ ,  $\lambda_2$  and  $\lambda_3$  are positive design constants. When the state trajectories reach the manifold  $\sigma = 0$ , sliding mode is said to be established. Now onwards, the system becomes parameter invariant [21] and its behavior is described as:

$$\sigma = \lambda_1 \iint e(t) dt dt + \lambda_2 \int e(t) dt + \lambda_3 e(t) = 0, \quad (3.7)$$

we differentiate Equation (3.7) w.r.t time and get:

$$\lambda_3 \ddot{e}(t) + \lambda_2 \dot{e}(t) + \lambda_1 e(t) = 0. \quad (3.8)$$

The Laplace transform of Equation (3.8) is:

$$S^2 E(s) + S \frac{\lambda_2}{\lambda_3} E(s) + \frac{\lambda_1}{\lambda_3} E(s) = 0. \quad (3.9)$$

Since  $\lambda_1$ ,  $\lambda_2$  and  $\lambda_3$  are positive design constants, hence the Laplace transform in Equation (3.9) is a Hurwitz polynomial and both of the roots lie on the left side of the S-plane. Hence, as  $t \rightarrow \infty$ ,  $e(t) \rightarrow 0$  and  $V_{out} \rightarrow V_d$ .

Implementation of SMC using Pulse Width Modulation (PWM) is based upon two well known theorems which sets the stage for the implementation of fixed frequency SMC. The first theorem [21] states that the discontinuous control  $u$  in SMC can be replaced theoretically with a smooth and continuous time function called equivalent control signal, such that  $0 < u_{eq} < 1$ . The second theorem states that, at sufficiently high frequency, the equivalent control coincides with the duty ratio of the PWM control [120].

The equivalent control  $u_{eq}$  of the system under sliding mode is derived by substituting the time derivative of the sliding surface equal to zero. Thus, setting  $\dot{\sigma} = 0$ , we get:

$$\dot{\sigma} = \lambda_1 \int e(t) dt + \lambda_2 e(t) + \lambda_3 \dot{e}(t) = 0. \quad (3.10)$$

Involving the dynamics of the system from Equation (3.1) and rearranging the

terms, we get:

$$\tilde{u}_{eq} = \frac{V_{in}}{V_{out}} - L \frac{\lambda_2}{\lambda_3} \frac{e(t)}{V_{out}} - L \frac{\lambda_1}{\lambda_3} \frac{\int e(t)dt}{V_{out}}. \quad (3.11)$$

Substituting  $\tilde{u} = (1 - u)$ , the expression of  $u_{eq}$  is derived from Equations (3.6) and (3.11) as:

$$u_{eq} = \left(1 - \frac{V_{in}}{V_{out}}\right) + L \frac{\lambda_2}{\lambda_3} \frac{(I_{ref} - I_L)}{V_{out}} + \frac{\lambda_1}{\lambda_3} \frac{\int (I_{ref} - I_L)dt}{V_{out}}. \quad (3.12)$$

Since the equivalent control signal  $u_{eq}$  coincides with the duty ratio  $d$  of PWM converter, we can write:

$$\begin{aligned} u_{eq} &= d = \frac{V_{con}}{V_{Pramp}} \\ \implies V_{con} &= u_{eq} \times V_{Pramp}, \end{aligned} \quad (3.13)$$

where  $V_{con}$  is the control signal to the PWM modulator and  $V_{Pramp}$  is the peak voltage of ramp signal, respectively. By choosing  $V_{Pramp} = V_{out}$  and using Equation (3.13), we get:

$$V_{con} = (V_{out} - V_{in}) + L \frac{\lambda_2}{\lambda_3} (I_{ref} - I_L) + L \frac{\lambda_1}{\lambda_3} \int (I_{ref} - I_L)dt, \quad (3.14)$$

$$V_{Pramp} = V_{out}. \quad (3.15)$$

It is worth mentioning that the proposed structure in Equation (3.14) differs from the PI controllers because of the term  $(V_{out} - V_{in})$ . It acts as an adaptive feed-forward gain which automatically changes, in an effort to nullify the disturbances in  $V_{in}$ . This adaptation is also reflected in Equation (3.15) which means that the peak amplitude of the ramp signal is modified in relation with  $V_{out}$ . It acts as an agent to change the modulation index in order to achieve faster dynamic response. Conditions to guarantee stability and avoid over modulation are discussed in Section 3.4. Another important difference between the two controllers is the way they are designed. The PI controllers are designed on the concept of small signal analysis which makes the response of the system specific to an operating

point while sliding mode controllers are large signal systems, where the design is independent from the operating point.

### 3.4 Stability of Sliding Mode Control

This section deals with the proof of stability and finite time convergence of the states to the sliding manifold.

#### 3.4.1 Existence of Sliding Mode Control

The existence and stability of SMC is ensured if the control law enforces the state trajectories towards the sliding manifold  $\sigma = 0$ . Mathematically, the following two constraints shall be satisfied in the neighborhood of the manifold:

$$\lim_{\sigma \rightarrow 0^+} \dot{\sigma} < 0, \quad (3.16)$$

$$\lim_{\sigma \rightarrow 0^-} \dot{\sigma} > 0. \quad (3.17)$$

For the proposed controller, we obtain the equation for  $\dot{\sigma}$  by using Equations (3.1) and (3.5) as:

$$\dot{\sigma} = \lambda_1 x_1(t) + \lambda_2 x_2(t) + \lambda_3 \left( \frac{V_{out}}{L} \tilde{u} - \frac{V_{in}}{L} \right), \quad (3.18)$$

where  $x_1(t) = \int e(t)dt$  and  $x_2(t) = e(t)$ . The specific conditions for the stable operation of the system are as follows:

Case 1:

When  $\sigma \rightarrow 0^+$ , then Constraint (3.16) states that  $\dot{\sigma} < 0$ . This turns Equation (3.18) into an inequality as:

$$\dot{\sigma} = \lambda_1 x_1(t) + \lambda_2 x_2(t) + \lambda_3 \left( \frac{V_{out}}{L} \tilde{u} - \frac{V_{in}}{L} \right) < 0. \quad (3.19)$$

The control law (3.4), in Case 1, takes the value  $u = 1$  ( $\tilde{u} = 0$ ). To ensure that Condition (3.19) remains true, the following constraint shall be satisfied:

$$\frac{\lambda_3}{L}V_{in} > \lambda_1|x_1(t)| + |\lambda_2x_2(t)|. \quad (3.20)$$

The biasing voltages of the operational amplifiers computing  $x_1(t)$  and  $x_2(t)$  are  $\pm 8$  and  $\pm 5$ , respectively. This physically limits the maximum and minimum values of  $x_1(t)$  and  $x_2(t)$ . Mathematically,  $|x_1(t)| < 8$  and  $|x_2(t)| < 5$ ; thus, by appropriate choice of design constants  $\lambda_1$ ,  $\lambda_2$  and  $\lambda_3$ , the constraint in Equation (3.20) is satisfied.

Case 2:

When  $\sigma \rightarrow 0^-$ , then Constraint (3.17) states that  $\dot{\sigma} > 0$ . This turns Equation (3.18) into inequality as:

$$\dot{\sigma} = \lambda_1x_1(t) + \lambda_2x_2(t) + \lambda_3\left(\frac{V_{out}}{L}\tilde{u} - \frac{V_{in}}{L}\right) > 0. \quad (3.21)$$

The control law will turn  $u = 0$  ( $\tilde{u} = 1$ ). To ensure that condition in Inequality (3.21) remains true, the following constraint shall be satisfied:

$$\lambda_3\frac{V_{out} - V_{in}}{L} > |\lambda_1x_1(t)| + |\lambda_2x_2(t)|. \quad (3.22)$$

The Inequality (3.22) is satisfied by an appropriate choice of design constants. It is important to notice that, if the output voltage of the converter is less than the input source voltage, then the inequality (3.22) is not satisfied. This requires careful selection of the initial conditions that guarantee the convergence of the state trajectories to  $\sigma = 0$ . At startup of the boost converter, this problem is solved by starting the converter in open loop and then closing the loop once the condition  $V_{out} > V_{in}$  is satisfied. Another simple way to solve the problem is by introducing a protection circuit that always ensures the control signal  $V_{con} < V_{Pramp}$  in the



PWM circuit, which in return results in stable switching of the power electronic switch until the condition  $V_{out} > V_{in}$  is achieved.

### 3.4.2 Finite Time Convergence to the Sliding Manifold

In order to show that the states converge to the sliding manifold  $\sigma = 0$  in finite time, we consider the following Lyapunov function:

$$V = \frac{1}{2}\sigma^2 \quad (3.23)$$

where its time derivative is given as:

$$\dot{V} = \sigma\dot{\sigma} \quad (3.24)$$

Since both the conditions (3.20) and (3.22) are satisfied, hence  $\dot{V}$  is real and negative, thus we write:

$$\dot{V} = -|\sigma|\xi \quad \text{where } \xi \in \mathfrak{R}^+ \quad (3.25)$$

It is shown in [121] that for any general case of equation (3.25) the following estimate holds true:

$$\dot{V} \leq -\delta\sqrt{2V} \quad (3.26)$$

The inequality (3.26) guarantees that the state trajectories of the system reach the manifold  $\sigma = 0$  in finite time  $t_{fs}$  [122] which is given as:

$$t_{fs} \leq \frac{1}{\delta} \sqrt{2V(\sigma(0))} \quad (3.27)$$

Once the state trajectories reach the sliding manifold, the behavior of the system is

completely described by the dynamics of the sliding surface as previously discussed in Section 3.3.

### 3.5 Sliding Surface and Parametrization of the Controller

In order to achieve the desired dynamics of the system during sliding mode, the controller is parametrized using Ackermann's formula. When the system is sliding on the manifold  $\sigma = 0$ , then the reduced order dynamics of the system are totally described by the sliding coefficients. Rearranging Equation (3.8), we get:

$$\frac{d^2}{dt^2}e(t) + \frac{\lambda_2}{\lambda_3} \frac{d}{dt}e(t) + \frac{\lambda_1}{\lambda_3}e(t) = 0. \quad (3.28)$$

The standard second order equation is given as:

$$\frac{d^2y(t)}{dt^2} + 2\zeta\omega_n \frac{dy(t)}{dt} + \omega_n^2 y(t) = 0. \quad (3.29)$$

Comparing coefficients of the Equations (3.28) with (3.29), we get:

$$\frac{\lambda_2}{\lambda_3} = 2\zeta\omega_n \quad \text{and} \quad \omega_n^2 = \frac{\lambda_1}{\lambda_3},$$

where  $\omega_n$  is the natural frequency and  $\zeta$  is the damping ratio. Recalling that the damping ratio in a linear time-invariant second order system corresponds to the response of the system, which is over damped for  $\zeta > 1$ , critically damped for  $\zeta = 1$  and under damped for  $\zeta < 1$ . In order to achieve a smooth and fast response with no overshoots, we choose  $\zeta = 1$ . Rearranging the above equation in terms of the bandwidth  $f_{bw}$  of the converter, we get:

$$\frac{\lambda_2}{\lambda_3} = 4\pi f_{bw} \quad \text{and} \quad \frac{\lambda_1}{\lambda_3} = 4\pi^2 f_{bw}^2. \quad (3.30)$$

For the desired bandwidth of 65 kHz, the calculations of the sliding coefficients using Equation (3.30) are as follows:

$$\frac{\lambda_2}{\lambda_3} = 4\pi f_{bw} = 4\pi(65k) = 816.4 \times 10^3,$$

$$\frac{\lambda_1}{\lambda_3} = 4\pi^2 f_{bw}^2 = 4\pi^2(65k)^2 = 2.6 \times 10^{13}.$$

It is important mention that the maximum allowable limits of the op-amps should be considered while parameterizing the controller. In our case, both  $V_{in}$  and  $V_{out}$  of the converter exceed the limits. This problem is solved by feeding  $V_{in}$  and  $V_{out}$  via voltage divider network with attenuation constant  $\gamma$ . For the desired output voltage of  $V_d = 24$  V, the reference voltage  $V_{ref}$  is kept as 2.5 V. Hence,  $\gamma$  is calculated as:

$$\gamma = \frac{V_{ref}}{V_d} = \frac{2.5}{24} = 0.104.$$

The combination of feedback resistor is calculated using  $\gamma$ . Selecting resistor  $R_1$  as 6.8 k $\Omega$ ,  $R_2$  is calculated as:

$$R_2 = \frac{\gamma}{1 - \gamma} R_1 = \frac{0.104}{1 - 0.104} \times 6.8 \text{ k} = 789.2 \text{ } \Omega.$$

Using a series combination of standard value resistors, we get  $\gamma = 0.103$ . The constant  $\gamma$  modifies the feedback control Equation (3.13) as:

$$u_{eq} = d = \frac{\gamma V_{con}}{\gamma V_{out}} = \frac{V_{con}}{\gamma V_{out}},$$

where  $V_{con}$  is computed from Equation (3.14) as:

$$V_c = (\gamma V_{out} - \gamma V_{in}) + \gamma L \frac{\lambda_2}{\lambda_3} (I_{ref} - I_L) + \gamma L \frac{\lambda_1}{\lambda_3} \int (I_{ref} - I_L) dt. \quad (3.31)$$

Equation (3.31) can be expressed as:

$$V_c = (\gamma V_{out} - \gamma V_{in}) + k_1(I_{ref} - I_L) + k_2 \int (I_{ref} - I_L) dt, \quad (3.32)$$

where  $k_1$  and  $k_2$  are:

$$k_1 = \gamma L \frac{\lambda_2}{\lambda_3} = 8.25, \quad (3.33)$$

$$k_2 = \gamma L \frac{\lambda_1}{\lambda_3} = 1.7 \times 10^6, \quad (3.34)$$

and  $V_{Pramp}$  is computed from Equation (3.15) as:

$$V_{Pramp} = \gamma V_{out}. \quad (3.35)$$

The output of op-amps computing  $x_1(t)$  and  $x_2(t)$  in Equation (3.18) are also scaled by the constant  $\gamma$  such that:

$$-0.52 \leq x_1(t) \leq 0.52,$$

$$-0.83 \leq x_2(t) \leq 0.83.$$

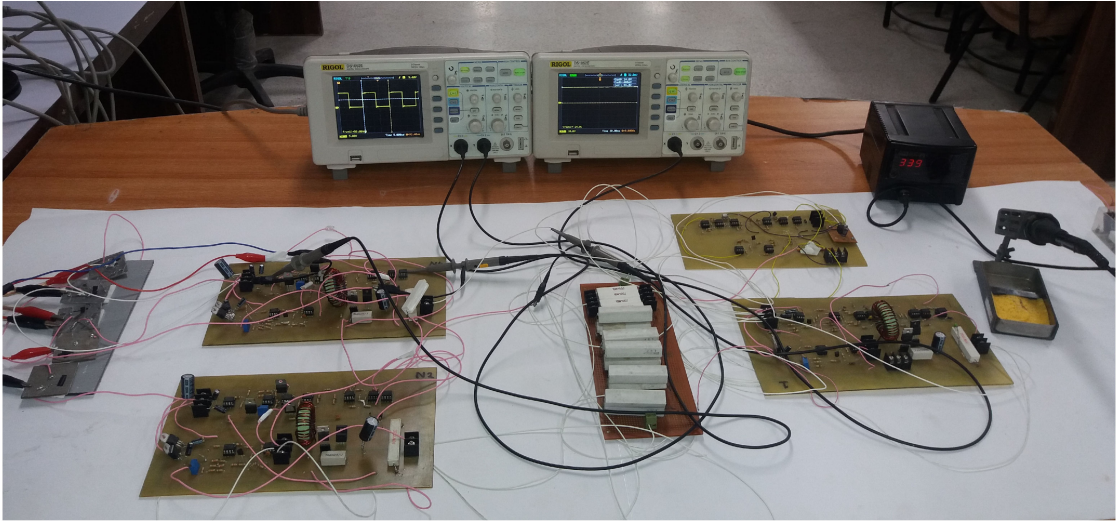
The integrator in Equation (3.32) is designed using op-amp circuit, where gain  $k_2 = 1/(R_{1i}C_{1i})$ . By selecting  $C_{1i} = 100$  pF, the value of  $R_{1i}$  is calculated as:

$$R_{1i} = \frac{1}{C_{1i} \times 1.7 \times 10^6} = 5.8 \text{ k}\Omega.$$

The outer PI control loop has a proportional gain of 8.2 and an integral gain of  $1/R_{2i}C_{2i} = 5000$ . The integral gain is achieved by selecting  $C_{2i} = 10$   $\mu$ F and  $R_{2i} = 20$  k $\Omega$ . In order to limit the maximum duty cycle of the power converter to 95%, a shunt regulator using TL431 with its reverse breakdown voltage adjusted at 4.8 V is placed at the output of the operational amplifier generating the control signal  $V_{con}$ . TL431 cannot be adjusted to regulate the output voltage lower than 2.5 V, hence a summing gain of 2 is introduced so that the signal  $V_{con}$  is greater than the minimum regulated voltage of TL431. This gain is then compensated

in Equation (3.13) by amplifying the ramp peak  $V_{Pramp}$  by the same gain. The hardware implementation of  $u_{eq}$  and  $V_{Pramp}$  is given as:

$$u_{eq} = d = \frac{2 \times V_{con}}{2 \times V_{Pramp}} = \frac{2 \times V_{con}}{2 \times \gamma V_d}. \quad (3.36)$$



(a)



(b)

FIGURE 3.4: Experimental set-up for the proposed technique. (a) 24 V setup; (b) 110 V setup.

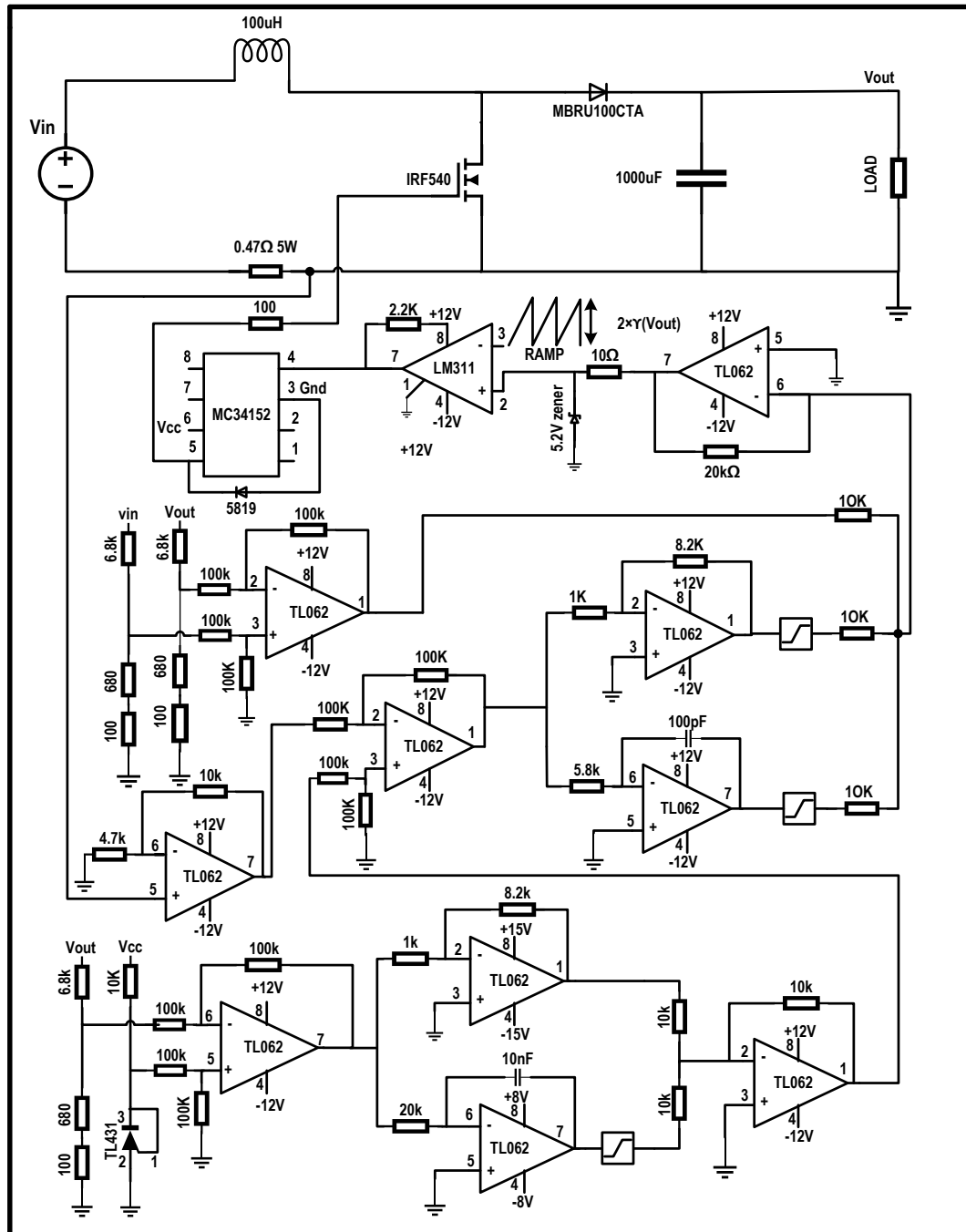


FIGURE 3.5: Schematic diagram of the proposed technique for voltage regulation in a single source using boost converter.

### 3.6 Results and Discussion

This section is devoted to the experimental results and their discussion. Both the open loop and closed loop responses are presented and the performance of the

later is discussed in comparison with conventional controllers. Fixed switching frequency for the sliding mode operation is selected to be 50 kHz and the experimental setup is shown in Figure 3.4. The complete circuit diagram for voltage regulation in a single source is shown in Figure 3.5.

### 3.6.1 Open Loop Response

In order to emphasize the need of the feedback control, the open loop response of the system is presented in Figure 3.6. The converter is operated, in open loop with a PWM signal having a 50% duty ratio. The calculated output of the converter at this signal is 24 V, but the experimental output is 22.8 V, which is 1.2 V less than the calculated output. This difference occurs due to the voltage drop in the parasitic resistance of the hardware components and the connecting leads. The output further drops to 20 V when an additional load of 47  $\Omega$  is connected to the existing 82  $\Omega$  load. Hence, it may be concluded that in open loop, the output of the power converter exhibits a steady state error that changes with variation in load resistors.

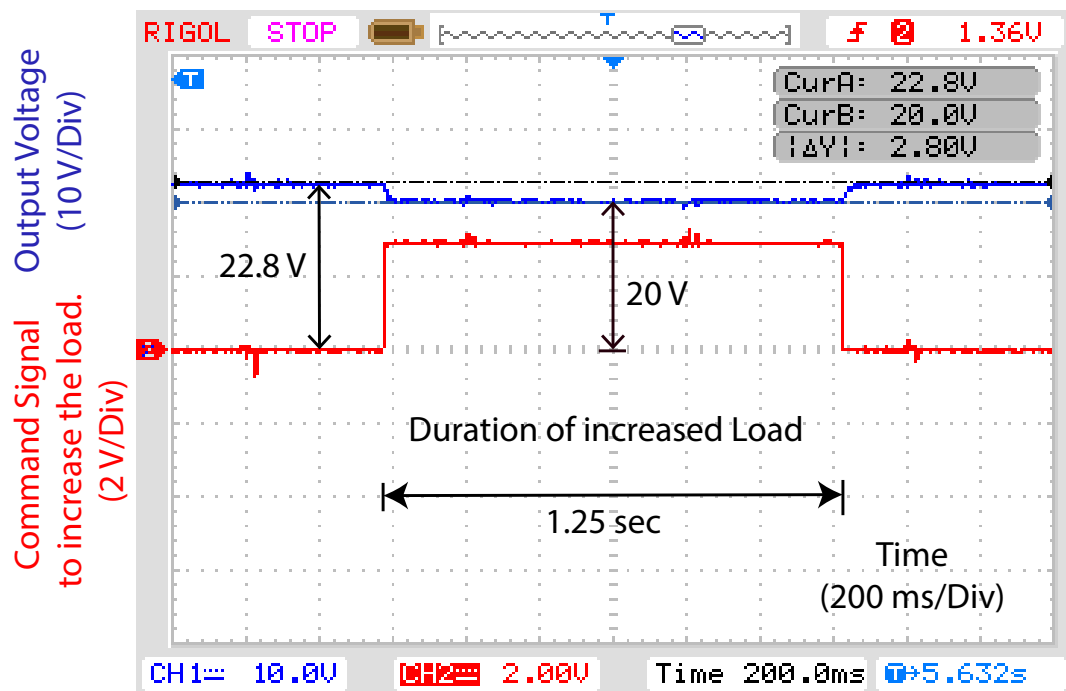


FIGURE 3.6: Output voltage of the boost converter in an open loop during rated load and full load.

### 3.6.2 Performance of Proposed Controller in Comparison with PI-Controller

The performance of the proposed technique is analyzed along with the conventional current-mode controller, having a PI loop each for voltage regulation and current tracking. For the sake of comparison, the bandwidth of the proposed technique is set to be the same as the current-mode controller.

#### 3.6.2.1 Dynamic Response

The dynamic response of the current-mode PI controller is presented in Figure 3.7a. The controller achieves 24 V with rise time of 43 ms and settles to final value in 80 ms. Figure 3.7b shows the response of the proposed fixed frequency SMC. The proposed controller has rise time of 40 ms and settling time of 75 ms which shows an appreciable improvement in the dynamic response of the closed loop system. The response is faster as compared to the current-mode PI controller due to the presence of a feed-forward term in the proposed technique.

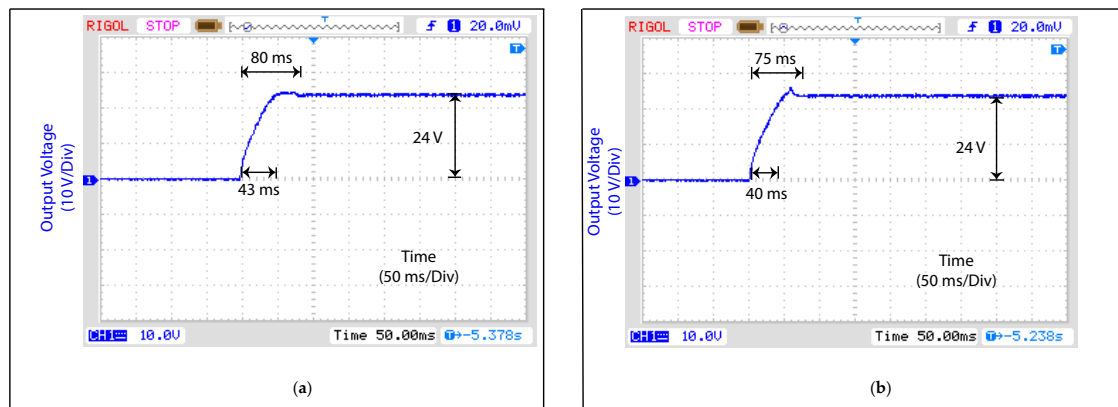


FIGURE 3.7: Step response of the system. (a) conventional current-mode controller; (b) fixed frequency Double Integral Sliding Mode Control (DI-SMC).

The switching sequence generated by the controller is shown in Figure 3.8a. The drain voltage resulting due to switching of MOSFET is shown on CH1 in Figure 3.8b. The CH2 in the same figure shows the inductor current. It shall be noticed



TABLE 3.1: Parameters of power converter.

Parameter	Value
Input Voltage	55 V
Output Voltage	110 V
Inductance of Coil	100 $\mu$ H
Output capacitance	1000 $\mu$ F
Max. Output power	2000 W

that the time period of switching sequence is constant, hence the objective of fixing the switching frequency in SMC is achieved by the proposed technique.

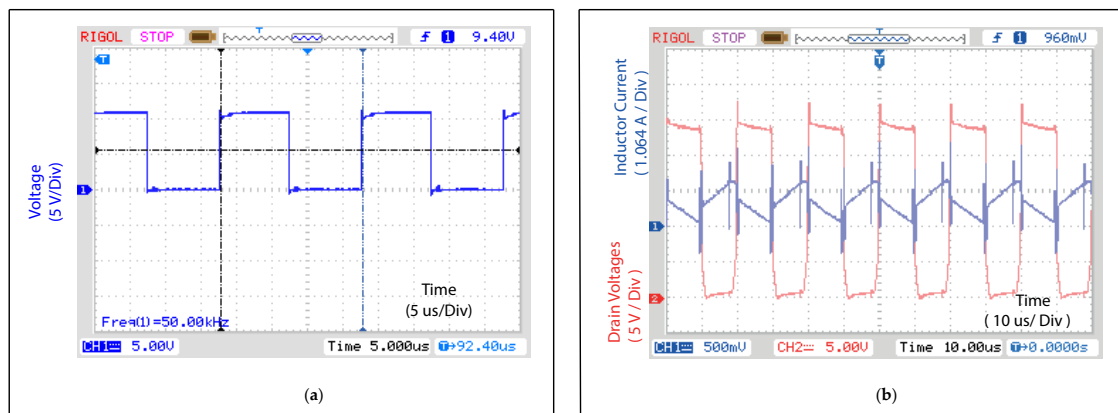


FIGURE 3.8: Fixed frequency operation of the converter. (a) switching signal; (b) drain voltage and inductor current.

The hardware can be easily scaled for operation at any desired output by proper selection of  $\gamma$ . The value of  $\gamma$  shall be selected such that the feedback signal does not exceed the power supply voltages of the operational amplifiers and other control circuitry. In order to observe the behavior of the controller for high voltage and large power applications, the technique is also applied to the converter with specifications shown in Table 3.1. The experimental setup is shown in Figure 3.4b where the input voltage is applied using four 12 V lead acid batteries connected in series having 200 AH current rating. The output is regulated at 110 V while delivering 1230 W to the load. Figure 3.9a shows the inductor current that is measured using a current to voltage conversion circuit while the dynamic response of the converter is shown in Figure 3.9b. For the sake of analysis, the output

TABLE 3.2: Output voltages for variations in input.

$V_{in}$	$V_{out}$
12.1	24.0
14.5	24.0
16.0	24.0
18.1	24.0

voltage is fed to the oscilloscope through a resistive network of 0.1 attenuation and is measured using its  $10 \times$  settings.

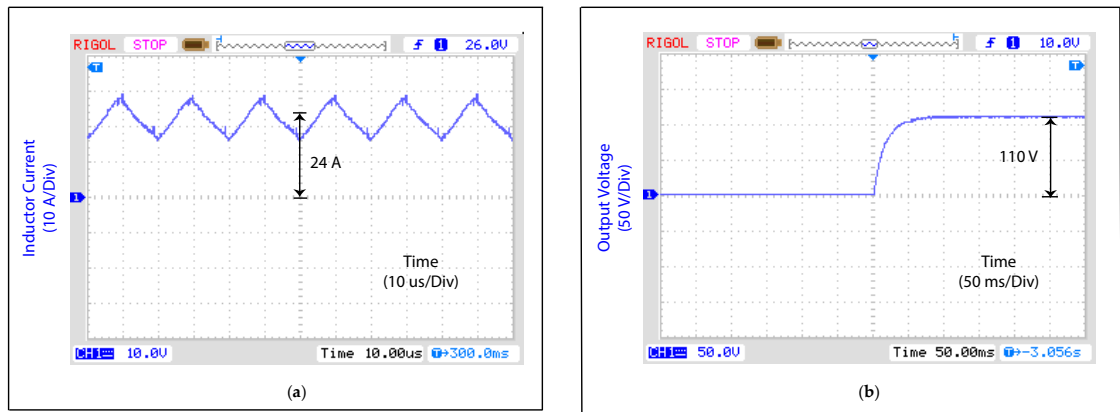


FIGURE 3.9: Performance of the DI-SMC during large power application. (a) inductor current; (b) step response.

### 3.6.2.2 Robustness of the Controller

The robustness of the controller is verified by applying a step change in load from  $82 \Omega$  to  $29.9 \Omega$ . This step change is emulated by connecting and disconnecting a  $47 \Omega$  resistor in parallel with  $82 \Omega$  load at a frequency of 10 KHz. The switching is achieved by using a Darlington paired Positive-Negative-Positive (PNP) power transistor (TIP142) whose base is driven by Negative-Positive-Negative (NPN) transistor (C828). Figure 3.10a shows that the conventional current-mode controller exhibits an undershoot of 4.1 V and recovers in  $640 \mu\text{s}$ . Figure 3.10b shows that the proposed DI-SMC exhibits an under-shoot of only 2.8 V and recovers in  $250 \mu\text{s}$  with no steady state error. Hence, the voltage dip during load transaction is reduced by 31.7%. This verifies the robustness of the proposed technique to a sudden change in load which is a key feature of SMC designs. The experimental

setup for the proposed controller is shown in Figure 3.4. The proposed controller is also tested for line variations. The test is performed by changing the input voltage from  $V_{in} = 12$  V to  $V_{in} = 18$  V. The controller operates effectively and the results are summarized in Table 3.2.

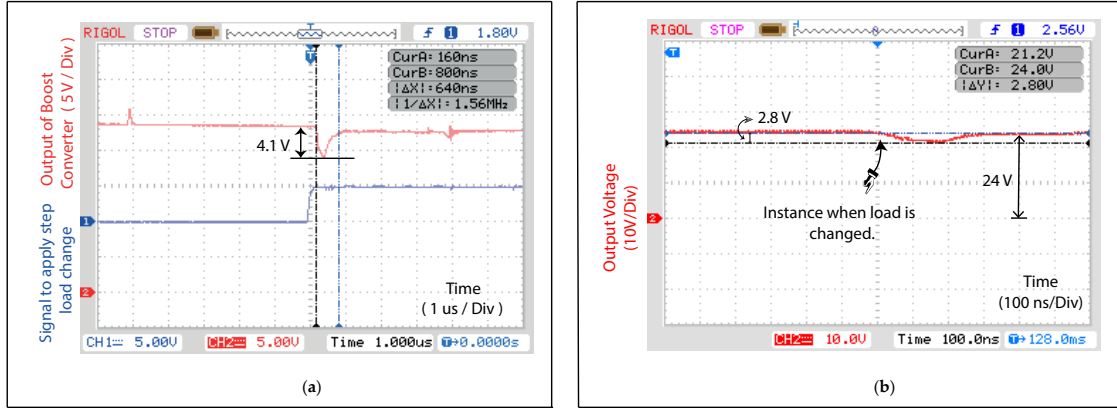


FIGURE 3.10: Experiment waveform of the output voltage when an additional load of  $47 \Omega$  is connected in parallel to  $82 \Omega$  load. (a) conventional current-mode controller; (b) fixed frequency DI-SMC.

### 3.6.3 Grid Testing for Fault Condition

The capability of the proposed technique to operate in a DC micro-grid is experimentally validated on a test rig comprising of three sources. An outer control loop based on a PI-controller provides reference current signal for the each source connected to the micro-grid. The tracking of the reference current is accomplished in each source by using a boost converter controlled by the proposed double integral type fixed frequency SMC. During the steady state condition, the bus voltage is 24 V and the currents supplied by the sources are 1.61 A, 1.63 A and 1.62 A, respectively. The system is operated at a partial load such that, if one source fails, the other two sources have sufficient power capability to fulfill the load demand. The fault in Source 2 is emulated by disconnecting its control signal. Figure 3.11a–c show the current of each source during the fault condition. Figure 3.11d shows the voltage transient at the load during the fault. The new currents supplied by Sources 1 and 3 are 2.42 A and 2.44 A, respectively, which corresponds to 0.82% error in load sharing. Hence, the load disturbances on the position of DC–DC

micro-grids have been effectively addressed, confirming that the proposed technique is capable of operation even during an instantaneous increase in the load demand or in case of a fault in the connected sources.

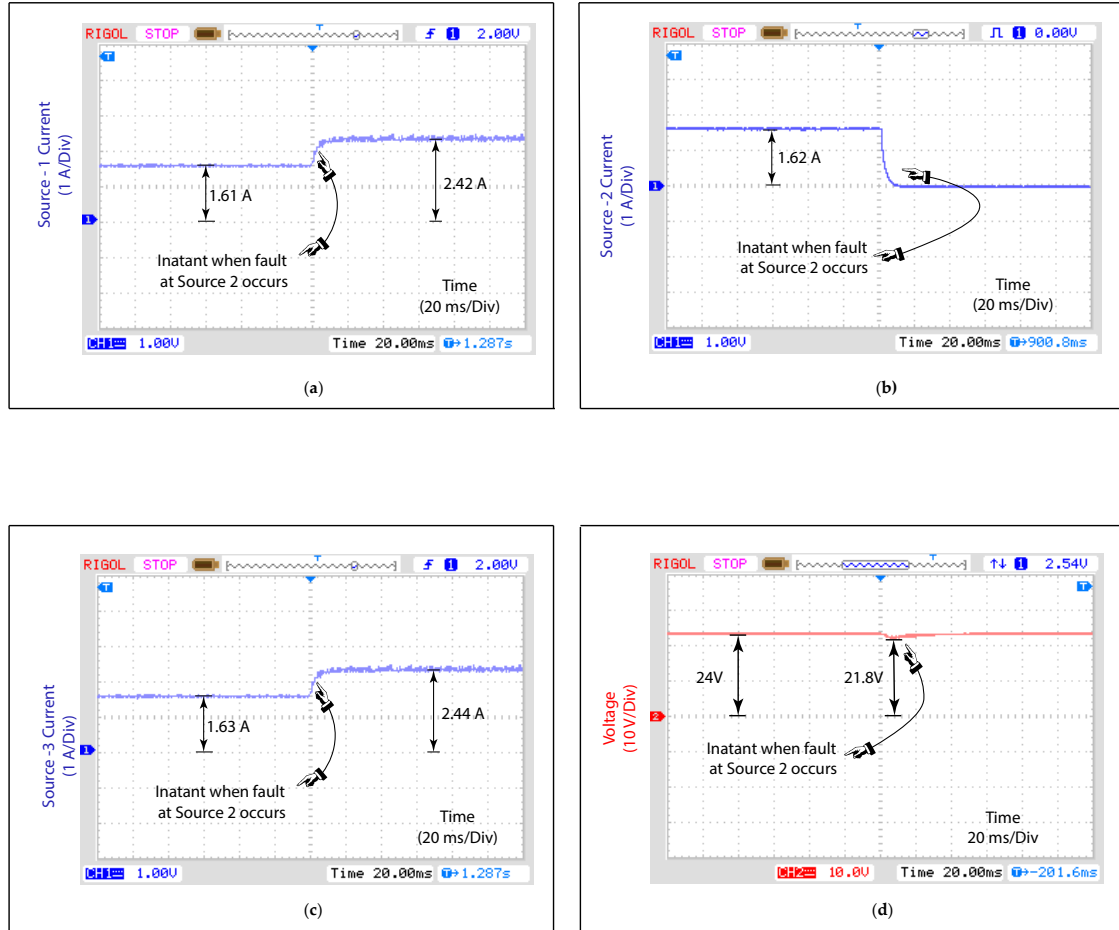


FIGURE 3.11: Grid operation of DI-SMC. (a) output current of Source-1; (b) output current of Source-2; (c) output current of Source-3. (d) Load voltage during fault condition.

### 3.7 Summary

In this chapter, voltage regulation of DC micro-grid using fixed frequency SMC with a novel double integral type sliding manifold is proposed along with a rigorous proof for the stability of the system. The controller is tested experimentally and the results show the desired performance of the proposed technique along with providing robustness against fluctuations in input voltages and change in load

conditions. A detailed discussion on parametrization of the controller, hardware design and circuit implementation is presented. The technique is also applied on a micro-grid test bench, having three sources and the results show satisfactory operation of the closed loop system. The controller is implemented using commercially available analogue ICs which eliminated the need of using expensive analogue-to-digital data acquisition cards along with phasing out the issues due to their finite sampling time. For the purpose of bench marking, the results are compared with conventional PI controller. The proposed technique improved the dynamic response of the closed loop system by reducing both, the rise time and the settling time. It is observed that a sudden voltage dip appears in the regulated voltage when an additional load is connected. This dip is reduced by 31.7% for the proposed controller as compared to that of the conventional PI controller.

# Chapter 4

## Power Quality Improvement

### 4.1 Introduction

A solution based on dual loop control structure is proposed in Chapter 3 and published in [123] where it is shown that fixed frequency SMC achieves better dynamic response in DC micro-grids. Now, this chapter is devoted to improve the power quality by achieving a robust, fixed frequency and parameter invariant solution. A fixed frequency SMC along with harmonic cancellation of the chattering signal in a micro-grid by utilizing a PI-type sliding manifold is presented. A dual loop control structure is used, where the inner current loop is based on the proposed SMC technique with fixed switching frequency. The outer control loop is based upon a conventional PI controller which provides reference signal to the inner loop. The proposed methodology achieves a wide range stable operation along with addressing the load sharing problem of parallel connected converters in a micro-grid. The objective of the presented research is not only to achieve required robustness and harmonic cancellation of chattering but also to outline the hardware design approach in accordance with mathematical calculations, while ensuring the stability of the system. Design of the controller hardware based on low cost commercially available IC's is presented in order to avoid use of discrete time signal processors which are more sensitive to electromagnetic interference.

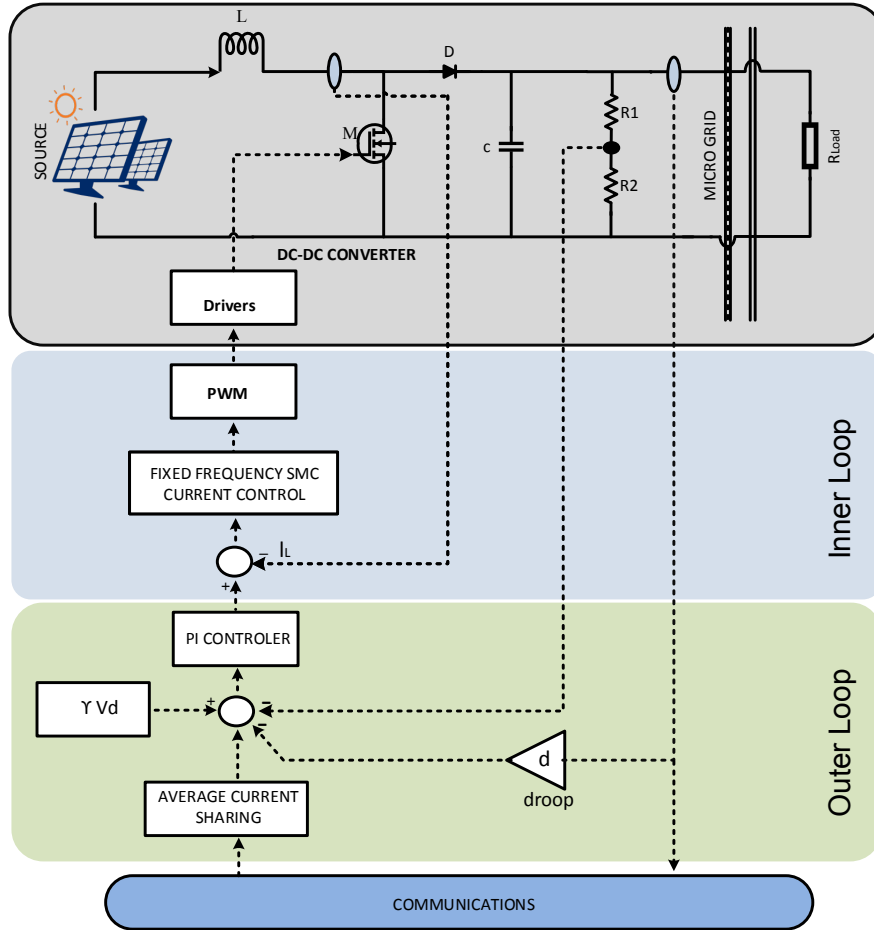


FIGURE 4.1: Structure of control loops in DC micro-grid using boost converter.

## 4.2 Design of Fixed Frequency SMC using PI-Type Sliding Manifold

The renewable energy resources and DERs supply power to the DC micro-grid via controllable DC-DC converters as shown in Fig. 4.1. Their connection to the grid results in parallel operation of these converters as shown in Fig. 4.2. The mathematical model of the system has been discussed in Chapter 3. To achieve the objective of better power quality by harmonic cancellation of the chattering signal we propose a PI-type sliding surface is designed as:

$$\sigma = k_1 \int e_i(t)dt + k_2 e_i(t) \tag{4.1}$$

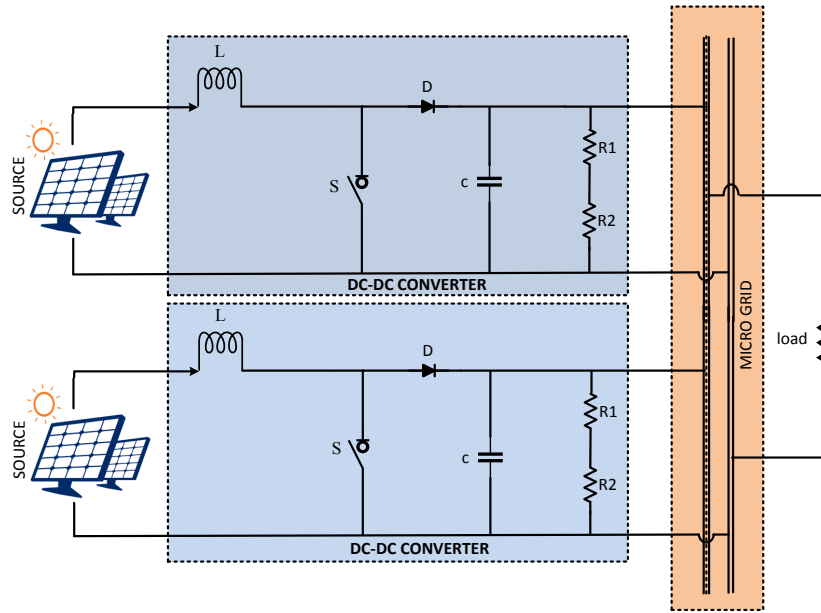


FIGURE 4.2: Block diagram showing parallel operation of power converter in a DC micro-grid.

where  $k_1, k_2$  are positive design constants and  $e_i(t)$  is the current error defined as:

$$e_i(t) = I_{ref} - I_L \quad (4.2)$$

where  $I_{ref}$  is the reference inductor current provided by the outer PI voltage control loop. The derivation of constant frequency SMC is based on equivalent control [21] method. The equivalent control signal  $u_{eq}$  is a theoretical continuous time signal that replaces the discontinuous control signal for the sake of mathematical analysis. The expression of  $u_{eq}$  for this system under sliding mode is computed by equating the time derivative of the sliding surface to zero. Thus we get:

$$\dot{\sigma} = k_1 e_i(t) + k_2 \dot{e}_i(t) = 0 \quad (4.3)$$

By using (3.1) and (4.3) we get:

$$\tilde{u}_{eq} = \frac{V_{in}}{V_{out}} - \frac{k_1}{k_2} \frac{L}{V_{out}} e_i(t) \quad (4.4)$$



We derive the equivalent control for the system by substituting  $\tilde{u}_{eq} = (1 - \tilde{u}_{eq})$  and using (4.2) we get:

$$u_{eq} = \left(1 - \frac{V_{in}}{V_{out}}\right) + \frac{k_1}{k_2} \frac{L}{V_{out}} (I_{ref} - I_L) \quad (4.5)$$

After the establishment of SM control when  $\sigma = 0$  is achieved, the equivalent control of the system equals the duty ration  $d$  in PWM converters [120].

$$u_{eq} = d = \frac{V_c}{V_{Pr}} \quad (4.6)$$

$$V_c = u_{eq} \times V_{Pr} \quad (4.7)$$

where  $V_{Pr}$  is the peak amplitude of ramp signal and  $V_c$  is the SM control based control signal which is PWM modulated to get a discontinuous control for the power electronic switch having a fixed switching frequency [120]. By using (4.5) and (4.7) and selecting ( $V_{Pr} = V_{out}$ ) we get the control equation as:

$$V_c = (V_{out} - V_{in}) + L \frac{k_1}{k_2} (I_{ref} - I_L) \quad (4.8)$$

and the peak of ramp signal  $V_{Pr}$  as:

$$V_{Pr} = V_{out} \quad (4.9)$$

The equivalent control is a theoretical signal that completely describes the sliding motion when  $\dot{\sigma} = \sigma = 0$  has been established [21]. Taking Laplace transform of  $\dot{\sigma} = 0$  in (4.3) we get:

$$Sk_2 E_i(S) + k_1 E_i(S) = 0 \quad (4.10)$$

The time domain solution of (4.10) ensures that  $e_i(t) \rightarrow 0$  and  $V_{out} \rightarrow V_d$ . Substituting these values in (4.8) and (4.9) we get:

$$V_c = (V_d - V_{in}) + L \frac{k_1}{k_2} (I_{ref} - I_L) \quad (4.11)$$

and the peak of ramp signal  $V_{Pr}$  as:

$$V_{Pr} = V_d \quad (4.12)$$

It shall be noticed that the proposed control structure in (4.11) does not have any adaptive tuning of  $V_{Pr}$ , as in previously proposed work in fixed frequency SMC. This simplifies the hardware implementation and solves the problem of modulation non-linearities which arise due to changing amplitude of modulating ramp signal. The structure of (4.11) contains the term  $(V_d - V_{in})$  which acts as feed forward gain and helps achieve smaller settling time as compared to conventional PID controllers.

### 4.2.1 Stability of the Controller

Sliding mode can exist on the manifold  $\sigma = 0$  if the following condition is satisfied [73].

$$\lim_{\sigma \rightarrow 0} \sigma \dot{\sigma} < 0 \quad (4.13)$$

By using (3.1) and (4.1) we derive the expression for  $\dot{\sigma}$  as:

$$\dot{\sigma} = k_1 e_i(t) + \tilde{u} \frac{k_2}{L} V_{out} - \frac{k_2}{L} V_{in} \quad (4.14)$$

when  $\sigma \rightarrow 0^+$  then according to (4.13),  $\dot{\sigma} < 0$  thus (4.14) is written as:

$$k_1 e_i(t) + \tilde{u} \frac{k_2}{L} V_{out} - \frac{k_2}{L} V_{in} < 0 \quad (4.15)$$

As  $\sigma \rightarrow 0^+$ , the control law (3.4) turns  $u = 1$  ( $\tilde{u} = 0$ ) and thus (4.15) is written as:

$$k_1 e_i(t) - \frac{k_2}{L} V_{in} < 0 \quad (4.16)$$

Since  $V_{in}$  is always positive, thus (4.16) is ensured to hold true if the following condition is fulfilled.

$$\left\| \frac{k_2}{L} V_{in} \right\| > \|k_1\| \quad (4.17)$$

When  $\sigma \rightarrow 0^-$  then according to (4.13),  $\sigma > 0$  and we write (4.14) as:

$$k_1 e_i(t) + \tilde{u} \frac{k_2}{L} V_{out} - \frac{k_2}{L} V_{in} > 0 \quad (4.18)$$

As  $\sigma \rightarrow 0^-$  the control law (3.4) turns  $u = 0$  ( $\tilde{u} = 1$ ) and (4.18) is written as:

$$k_1 e_i(t) + \frac{k_2}{L} V_{out} - \frac{k_2}{L} V_{in} > 0 \quad (4.19)$$

The following conditions shall be satisfied to ensure that (4.19) remains true.

$$\left\| \frac{k_2}{L} (V_{out} - V_{in}) \right\| > \|k_1\| \quad (4.20)$$

For boost converter  $V_{out} > V_{in}$  and hence (4.17) and (4.20) are easily satisfied by appropriate selection of  $k_1$  and  $k_2$ .

## 4.2.2 Selection of Sliding Constants

When the system has entered the sliding phase then the dynamics of the system are completely described by manifold  $\sigma = 0$ , thus by using (4.1) we get:

$$k_1 \int e_i(t) dt + k_2 e_i(t) = 0 \quad (4.21)$$

Taking time derivative of (4.21) we get:

$$k_1 e_i(t) + k_2 \dot{e}_i(t) = 0 \quad (4.22)$$

$$\dot{e}_i(t) = -\frac{k_1}{k_2} e_i(t) \quad (4.23)$$

Since  $k_1$  and  $k_2$  are positive design constants, hence as  $e_i(t) \rightarrow 0$ . The rate of decay of  $e_i(t)$  is controlled by the ration of  $k_1$  to  $k_2$ . The time domain solution of (4.23) is:

$$e_i(t) = e_{io} e^{-\left(\frac{k_1}{k_2}\right)t} \quad (4.24)$$

where  $e_{io}$  is the initial value of error. It is important to note that the decay rate of the error signal is controlled by the ratio of  $k_1$  to  $k_2$ . Large values of  $k_1/k_2$  leads to faster decay of the error but at the cost of increased control effort (large duty ratio). This causes high in-rush current at the start up of the converter which may trigger the over circuit protection circuits in the source supply (renewable energy resource). Hence there is a compromise in selection of the ratio. Primarily, the constants  $k_1$  and  $k_2$  are selected such that constraint for stability in (4.17) is satisfied. We select  $(k_2 V_{in}/L)$  to be 1.2 times greater than  $k_1$ , hence the inequality (20) is transformed into equation as:

$$\left\| \frac{k_2}{L} V_{in} \right\| = 1.2 \|k_1\| \quad (4.25)$$

For  $V_{in} = 12$  V,  $L = 100 \times 10^{-6}$  H, we get  $k_1/k_2 = 10 \times 10^4$ . Assuming  $k_2 = 1$  we get  $k_1 = 10 \times 10^4$ . These values of  $k_1$  and  $k_2$  also satisfy the constraints in (4.20) for  $V_{out} = 24$  V.

### 4.2.3 Parameterization of Controller

In this subsection calculations for the specific case are presented. Both  $V_{in}$  and  $V_{out}$  exceed the maximum allowable limits of op-amps and are fed through a resistor network with attenuation constant  $\beta$ . By selecting reference voltage  $V_{ref}$  of 2.5 V

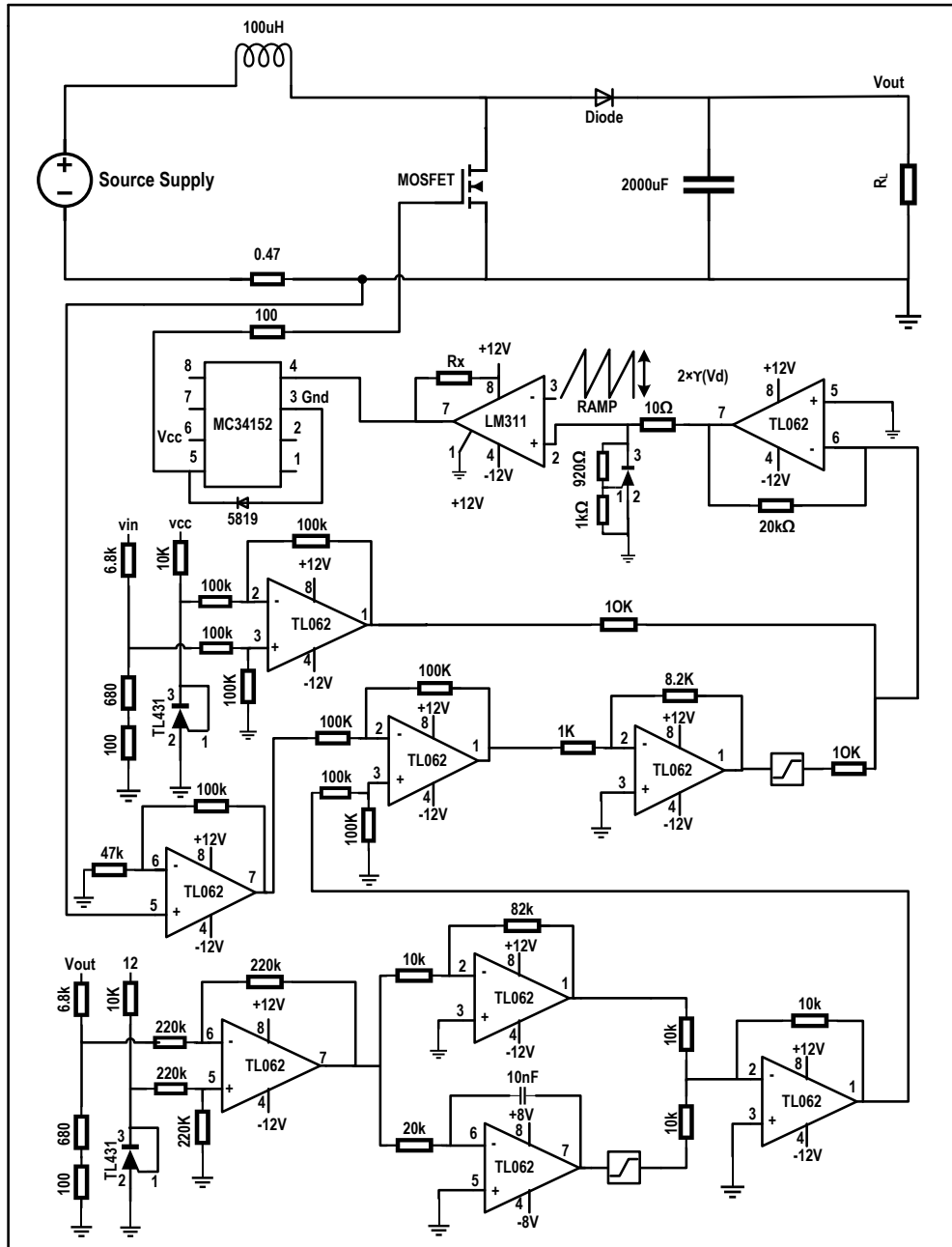


FIGURE 4.3: Schematic of the proposed technique for voltage regulation in a single renewable energy resource.

we calculate  $\beta$  as:

$$\beta = \frac{V_{ref}}{V_d} = \frac{2.5}{24} = 0.104 \quad (4.26)$$

Selecting  $R_1 = 6.8 \text{ k}\Omega$ ,  $R_2$  is computed as:

$$R_2 = \frac{\beta}{1 - \beta} R_1 = 789 \text{ }\Omega \quad (4.27)$$

The constant  $\beta$  is multiplied and divided in the control law as:

$$u_{eq} = \frac{\beta V_c}{\beta V_{Pr}} = \frac{V_c^*}{V_{Pr}^*} \quad (4.28)$$

where

$$V_c^* = \beta V_d - \beta V_{in} - \beta L \frac{k_1}{k_2} (I_{ref} - I_L) \quad (4.29)$$

and peak of ramp signal becomes:

$$V_{Pr}^* = \beta V_d \quad (4.30)$$

To use TL431 and limit the maximum duty cycle, gain of two is applied to both  $V_{Pr}$  and  $V_c^*$ . This gain has no effect on control law as same constant is multiplied in numerator and denominator. The control law becomes:

$$u_{eq} = d = \frac{2 \times V_c^*}{2 \times V_{Pr}^*} \quad (4.31)$$

### 4.3 Hardware Description

The boost converter used in the experiments has filter capacitance,  $C = 2000 \text{ }\mu\text{F}$ , and inductor coil having  $L = 100 \text{ }\mu\text{H}$ . A metal oxide field effect transistor (MOS-FET), IRF540 is used as power electronic switch. It's on resistance is  $0.06 \text{ }\Omega$

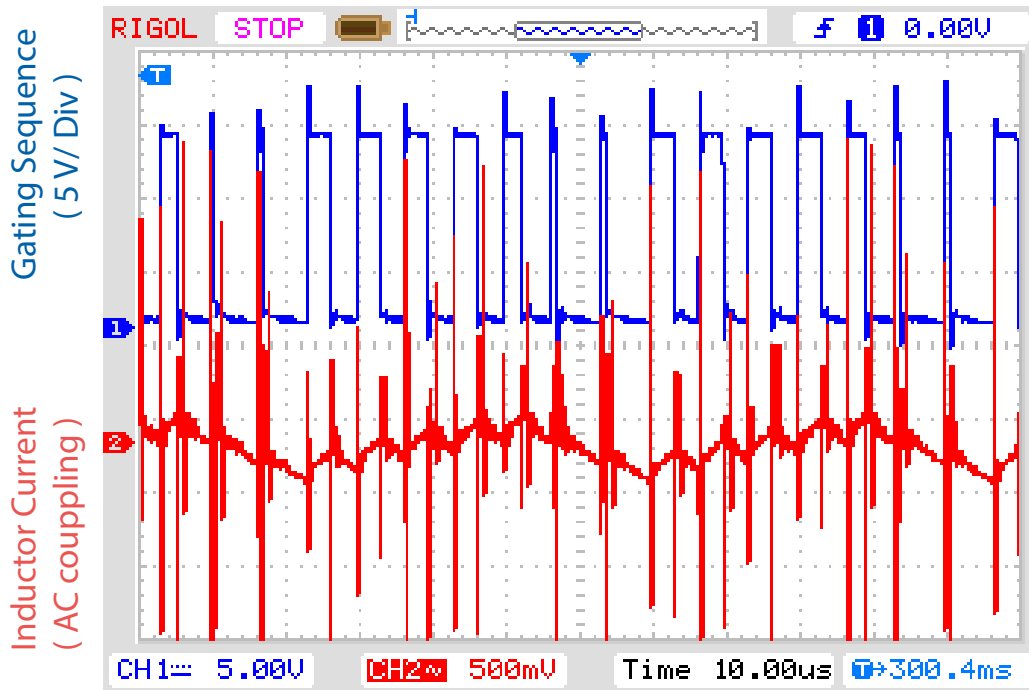


FIGURE 4.4: The CH. 1 shows chattering along with low frequency oscillations for  $R_x = 10\text{ k}\Omega$  while CH. 2 shows the generated gating sequence as a consequence of improper selection of  $R_x$ .

and can sustain a continuous drain current of 20 A. The selected switching frequency for fixed frequency SMC is 32 kHz. The selection of switching frequency is a compromise between switching losses and maximum allowable amplitude of chattering (ripples in the output). The efficiency of the converter also decreases with increasing switching frequency because of increase in switching losses. The designed converter has an efficiency of 92%. Experiments reveal that for proper switching of the MOSFET, the resistance seen at the drain of the device shall be less than  $47\ \Omega$ , so that the body diode capacitance of the device can be easily discharged. If this issue is not taken care off, then it may take significantly high time for the MOSFET to turn off. To ensure discharge of gate capacitance a resistor of  $47\text{ k}\Omega$  is placed between gate and source of the device. Adjustable shunt type voltage regulator TL431 is used to generate reference signal of 2.5 V. It is important to mention that experimentally some tuning of the reference signal may be required. The inductor current is measured by placing a resistor  $R_{Me} = 0.47\ \Omega$ , in the return path of  $I_L$ . By Ohm's law  $I_L = V_{Me}/R_{Me} = 2.1V_{Me}$ . Thus the voltage  $V_{Me}$  is amplified by a gain of 2.1, before being fed to the controller circuitry.

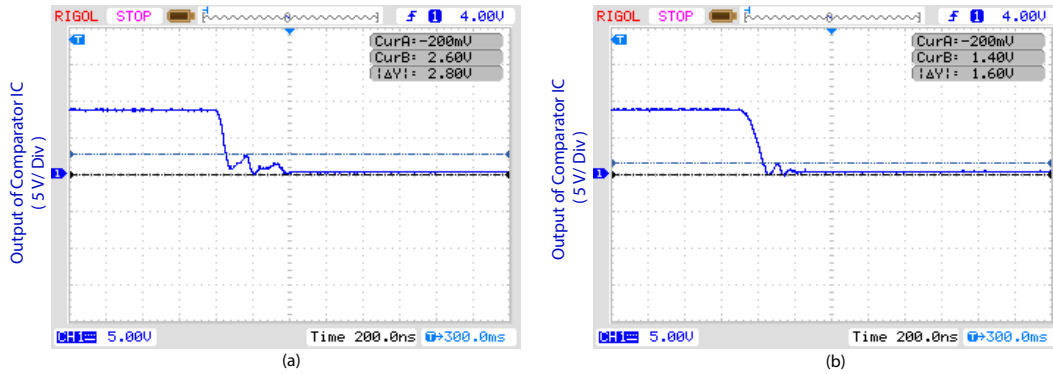


FIGURE 4.5: Output of comparator IC LM311 showing oscillations at crossover  
 (a) For  $R_x = 1 \text{ k}\Omega$  and  $V_{cc} = 9 \text{ V}$  (b) For  $R_x = 333 \Omega$  and  $V_{cc} = 9 \text{ V}$ .

TABLE 4.1: Voltage regulation at different input source voltages.

Reading No.	Input source voltage	Output Voltage
1	11.5	24.0
2	13.0	24.0
3	14.5	24.0
4	16.0	24.0
5	17.5	24.0

## 4.4 Experimental Setup and Results

The experiments are performed using Rigol oscilloscope having two channels of 70 MHz bandwidth. The maximum sampling rate is 1G samples/sec. To record the controller behavior under varying input voltages, Matrix precision supplies accurate to 0.1 decimal place are used. The op-amps are powered with  $\pm 15 \text{ V}$  using same power supplies. The steady state behavior is measured with oscilloscope settings of 10 V/div. It is worth mentioning that at 5 V/div and 10 V/div settings, the oscilloscope has an accuracy to one decimal place. Thus any voltage above 23.95 V will be rounded off to 24.0 V indicating that the steady state error is less than  $\pm 0.2\%$ .

### 4.4.1 Pulse Width Modulation Circuit

PWM signal is generated using IC (LM311) that compares  $V_c$  with a ramp signal having peak amplitude of  $V_{Pr}$ . This comparator IC (LM311) has an advantage



of isolated common mode input. The design engineer has a liberty to refer the output of the comparator to ground or  $V_{cc}$ . Referring the output of the IC to ground inverts the output signal with respect to input signal. However, it is important to mention that the rise time of the output pulse depends upon the resistor  $R_x$  in Fig. 4.3. For large values of  $R_x$ , the rise time of the output pulse is significantly high and it takes large time to reach 1.75 V which is logic 1 for MOSFET gate driver MC34152. This causes a significant delay in the switching command to MOSFET. For example with  $R_x = 10\text{ k}\Omega$  and frequency of ramp signal  $f_s = 150\text{ kHz}$ , the duty ratio can not exceed 42% even when  $V_{out} = 0$  (feedback signal disconnected). This is a non-linear behavior which is introduced because of high rise time of the comparator when  $R_x$  is not properly selected. In this case the comparator IC fails to generate a duty ratio equal to  $(V_c/V_{Pr})$ . As a result a false duty cycle is generated that increases  $I_L$  in each switching cycle, causing  $V_{out}$  to increase. The controller generates lower  $V_c$  to control the output voltage drift but because of above mentioned non-linearity, the duty cycle does not change accordingly. Finally the output increases to a level where the controller makes the duty ratio significantly small resulting in decreasing the inductor current in successive cycles. This results in low frequency oscillations in the output voltage other than chattering (ripples in power electronic literature). These low frequency oscillations along with the gating signal are shown in Fig. 4.4. It shall be noticed that this non-linearity is a type of actuator saturation and belongs to a class of unmatched disturbances and can not be canceled by SMC. Thus it is important to eliminate them in proper hardware design. For mid range values of  $R_x$  the output of comparator may oscillate at crossing points as shown in Fig. 4.5(a). This may occur when one of the inputs is a ramp signal or the source resistance generating input signal is high. The problem is solved by adding a small hysteresis band using positive feedback or by lowering both  $R_x$  and the supply voltage of LM311. Lowering  $R_x$  and the supply voltage of LM311 also lowers the peak of oscillations at crossover to be less than 1.75 V and hence MC34152 will not get false trigger

as shown in Fig. 4.5(b).

#### 4.4.2 Step Response of the Closed Loop System

The performance of the controller is tested at different load conditions. The input voltage of the converter is switched at 400 mHz to obtain step response of the system. The switching action is accomplished by TIP147, a PNP power transistor, that connects and disconnects  $V_{in}$  according to a 400 mHz square wave. The complete response of the closed loop system is shown in Fig. 4.7. The controller maintains 24 V for different load condition ( $18 \Omega \leq R_L \leq 100 \Omega$ ) and the output is shown in Fig. 4.6. The steady state error of the controller is zero because of the presence of an integrator in the outer voltage control loop. The output ripple during steady state operation is shown in Fig. 4.8. The inductor current at steady state is shown in Fig. 4.9. Fig. 4.8 and Fig. 4.9 shows the gating signal at the output of comparator IC LM311 and MOSFET driver MC34152 respectively. The major advantage of MC34152 is its high slew rate that reduces switching losses.

#### 4.4.3 Robustness to Load and Line Variations

To verify the robustness of the controller and note its behavior under changing load conditions, a setup is designed to switch load resistance from  $82 \Omega$  to  $29.87 \Omega$ . This is accomplished by switching a  $82 \Omega$  resistor in parallel to the existing  $47 \Omega$  load. A power transistor TIP147 driven by C1383 is used to switch this additional load at a frequency of 10 kHz. Fig. 4.11 shows the output of the converter when the load is changed from  $82 \Omega$  to  $29.87 \Omega$ . The system recovers from the step load change in less than  $250 \mu s$ . This demonstrates excellent disturbance rejection performance of the controller which is the key feature of SMC. Moreover, the performance of the controller under variable input voltages is also tested and the observations are presented in Table 4.1.

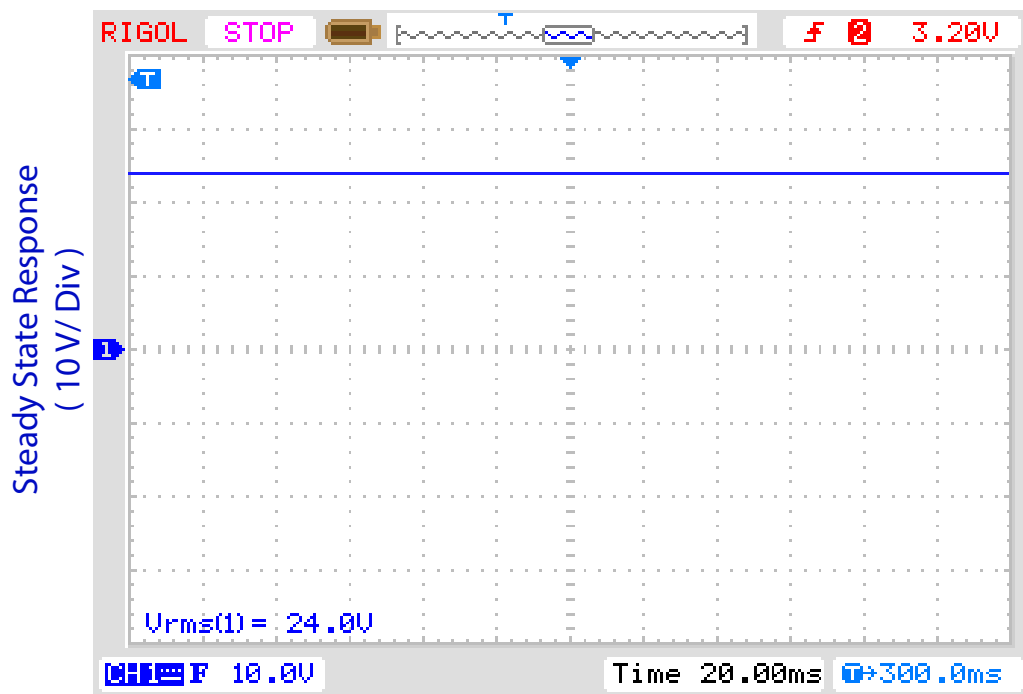


FIGURE 4.6: Steady state response of the closed loop system.

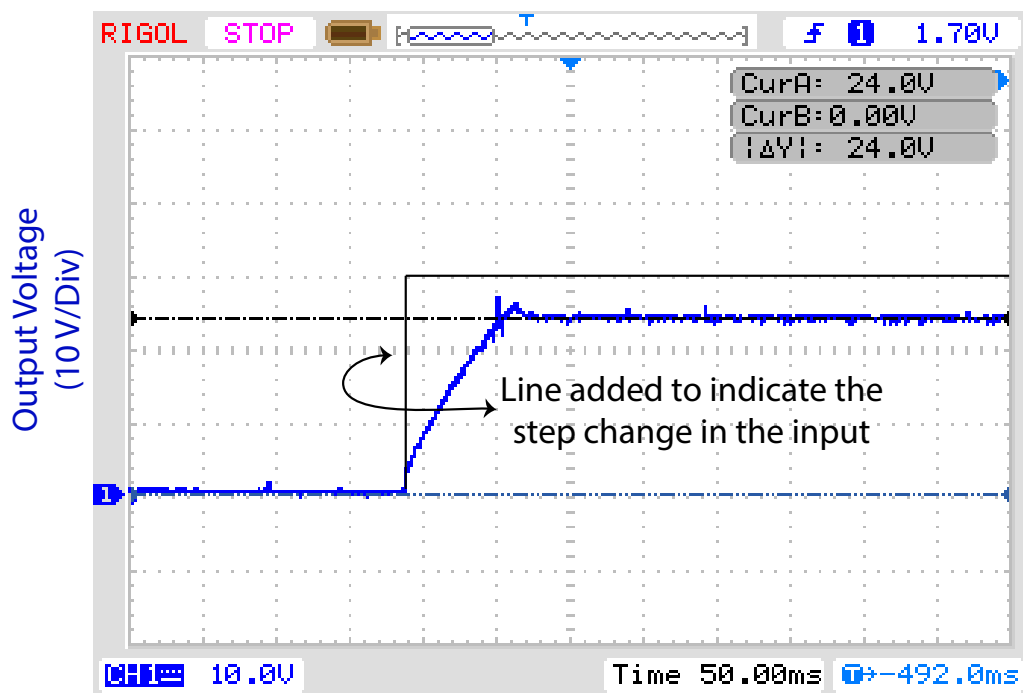


FIGURE 4.7: Complete response of the system with step change in input voltage from 0 V to  $V_{in}$ .

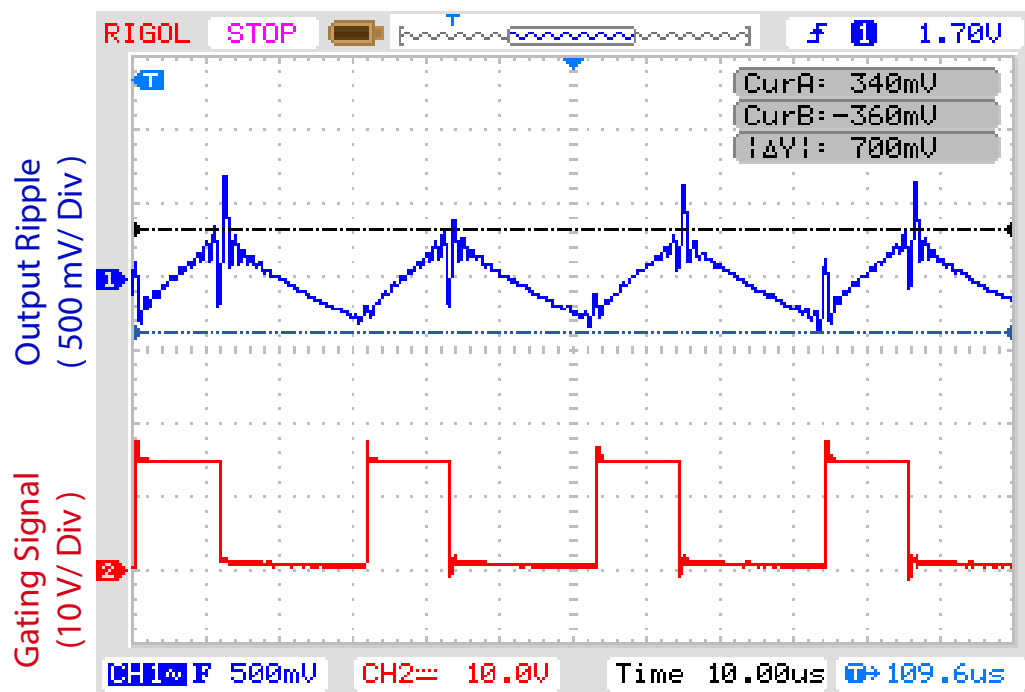


FIGURE 4.8: The CH. 1 shows the ripple/chattering in the output voltage at  $82\ \Omega$  load resistor while CH. 2 shows the gating signal at the output of MC34152.

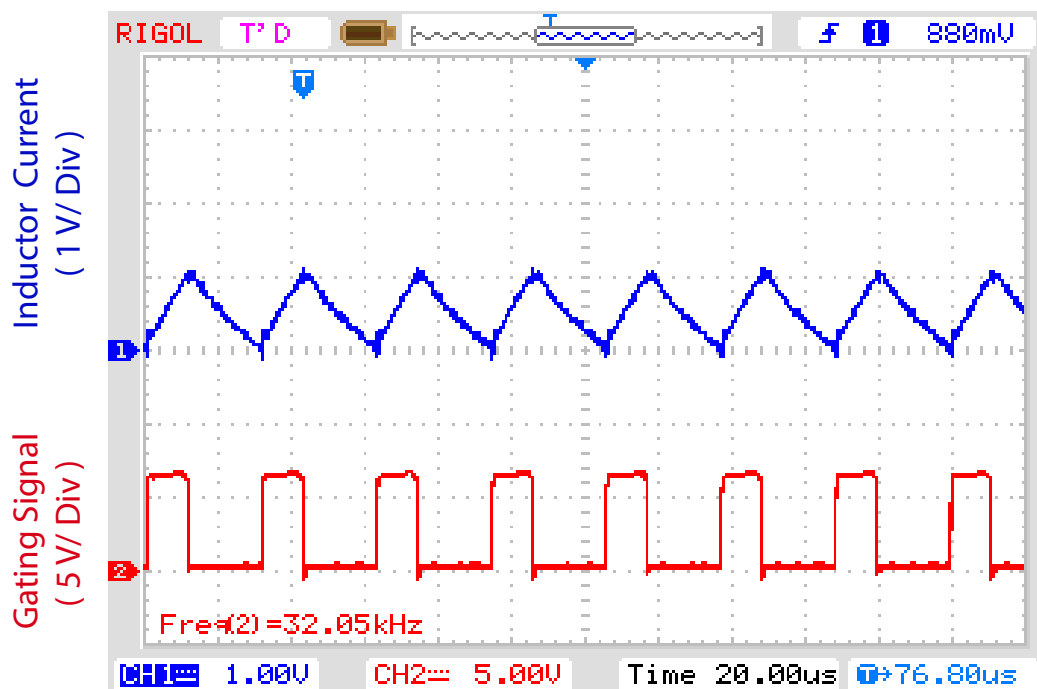


FIGURE 4.9: The CH. 1 shows the inductor current at steady state when operating at  $82\ \Omega$  load resistor while CH. 2 shows the gating signal observed at the output of LM311.

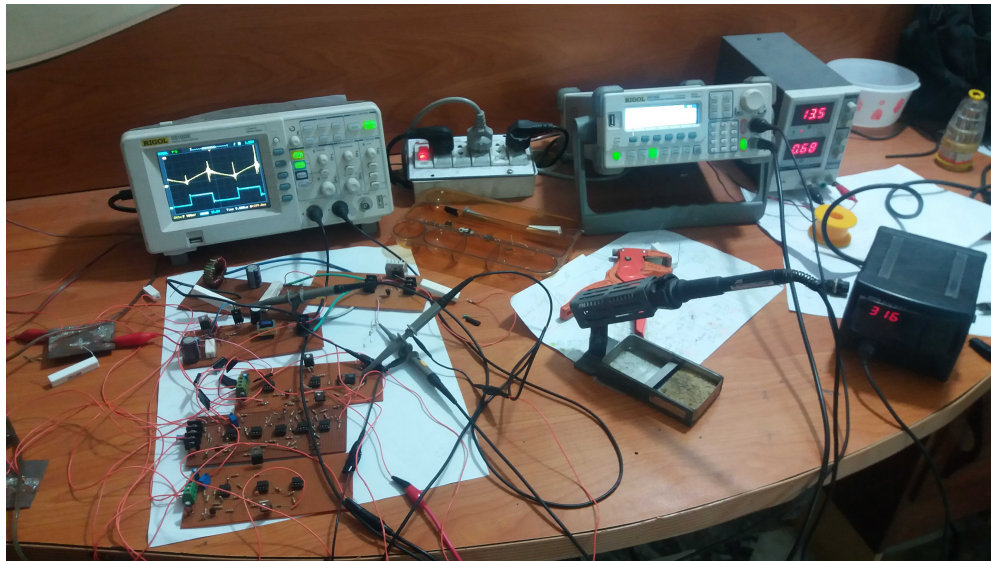
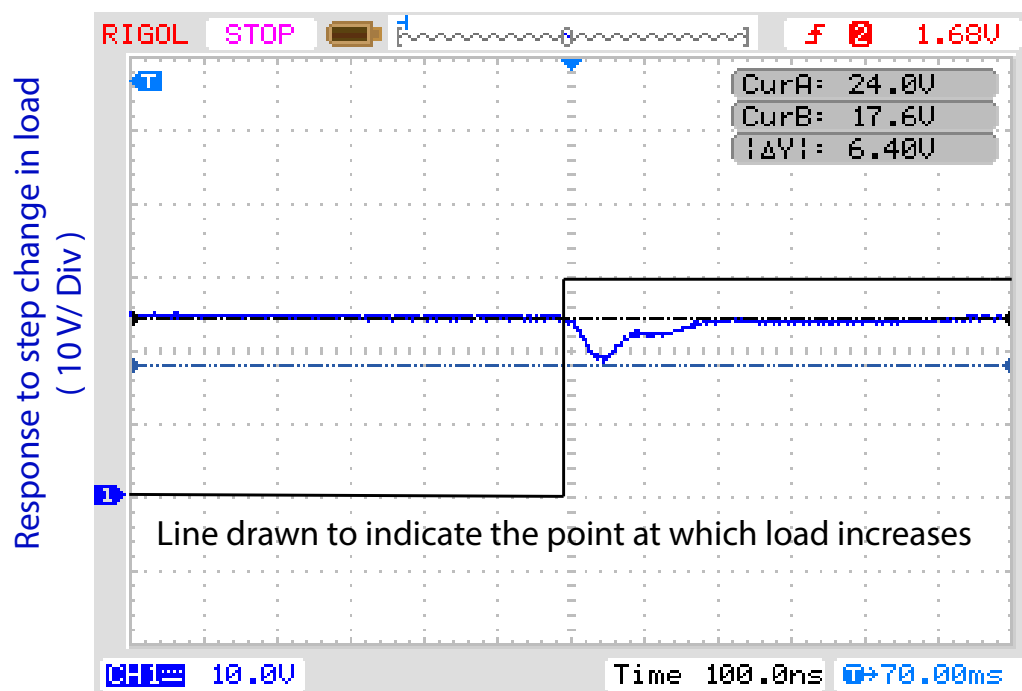


FIGURE 4.10: Hardware setup for the closed loop system.

FIGURE 4.11: Response of the system to step change in load from  $82\ \Omega$  to  $29.83\ \Omega$

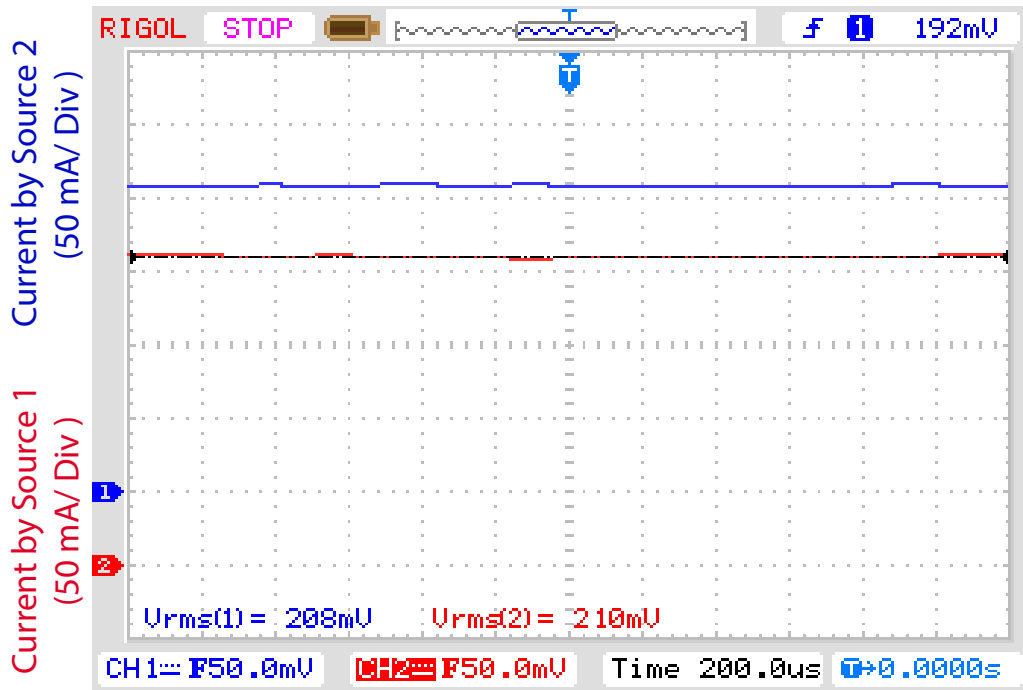


FIGURE 4.12: Current sharing of the two sources using proposed controller.

#### 4.4.4 Grid Operation

The ability of the technique to control a DC micro-grid is evaluated on a scaled down micro-grid having two sources and a single load as shown in Fig. 4.2. An outer control loop provides reference current signal for both the sources operated by the proposed controller. Fig. 4.12 shows the currents of each source while feeding a load of  $56 \Omega$ . The current delivered by Source 1 is 208 mA, while Source 2 contributes current of 210 mA. The proposed technique maintains the desired grid voltage with load sharing error of less than 1%. Fig. 4.10 shows the complete hardware setup for the closed loop system. Due to the fixed switching frequency of the proposed technique, harmonic cancellation of chattering is possible. Chattering is reduced in the proposed technique by adjusting the phase of two switching sequences such that the harmonics present in chattering signal of Source 1 are canceled by the harmonic contents in chattering signal of Source 2. Fig. 4.13(a) shows the chattering due to single source having peak-peak amplitude of 180 mV with RMS value of 59.3 mV. A significant reduction in chattering is observed when the phase of the switching sequence of Source 2 is adjusted to cancel the harmonic contents of chattering due to Source 1. Fig 4.13(b) shows that the RMS value of

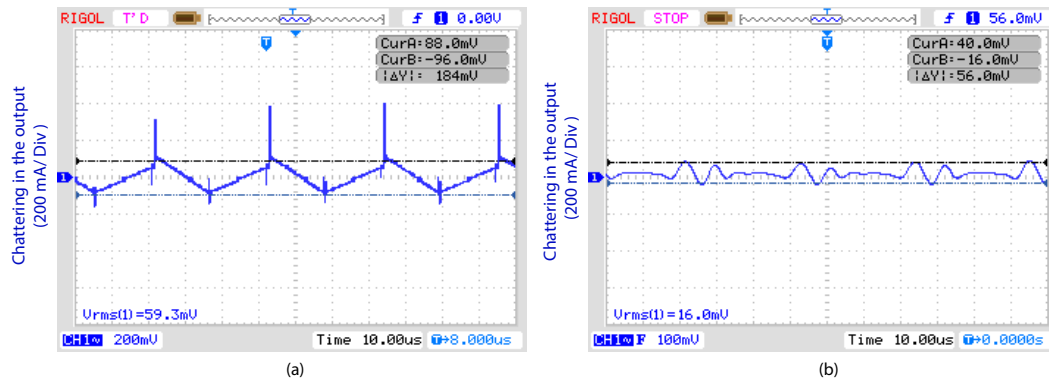


FIGURE 4.13: Harmonic cancellation of chattering in the output (a) Chattering due to single source. (b) Chattering in the output when the harmonics in chattering signal of Source 2 cancels the harmonics from Source 1.

chattering falls to 16 mV only, while its peak-peak amplitude is reduced to only 56 mV.

## 4.5 Summary

The voltage control of DC bus bar in micro-grids under uncertain load conditions is addressed. The experimental results show that the proposed technique is robust against input voltage variations and load changes, while maintaining fixed switching frequency. The chapter discusses the circuit design and component selection in detail. The results show the good performance of the closed loop system based on renewable energy resources. Furthermore, the technique is demonstrated on a scaled down micro-grid with two sources. Improvement of power quality by harmonic cancellation of chattering is demonstrated in the hardware.

# Chapter 5

## A Novel Filter Extracted Equivalent Control Based SMC

### 5.1 Introduction

Disturbance rejection, order reduction and capability to handle systems with unmodeled dynamics are the key properties of SMC that make it a good choice to control non-linear systems with perturbations. The system under SMC becomes invariant to parametric changes and its performance is completely robust against matched disturbances [19–21]. Due to these properties, SMC finds a wide range of applications in motor control, power electronics, robotics, micro-grids and automotive control [104, 124–129]. Moreover the complexity of feedback control design is reduced by SMC because it decouples the system into reduced order dynamics [102].

### 5.2 Issue in SMC Implementation

The SMC is ideally implemented using a discontinuous function that operates the switch at infinite frequency. Thus, forcing the state trajectories to slide along the designed manifold towards the origin. However, it is not possible to achieve



infinite switching frequency in physical systems. The first realistic approach towards SMC implementation is presented in [26], where the discontinuous *sign* function is replaced by a hysteresis comparator which is tuned to limit the maximum switching frequency according to the physical limits of the system. The scheme results in finite, but time varying switching frequency [27]. As a result, finite magnitude oscillations, known as chattering, appear in the output of the system [28]. The chattering is acceptable within limits for a particular system. However, the problem of variable switching frequency becomes a serious issue for electronic converters. They need a fixed frequency operation [29–31] because they consist of passive energy storing components (inductors and capacitors) and their correct size primarily depend upon the switching frequency. Moreover, the varying switching frequency degrades the power quality and makes it non-trivial to suppress electromagnetic interference (EMI) [32].

### 5.3 Fixed Frequency SMC

The researchers have proposed different methods to address the above mentioned problem by fixing the switching frequency in SMC. A method using a comparator with adaptive hysteresis band is proposed in [130–132]. This method varies the hysteresis band such that the switching frequency remains fixed. This adaptation requires knowledge of the system states and consequently needs additional sensors and state observers that increase the implementation cost and complexity.

The schemes in [133–136] use an additional PI control loop that adjusts the width of the hysteresis band in order to achieve fixed switching frequency. This design requires the dynamics of the Frequency Control Loop (FCL) to be much slower as compared to the dynamics of the voltage and current control loops, as the faster dynamics may cause interaction with the outer control loops [133, 134], hence the stability of the linearized system may not be ensured in this scenario [135, 136]. In [137], the authors have proposed a FCL that monitors the time period of each switching cycle and compares it with a reference switching period. The difference

in switching period is fed to a frequency regulation controller that updates the values of hysteresis band accordingly. The common drawback of these schemes is the addition of another control loop that increases the cost and complexity of the design.

The techniques presented in [138, 139] demonstrates the use of external signal to enforce constant switching frequency in SMC. The scheme shows good results when the switching frequency is kept low as compared to the time constant of the system. However, if the frequency is increased, the system states drift away causing a steady state error.

In [140], Zero Average Dynamics (ZAD) method is used to achieve fixed switching frequency and is practically demonstrated in [141]. The scheme works by computing a duty ratio that ensures a zero T-periodic mean of the switching function. As a result the switching frequency is fixed during the steady state operation and the closed loop behavior of the system is near to ideal SMC. However, complex calculations and requirement of fast processor are major drawbacks of this scheme.

Fixed switching frequency in SMC using pulse width modulation (PWM) is reported in [35, 142]. The authors have smoothened the control law within a boundary layer. In this boundary the discontinuous function is replaced by a smooth linear function which is PWM implemented to achieve fixed switching frequency. The drawback of this technique is that it sacrifices the disturbance rejection performance in this boundary layer. The fixed switching frequency using PWM is also reported in [123, 143–147]. However in this work the ideal equivalent control signal, computed from the measured system states, is PWM modulated. The scheme is named as PWM-SMC. In [148, 149] a bandwidth based parameter selection of the sliding surface is proposed for PWM-SMC. It is important to emphasize that in PWM-SMC, the ideal equivalent control does not evolve from a discontinuous function, rather it is computed from the measured states of the system, which may result in degrading the of inherent properties of SMC like order reduction and disturbance rejection [4, 137]. Another disadvantage of this scheme is the

requirement of larger number of components as compared to hysteresis modulation based SMC. It is important to mention that the actual equivalent control of the system can be extracted from the discontinuous control and its first evidence is found in [150], where chattering reduction is achieved by tuning the gain of the discontinuous function according to the Filter Extracted Equivalent Control (FEEC). The scheme achieves reduction in chattering amplitudes, however the switching frequency of the system is not fixed.

Hence, it may be concluded that the existing techniques for fixing frequency in SMC are either too complex or they compromise one or the other properties of SMC. Consequently, there is a need for a comprehensive, fixed frequency SMC design which is low cost, simple to implement using commercially available integrated circuits (ICs) and also retains the inherent properties of SMC.

In this chapter of the thesis a novel method for fixing the switching frequency in SMC is proposed. The actual equivalent control of the system is extracted from the discontinuous function by means of a low pass filter and is used to achieve fixed frequency SMC which to the best of authors' knowledge, has not been previously reported. The technique is implemented on a boost converter and the results are compared with existing PWM-SMC having a double integral type sliding surface. The experimental results demonstrate that the proposed technique achieves zero steady state error with improved dynamic response, and also exhibits better disturbance rejection properties as compared to PWM-SMC.

## 5.4 Proposed Technique

The proposed technique is demonstrated on a boost type DC-DC converter. Conventionally, the two state variables are the inductor current  $I_L$  and the output voltage  $V_{out}$ . Using circuit analysis techniques in Fig. 5.1, the mathematical model

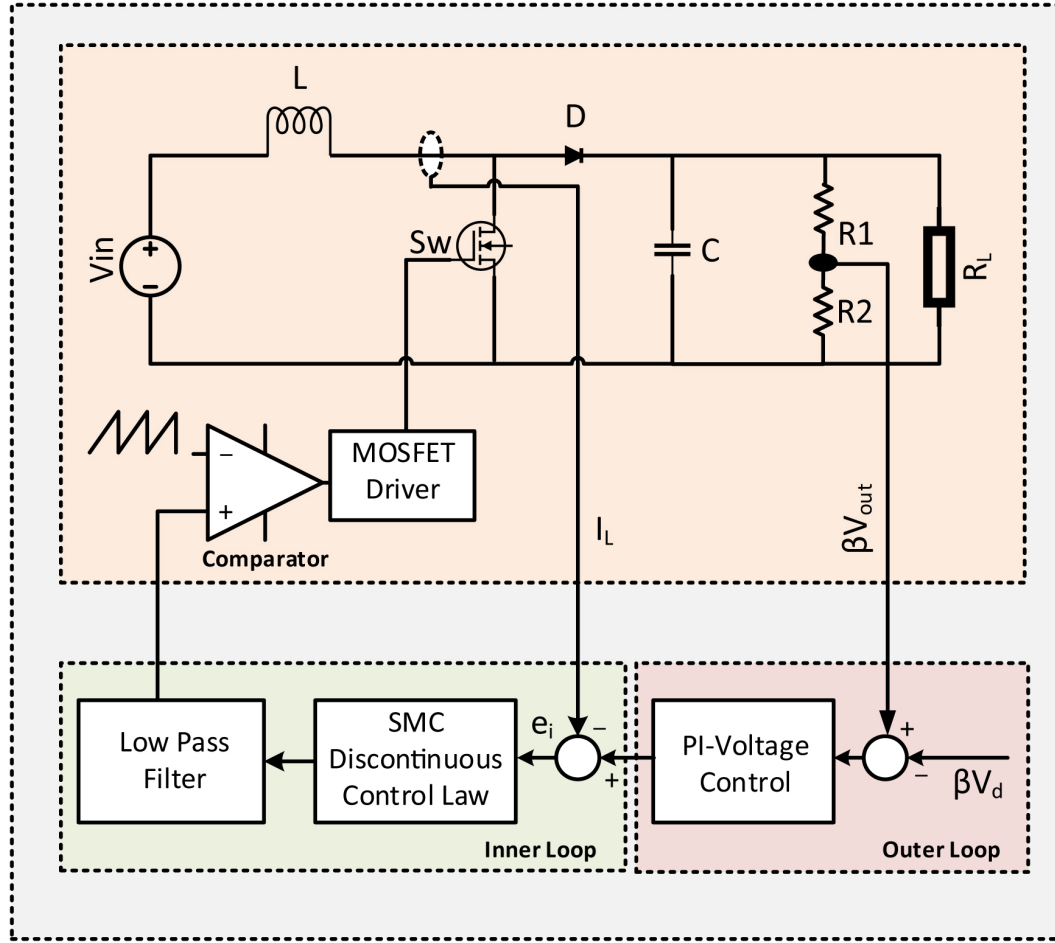


FIGURE 5.1: Block digram of the proposed filter extracted equivalent control based sliding mode control (FEEC-SMC) for voltage regulation in boost converter.

of the converter is derived as:

$$\begin{aligned} \dot{I}_L &= -\tilde{u} \frac{1}{L} V_{out} + \frac{V_{in}}{L} \\ \dot{V}_{out} &= \tilde{u} \frac{1}{C} I_L - \frac{V_{out}}{R_L C} \end{aligned} \quad (5.1)$$

where  $V_{in}$  is the input voltage of the converter. The control input is denoted by  $u$  while  $\tilde{u} = (1 - u)$ . The inductance ( $\mu H$ ), capacitance ( $\mu F$ ) and load resistance ( $\Omega$ ) are denoted by  $L$ ,  $C$ ,  $R_L$ . The power electronic converters are designed to operate as a switch and can be either ON or OFF. Therefore, the input signal of the converter is discrete in nature and mathematically  $u \in \{0, 1\}$ .

The boost converters exhibit a non-minimum phase nature [114] which makes it

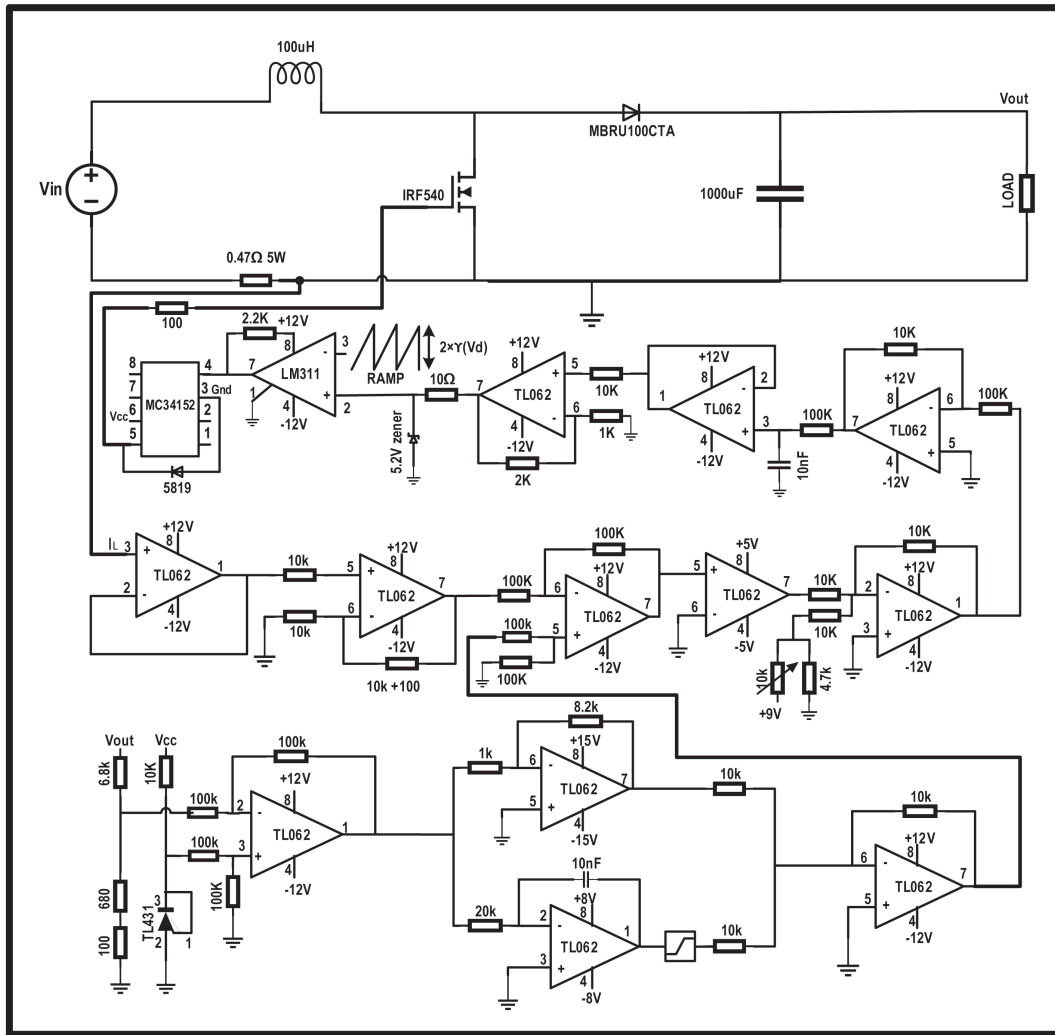


FIGURE 5.2: Complete circuit diagram of the proposed FECC-SMC.

more difficult to control as compared to other converters. The system becomes unstable if the feedback is designed based upon output voltage only.[116]. However, the problem is solved by a cascade control scheme, where a two loop based structure is designed to control the inductor current and output voltage. This is an application of singular perturbation theory that can be applied where the motion rate of inner loop is much faster as compared to the outer loop [117, 118]. The outer loop for voltage control is implemented using PI controller. Defining the error voltage  $e_v$  as:

$$e_v = V_{ref} - V_{out} \quad (5.2)$$

where  $V_{ref}$  and  $V_{out}$  are the reference and output voltages respectively. A PI controller for the outer loop is designed as:

$$i_{ref}^* = K_p e_v + K_i \int_0^t e_v dt \quad (5.3)$$

where  $K_p$  and  $K_i$  are the proportional and integral gains respectively while  $i_{ref}^*$  is the reference current for the inner current loop. If a feed forward reference current  $i_{fd}$  is also considered in (5.3), then the reference current  $I_{ref}$  is written as:

$$I_{ref} = i_{fd} + i_{ref}^* \quad (5.4)$$

The equilibrium points of the system are obtained by setting the time derivatives in (5.1) to zero. Hence we get,

$$V_{out} = V_d \quad (5.5)$$

$$I_{Leq} = \frac{V_d^2}{R_L V_{in}} \quad (5.6)$$

where  $V_d$  and  $I_{Leq}$  are the desired capacitor voltage and the inductor current at the equilibrium.

The sliding surface  $\sigma$  for the inner current loop is designed on the basis of current error as:

$$\sigma = I_{ref} - I_L \quad (5.7)$$

The control law that enforces  $I_L$  to track  $I_{ref}$  is defined as:

$$u = \frac{1}{2}(1 + \text{sign}(\sigma)) \quad (5.8)$$

The stability of the system can be ensured by applying the convergence condition  $\sigma \dot{\sigma} < 0$ . By using the dynamics of the system from (5.1) we get:

$$\dot{\sigma} = \tilde{u} \frac{1}{L} V_{out} - \frac{V_{in}}{L} \quad (5.9)$$

The condition  $\sigma\dot{\sigma} < 0$  is satisfied if:

$$\|V_{out}\| > \|V_{in}\| \quad (5.10)$$

Stability condition in terms of the equivalent control  $u_{eq}$  can be written as:

$$0 < u_{eq} = 1 - \frac{V_{in}}{V_{out}} < 1 \quad (5.11)$$

Analysis of (5.10) shows that  $V_{out}$  shall be greater than  $V_{in}$ , in order to ensure the stable operation of the converter. It is important to note that when a physical converter is initially turned on, its output voltage  $V_{out}$  may be less than  $V_{in}$ . Practically this problem can be worked out by operating the system in an open loop manner and finally plugging in the controller when  $V_{out} > V_{in}$ . For PWM based control, the problem can be solved by using a voltage limiter circuit that keeps the control signal  $V_c$  less than the peak amplitude of the modulating ramp signal. This ensures the stable switching operation until  $V_{out} > V_{in}$ . This study also uses a voltage limiter circuit which is easily realized by using a zener diode.

Ideally, SMC operates the switch at infinite frequency but however, due to physical constraints the system needs to operate at finite frequency. This causes the state to oscillate within a boundary layer of width  $\Delta$  close to the sliding manifold  $\sigma = 0$ . These oscillations consist of two components. The low frequency component coincides with equivalent control of the system and can be obtained from the actual discontinuous control by means of a low pass filter [21]. The time constant of the low pass filter shall be selected such that the low frequency component passes without any distortion while the high frequency component is removed. In this research a first order low pass filter having time constant  $\tau = R_{fl}C_{fl}$ , where  $R_{fl}$  is the resistance and  $C_{fl}$  is the capacitance of the filter used. The mathematical relationship between the discontinuous control input  $u$  and the output of the filter  $y(t)$  is obtained using Kirchhoff's voltage law as:

$$u = R_{fl}i(t) + y(t)$$

using the dynamics of first order low pass filter we get:

$$u = R_{fl}C_{fl}\frac{d}{dt}y(t) + y(t)$$

and finally we can get:

$$u = \tau\frac{d}{dt}y(t) + y(t) \quad (5.12)$$

where  $i(t)$  is the instantaneous current through the filter capacitor. It is shown in [21, 151] that the output of this filter gives  $u_{eq}$  under following ideal condition:

$$\lim_{\tau \rightarrow 0, f \rightarrow \infty} y(t) = u_{eq} \quad (5.13)$$

where  $f$  is the switching frequency. As  $f$  increases, the motion of the states becomes more near to ideal SMC and the width  $\Delta$  in which the states oscillates, approach zero. Hence as  $f \rightarrow \infty$ ,  $\Delta \rightarrow 0$ . The necessary condition to filter out the high frequency component and extract  $u_{eq}$  is that the switching frequency must be much higher than  $1/\tau$  or equivalently:

$$\frac{1}{f} \ll \tau \quad (5.14)$$

It is important to note that the FEEC contains information regarding the parameter changes and disturbances acting upon the system. The equivalent control under SMC coincides with the duty ratio of PWM converters [120, 152], establishing the relationship  $u_{eq} = d$  which provides the basic theoretical background for development of PWM based SM-controllers. Once the  $u_{eq}$  is extracted, the control signal  $V_c$  for PWM implementation is derived as:

$$u_{eq} = d = \frac{V_c}{V_{ramp}} \quad (5.15)$$

where  $V_{ramp}$  is the peak voltage of modulating ramp signal. The switching sequence provided by PWM according to (5.15) results in a fixed frequency operation of the



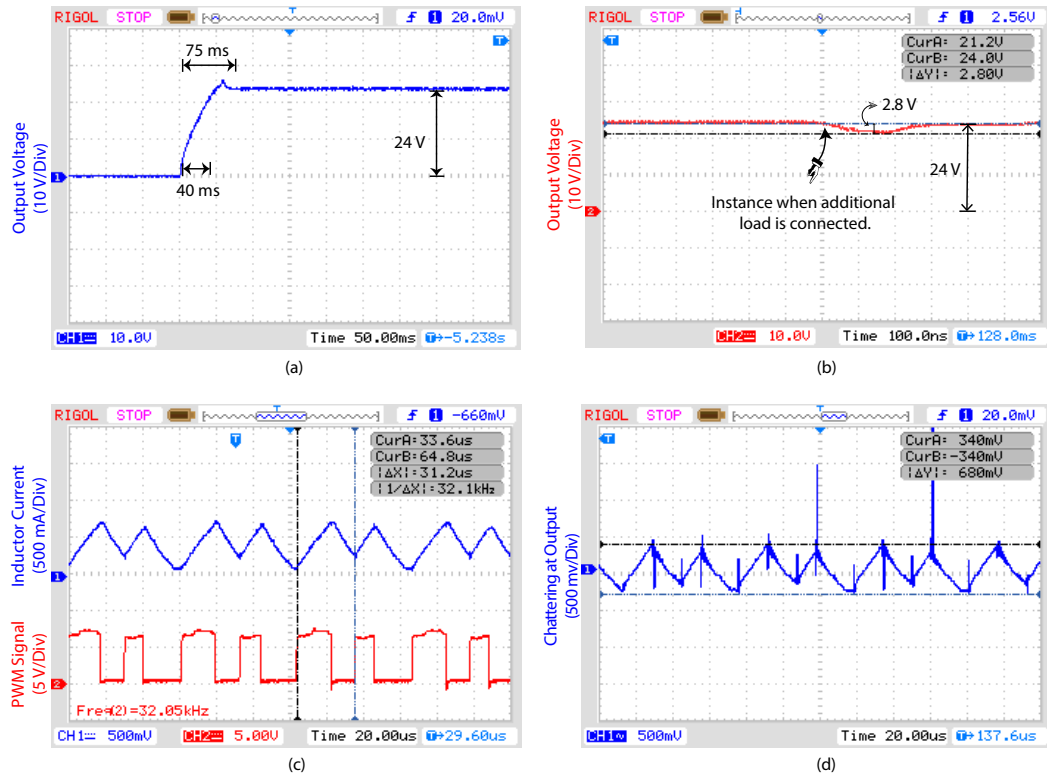


FIGURE 5.3: Experimental waveforms of the closed loop system with PWM-SMC. (a) Step response of the closed loop system. (b) Output voltage when load is shifted from 82  $\Omega$  to 29.88  $\Omega$  (c) Inductor current and gating signal at output of LM311 during steady state operation. (d) Chattering in the output voltage.

SM-controller.

## 5.5 PWM-SMC with Double Integral Type Sliding Surface

For bench marking purpose, PWM-SMC is implemented and for the sake of completeness and better understanding, its design is also presented. In order to ensure best performance, a double integral type sliding surface is chosen [119, 123]. The sliding manifold  $\sigma$  is defined as:

$$\sigma = c_1 \int \int e_i(t) dt dt + c_2 \int e_i(t) dt + c_3 e_i(t) \quad (5.16)$$

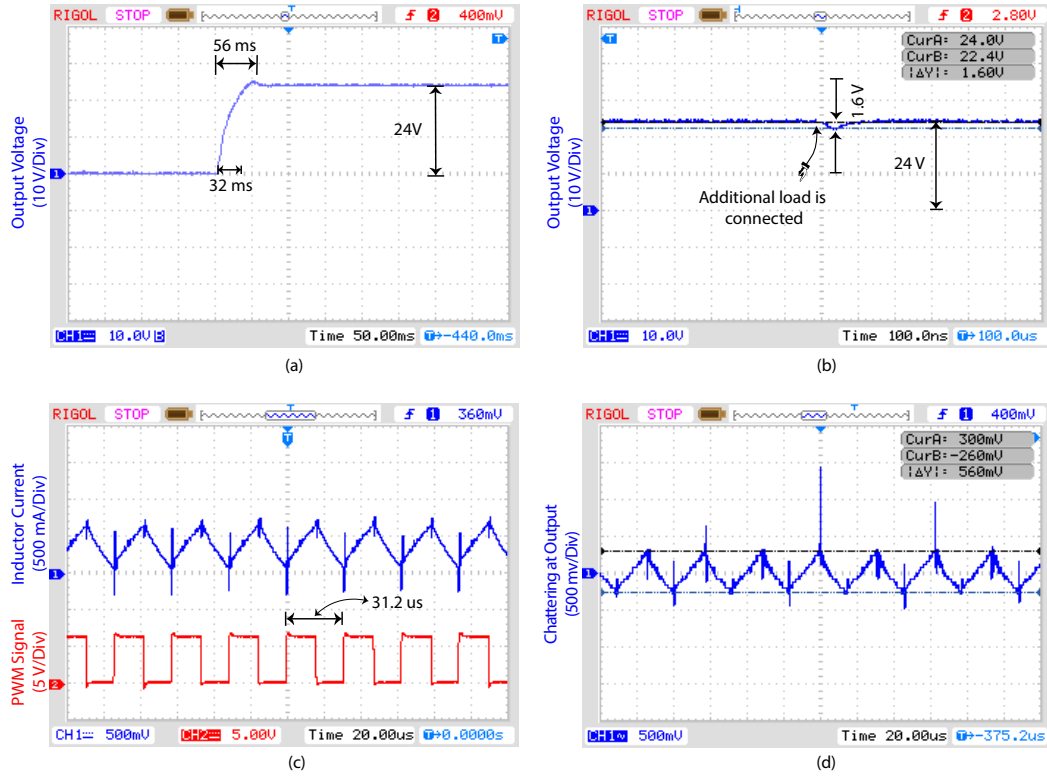


FIGURE 5.4: Experimental waveforms of the closed loop system with FECC-SMC. (a) Step response of the closed loop system. (b) Output voltage when load is shifted from  $82 \Omega$  to  $29.88 \Omega$  indicating robustness of the closed loop system. (c) Inductor current and gating signal at output of LM311 during steady state operation. (d) Chattering in the output voltage.

where  $e_i(t) = (I_{ref} - I_L)$ . Mathematically the ideal equivalent control signal  $u_{eq(ide)}$  for PWM-SMC is derived by putting  $\dot{\sigma} = 0$ . Thus we get:

$$\dot{\sigma} = c_3 \dot{e}_i(t) + c_2 e_i(t) + c_1 \int e_i(t) dt = 0 \quad (5.17)$$

Using (5.1) and (5.17) we get:

$$\tilde{u}_{eq(ide)} = \frac{V_{in}}{V_{out}} - L \frac{c_2}{c_3} \frac{e_i(t)}{V_{out}} - L \frac{c_1}{c_3} \frac{\int e_i(t) dt}{V_{out}}$$

By using definition  $\tilde{u} = (1 - u)$  we get:

$$u_{eq(ide)} = \left(1 - \frac{V_{in}}{V_{out}}\right) + L \frac{c_2}{c_3} \frac{(I_{ref} - I_L)}{V_{out}} + L \frac{c_1}{c_3} \frac{\int (I_{ref} - I_L) dt}{V_{out}} \quad (5.18)$$

Choosing  $V_{ramp} = V_{out}$  we derive  $V_c$  as:

$$\begin{aligned} V_c &= (V_{out} - V_{in}) + L \frac{c_2}{c_3} (I_{ref} - I_L) \\ &+ L \frac{c_1}{c_3} \int (I_{ref} - I_L) dt \end{aligned} \quad (5.19)$$

while

$$V_{ramp} = V_{out}$$

It is important to note that the magnitude of the ramp signal needs to be adaptively changed with respect to  $V_{out}$ . This makes this technique robust to input voltage variations as compared to conventional PID controllers [153]. However, this adaptive nature of  $V_{ramp}$  adds complexity to the design and causes over modulation of PWM signal during start up. Additional circuitry is required to prevent this over modulation. A salient feature of the proposed FECC-SMC is that it achieves robustness against input voltage variations without requiring adaptive control of the ramp signal.

### 5.5.1 Stability of Inner Loop

Sliding mode can only exist on manifold  $\sigma = 0$  if the following constraint is satisfied.

$$\lim_{\sigma \rightarrow 0} \sigma \dot{\sigma} < 0 \quad (5.20)$$

Using (5.1) and (5.16) we get:

$$\dot{\sigma} = c_1 \int e_i(t) dt + c_2 e_i(t) + c_3 \left( \frac{V_{out}}{L} \tilde{u} - \frac{V_{in}}{L} \right) \quad (5.21)$$

The control law for the system is defined as:

$$u = \frac{1}{2} + \frac{1}{2} \text{sign}(\sigma) \quad (5.22)$$

when  $\sigma \rightarrow 0^+$  then (5.20) implies that  $\dot{\sigma} < 0$ . The control law turns  $u = 1$ . This

gives the following condition:

$$\frac{c_3}{L}V_{in} > c_1\|g_1(t)\| + c_2\|g_2(t)\| \quad (5.23)$$

where  $g_1(t) = \int e_i(t)dt$  and  $g_2(t) = e_i(t)$ . The output of both the op-amps calculating  $g_1(t)$  and  $g_2(t)$  are limited to  $\pm 5$  and  $\pm 8$ , thus mathematically:

$$\begin{aligned} \|g_1(t)\| &< 5 \\ \|g_2(t)\| &< 8 \end{aligned} \quad (5.24)$$

Now by appropriate choice of  $c_1$ ,  $c_2$  and  $c_3$  the inequality (5.23) is satisfied. When  $\sigma \rightarrow 0^-$  then the control law sets  $u = 0$  and stability is guaranteed if  $\dot{\sigma} > 0$ . By using equation (5.21) we get the following condition:

$$\frac{c_3}{L}(V_{out} - V_{in}) > c_1\|g_1(t)\| + c_2\|g_2(t)\| \quad (5.25)$$

Again by appropriate choice of design constants, (5.25) is satisfied. Finally for the sake of protection the maximum duty cycle of the PWM output is limited to 95%. TL431 cannot regulate voltages lower than 2.5 V. Hence  $V_c$  and  $V_{ramp}$  both are amplified by a gain of 2 and TL431 is adjusted to clip voltages above 4.8 V. It is important to mention that this gain of 2 has no effect on the duty ratio in this particular scenario because the same constant is multiplied in the numerator and denominator of the fraction. Thus the control law becomes:

$$d = \frac{2 \times V_c}{2 \times V_{ramp}} \quad (5.26)$$

## 5.6 Experimental Results and Discussion

The performance of the above mentioned controllers is compared on the following basis of steady state error, transient response and robustness to load variations.

TABLE 5.1: Parameters of Buck Converter

Description	Symbol	Value
Input voltage	$V_{in}$	12 V
Desired output voltage	$V_d$	24 V
Capacitance	$C$	1000 $\mu$ F
Capacitor ESR	$r_C$	21 $m\Omega$
Inductance of coil	$L$	100 $\mu$ H
Resistance of coil	$r_L$	0.18 $\Omega$
Switching frequency	$f_{SW}$	32 kHz
Load resistance	$R_L$	100 - 15 $\Omega$

### 5.6.1 Experimental Setup

The parameters of the boost converter are shown in Table 5.1 while the complete schematic of the controller is shown in Fig. 5.2. The electronic switch consists of a power MOSFET IRF540 with 0.06  $\Omega$  channel resistance with maximum current capability of 20 A. The converter is operated with switching frequency of 32 kHz. It is important to note that increasing the switching frequency also increases the switching losses whereas lower switching frequency increases the chattering amplitude. Thus there is a compromise between the two factors. The efficiency of the converter also drops with increase in the switching frequency due to increase in switching losses. The efficiency of the boost converter is measured to be 93%.

It is observed experimentally that the equivalent resistance at the drain of the MOSFET shall be small enough to timely discharge the body diode capacitance, otherwise it may take significantly large time to discharge and hence the turn off time of the device may be adversely effected. A resistor of 47 k $\Omega$  is placed between the gate and the source of the device to ensure the discharge of the gate capacitance. To measure instantaneous inductor current a resistor of 0.47  $\Omega$  is placed in the return path of the inductor current. By Ohm's law inductor current  $I_L = V_{me}/R_{me} = 2.1V_{me}$ . Hence the voltage sensed at  $R_{me}$  is amplified by a gain of 2.1 to give exact value of the inductor current. All the waveforms presented in this research are obtained using 70 MHz Rigol oscilloscope having sampling rate of 1 G samp/sec. The control circuitry is powered with 0.1 V accurate power supply.

### 5.6.2 Steady State Error

Fig. 5.3 presents the response of the boost converter with PWM-SMC. Fig. 5.4 shows the response of the proposed FEEC-SMC. Both the controllers have zero steady state error and their output voltage converges to the desired 24 V as shown in Fig. 5.3(a) and Fig. 5.4(a). It is worth mentioning that FEEC-SMC achieves zero steady state error without having any integral term in the sliding surface. This factor simplifies the design and makes the proposed technique cost effective as compared to PWM-SMC design.

### 5.6.3 Transient Response

The transient response of the system is obtained by switching the input voltage at 0.4 Hz using Rigol function generator. The output of the function generator is applied to the base of a NPN transistor C1383 which drives a PNP power transistor TIP147 so that  $V_{in}$  is connected and disconnected accordingly. The experimental results show that the rise time ( $t_r$ ) for the PWM-SMC is 40 ms and its settling time ( $t_s$ ) is 75 ms. The  $t_r$  and  $t_s$  for the closed loop system obtained using FEEC-SMC are 32 ms and 56 ms respectively. This indicates an improvement of 20% in  $t_r$  and 25.3% in  $t_s$  which is a direct consequence of the fact that the discontinuous function is directly implemented and no indirect approach is adopted to compute equivalent control.

### 5.6.4 Robustness to Load Variations

In order to establish the robustness of proposed FEEC-SMC, experiments are conducted by abruptly increasing the load resistance. A switching network is used to increase the load by connecting a resistor of 47  $\Omega$  in addition to the existing 82  $\Omega$  load. Fig. 5.3(b) shows that PWM-SMC exhibits an undershoot of 2.8 V while FEEC-SMC shows 42.86% improvement by reducing the voltage dip to 1.6



FIGURE 5.5: Experimental setup to evaluate the performance of the controllers.

V only. PWM-SMC recovers in  $250 \mu\text{s}$  while FEEC-SMC recovers in  $85 \mu\text{s}$  which shows an improvement of 66% in recovery time.

## 5.7 Summary

In this research a novel FEEC based approach is proposed to fix the switching frequency in sliding mode controllers for analogue circuits and power electronic converters. The discontinuous function inherently responsible for the robustness of the SM controller is filtered to extract the equivalent control of the system which is pulse width modulated to achieve fixed switching frequency. Conditions and constraints that apply to extract the equivalent control without distortion are highlighted. For the purpose of benchmarking, the results are compared with PWM-SMC having a double integral sliding manifold. The proposed FEEC-SMC shows better results in terms of transient response and reduces both  $t_r$  and  $t_s$  by 20% and 25.3% respectively. Moreover, the voltage sag at load transient is reduced by 42.86%. FEEC-SMC achieves zero steady state error without any integral term in the sliding surface which gives it an advantage over PWM-SMC which requires a double integral type sliding surface to achieve zero steady state error. In contrast

with PWM-SMC, the FEEC-SMC achieves robustness against input voltage variations without requiring complex adaptive control of the ramp signal. Moreover, because of the direct implementation of the discontinuous function, FEEC-SMC exhibits properties like order reduction and parameter invariance which are lost if the ideal equivalent control is constructed without involving a discontinuous function.



# Chapter 6

## Conclusion and Future Work

The first section of the chapter is devoted to the summary of the thesis along with the concluding remarks. Possible direction for the future research are presented in the later part of this chapter.

### 6.1 Conclusion

The features like disturbance rejection, parameter invariance and ease of implementation make SMC a good choice for systems having unknown or perturbed parameters. SMC operation can be divided into two phases, namely the reaching phase and the sliding phase. Once the state trajectories have reached the sliding manifold, the system becomes parameter invariant and is completely robust against all kinds of matched disturbances. These features make it an attractive solution for controlling grid connected converters.

However, SMC has a drawback of operating the power converter at variable switching frequency which results in degrading the power quality. This thesis introduces a fixed frequency sliding mode controller that does not suffer from this predicament. The controller is tested experimentally and the results show the desired performance of the proposed technique along with providing robustness against fluctuations in input voltages and change in load conditions. A detailed discussion

on parametrization of the controller, hardware design and circuit implementation is presented. The technique is also applied on a micro-grid test bench, having three sources and the results show satisfactory operation of the closed loop system. The controller is implemented using commercially available analogue ICs which eliminated the need of using expensive analogue-to-digital data acquisition cards along with phasing out the issues due to their finite sampling time. For the purpose of bench marking, the results are compared with conventional PI controller. The proposed technique improved the dynamic response of the closed loop system by reducing both, the rise time and the settling time. It is observed that a sudden voltage dip appears in the regulated voltage when an additional load is connected. This dip is reduced by 31.7% for the proposed controller as compared to that of the conventional PI controller.

The above mentioned methodology is also applied to another challenging problem in DC micro-grid regarding degradation of power quality due to chattering. Power quality is a widely addressed topic in AC grid systems but however, these issues have not been discussed by research community in depth regarding DC grids because previously all the transmission were based on AC systems only. But due to the recent advancements in power semiconductor industry, DC micro-grids have become an attractive solution to integrate generations based on renewable energy resources. A significant improvement in power quality is achieved by harmonic cancellation of chattering in the output of the converters. Moreover, the experimental results show good performance of the controller under different loads and uncertain input voltage conditions.

Finally a novel FEEDC based approach is proposed to fix the switching frequency in sliding mode controllers for analogue circuits and power electronic converters. The discontinuous function inherently responsible for the robustness of the SM controller is filtered to extract the equivalent control of the system which is pulse width modulated to achieve fixed switching frequency. Conditions and constraints that apply to extract the equivalent control without distortion are highlighted. For the purpose of benchmarking, the results are compared with PWM-SMC having

a double integral sliding manifold. The proposed FEEC-SMC shows better results in terms of transient response and reduces both  $t_r$  and  $t_s$  by 20% and 25.3% respectively. Moreover, the voltage sag at load transient is reduced by 42.86%. FEEC-SMC achieves zero steady state error without any integral term in the sliding surface which gives it an advantage over PWM-SMC which requires a double integral type sliding surface to achieve zero steady state error. In contrast with PWM-SMC, the FEEC-SMC achieves robustness against input voltage variations without requiring complex adaptive control of the ramp signal. Moreover, because of the direct implementation of the discontinuous function, FEEC-SMC exhibits properties like order reduction and parameter invariance may not be guaranteed if the ideal equivalent control is constructed without involving a discontinuous function.

## 6.2 Future Work

The directions for future work originating from the presented research are as follows:

- Improvements that may result from the use of different sliding manifolds other than those presented in this thesis shall be explored.
- Analysis may be extended to the study of the proposed technique in more diverse networks including different types of power converters, controlled by various local techniques, other than the one presented in this research.
- In modern renewable energy systems, the economics related to the produced energy is of great importance. Therefore, one of the possible direction for future work is to evaluate the proposed technique on the basis of fuel economy and efficiency of the closed loop system.
- FEEC based fixed frequency SMC may be applied to other types of converters like buck converter, cuk converter and Z-source converters.

- Power electronic converters are a basic component in regenerative braking of hybrid electrical vehicles. FEED based SMC may be applied to improve the transient response of the system along with increasing the robustness of the system.

# Bibliography

- [1] J. Mahdavi, A. Emadi, and H. Toliyat, “Application of state space averaging method to sliding mode control of pwm dc/dc converters,” in *Industry Applications Conference, 1997. Thirty-Second IAS Annual Meeting, IAS '97., Conference Record of the 1997 IEEE*, vol. 2, Oct 1997, pp. 820–827 vol.2.
- [2] B. Choi, *Pulsewidth modulated dc-to-dc power conversion: circuits, dynamics, and control designs*. John Wiley & Sons, pp. 120-150, 2013.
- [3] D. Mitchell, *Dc-Dc Switching Regulator Analysis*, ser. Electronics (McGraw-Hill). McGraw-Hill Ryerson, Limited, pp. 200-210, 1988.
- [4] R.-J. Wai and L.-C. Shih, “Design of voltage tracking control for dc–dc boost converter via total sliding-mode technique,” *IEEE Transactions on Industrial Electronics*, vol. 58, no. 6, pp. 2502–2511, 2011.
- [5] M. Ahmeid, M. Armstrong, M. Al-Greer, and S. Gadoue, “Computationally efficient self-tuning controller for dc–dc switch mode power converters based on partial update kalman filter,” *IEEE Transactions on Power Electronics*, vol. 33, no. 9, pp. 8081–8090, 2017.
- [6] X. Li, M. Chen, H. Shinohara, and T. Yoshihara, “Design of an auto-tunable pid controller for buck converters through a robust h synthesis approach,” *IEICE Communications Express*, vol. 5, no. 1, pp. 7–12, 2016.
- [7] S.-C. Tan, Y.-M. Lai, and C.-K. Tse, *Sliding mode control of switching power converters: techniques and implementation*. CRC press, pp. 130-140, 2011.

- 
- [8] A. El Khateb, N. A. Rahim, J. Selvaraj, and M. N. Uddin, “Fuzzy-logic-controller-based sepic converter for maximum power point tracking,” *IEEE Transactions on Industry Applications*, vol. 50, no. 4, pp. 2349–2358, 2014.
- [9] C. Cecati, F. Ciancetta, and P. Siano, “A multilevel inverter for photovoltaic systems with fuzzy logic control,” *IEEE Transactions on Industrial Electronics*, vol. 57, no. 12, pp. 4115–4125, 2010.
- [10] J. Chen, C. Xu, C. Wu, and W. Xu, “Adaptive fuzzy logic control of fuel-cell-battery hybrid systems for electric vehicles,” *IEEE Transactions on Industrial Informatics*, vol. 14, no. 1, pp. 292–300, 2018.
- [11] K. Kamalpathi, N. Priyadarshi, S. Padmanaban, J. Holm-Nielsen, F. Azam, C. Umayal, and V. Ramachandaramurthy, “A hybrid moth-flame fuzzy logic controller based integrated cuk converter fed brushless dc motor for power factor correction,” *Electronics*, vol. 7, no. 11, p. 288, 2018.
- [12] Y.-J. Liu, S. Lu, S. Tong, X. Chen, C. P. Chen, and D.-J. Li, “Adaptive control-based barrier lyapunov functions for a class of stochastic nonlinear systems with full state constraints,” *Automatica*, vol. 87, pp. 83–93, 2018.
- [13] C. Elmas, O. Deperlioglu, and H. H. Sayan, “Adaptive fuzzy logic controller for dc–dc converters,” *Expert Systems with Applications*, vol. 36, no. 2, pp. 1540–1548, 2009.
- [14] S. Li, Y. Sun, M. Ramezani, and Y. Xiao, “Artificial neural networks for volt/var control of der inverters at the grid edge,” *IEEE Transactions on Smart Grid*, vol. 15, no. 4, pp. 1103–1114, 2018.
- [15] R.-J. Wai, L.-C. Shih *et al.*, “Adaptive fuzzy-neural-network design for voltage tracking control of a dc–dc boost converter,” *IEEE Trans. Power Electron*, vol. 27, no. 4, pp. 2104–2115, 2012.
- [16] N. Chettibi, A. Mellit, G. Sulligoi, and A. M. Pavan, “Adaptive neural network-based control of a hybrid ac/dc microgrid,” *IEEE Transactions on Smart Grid*, vol. 9, no. 3, pp. 1667–1679, 2018.

- [17] W.-J. Liu, "Decentralized sliding mode control for multi-input complex interconnected systems subject to non-smooth nonlinearities," *Asian Journal of Control*, vol. 20, no. 3, pp. 1171–1181, 2018.
- [18] C. Zaafour, B. Torchani, A. Sellami, and G. Garcia, "Uncertain saturated discrete-time sliding mode control for a wind turbine using a two-mass model," *Asian Journal of Control*, vol. 20, no. 2, pp. 802–818, 2018.
- [19] Y. Pan, C. Yang, L. Pan, and H. Yu, "Integral sliding mode control: Performance, modification, and improvement," *IEEE Transactions on Industrial Informatics*, vol. 14, no. 7, pp. 3087–3096, 2018.
- [20] S. Mobayen, "Chaos synchronization of uncertain chaotic systems using composite nonlinear feedback based integral sliding mode control," *ISA transactions*, vol. 77, pp. 100–111, 2018.
- [21] V. Utkin, J. Guldner, and J. Shi, *Sliding mode control in electro-mechanical systems*. CRC press, pp. 235-240, 2009, vol. 34.
- [22] H. Chung, S. Y. R. Hui, and K. K. Tse, "Reduction of power converter emission using soft switching technique," *IEEE Transactions on Electromagnetic Compatibility*, vol. 40, no. 3, pp. 282–287, Aug 1998.
- [23] F. Pareschi, R. Rovatti, and G. Setti, "Emi reduction via spread spectrum in dc/dc converters: State of the art, optimization, and tradeoffs," *IEEE Access*, vol. 3, pp. 2857–2874, 2015.
- [24] A. Isidori, *Nonlinear Control Systems*, 3rd ed., M. Thoma, E. D. Sontag, B. W. Dickinson, A. Fettweis, J. L. Massey, and J. W. Modestino, Eds. Secaucus, NJ, USA: Springer-Verlag New York, Inc., pp. 148-151, 1995.
- [25] Y. M. Alsmadi, V. Utkin, M. Haj-Ahmed, L. Xu, and A. Y. Abdelaziz, "Sliding-mode control of power converters: Ac/dc converters & dc/ac inverters," *International Journal of Control*, pp. 1–15, 2018.
- [26] R. Venkataramanan, "Sliding mode control of power converters," Ph.D. dissertation, California Institute of Technology, pp. 73-163, 1986.

- 
- [27] M. Carpita and M. Marchesoni, "Experimental study of a power conditioning system using sliding mode control," *IEEE transactions on power electronics*, vol. 11, no. 5, pp. 731–742, 1996.
- [28] J. A. González, A. Barreiro, S. Dormido, and A. Baños, "Nonlinear adaptive sliding mode control with fast non-overshooting responses and chattering avoidance," *Journal of the Franklin Institute*, vol. 354, no. 7, pp. 2788–2815, 2017.
- [29] D. B. W. Abeywardana, B. Hredzak, and V. G. Agelidis, "A fixed-frequency sliding mode controller for a boost-inverter-based battery-supercapacitor hybrid energy storage system," *IEEE Transactions on Power Electronics*, vol. 32, no. 1, pp. 668–680, 2017.
- [30] P. R. Mohanty and A. K. Panda, "Fixed-frequency sliding-mode control scheme based on current control manifold for improved dynamic performance of boost pfc converter," *IEEE Journal of Emerging and Selected Topics in Power Electronics*, vol. 5, no. 1, pp. 576–586, 2017.
- [31] M. Gao, D. Wang, Y. Li, and T. Yuan, "Fixed frequency pulse-width modulation based integrated sliding mode controller for phase-shifted full-bridge converters," *IEEE Access*, vol. 6, pp. 2181–2192, 2018.
- [32] F. Pareschi, R. Rovatti, and G. Setti, "Emi reduction via spread spectrum in dc/dc converters: State of the art, optimization, and tradeoffs," *IEEE Access*, vol. 3, pp. 2857–2874, 2015.
- [33] P. R. Mohanty and A. K. Panda, "Fixed-frequency sliding-mode control scheme based on current control manifold for improved dynamic performance of boost pfc converter," *IEEE Journal of Emerging and Selected Topics in Power Electronics*, vol. 5, no. 1, pp. 576–586, March 2017.
- [34] Y. He and F. Luo, "Sliding-mode control for dc–dc converters with constant switching frequency," *IEE Proceedings-Control Theory and Applications*, vol. 153, no. 1, pp. 37–45, 2006.



- 
- [35] J. Ye, P. Malysz, and A. Emadi, "A fixed-switching-frequency integral sliding mode current controller for switched reluctance motor drives," *IEEE Journal of Emerging and Selected Topics in Power Electronics*, vol. 3, no. 2, pp. 381–394, 2015.
- [36] S. H. Chincholkar and C.-Y. Chan, "Design of fixed-frequency pulsewidth-modulation-based sliding-mode controllers for the quadratic boost converter," *IEEE Transactions on Circuits and Systems II: Express Briefs*, vol. 64, no. 1, pp. 51–55, 2017.
- [37] M. Rashad, M. Ashraf, A. I. Bhatti, D. M. Minhas, and B. A. Ahmed, "Mathematical modeling and stability analysis of dc microgrid using sm hysteresis controller," *International Journal of Electrical Power & Energy Systems*, vol. 95, pp. 507–522, 2018.
- [38] M. Rashad, U. Raoof, M. Ashraf, and B. Ashfaq Ahmed, "Proportional load sharing and stability of dc microgrid with distributed architecture using sm controller," *Mathematical Problems in Engineering*, vol. 2018, pp. 107–123, 2018.
- [39] N. L. Díaz, A. C. Luna, J. C. Vasquez, and J. M. Guerrero, "Centralized control architecture for coordination of distributed renewable generation and energy storage in islanded ac microgrids," *IEEE Transactions on Power Electronics*, vol. 32, no. 7, pp. 5202–5213, 2017.
- [40] P. Faria, J. Spínola, Z. Vale *et al.*, "Distributed energy resources scheduling and aggregation in the context of demand response programs," *Energies*, vol. 11, no. 8, pp. 1–17, 2018.
- [41] F. Drfler, J. W. Simpson-Porco, and F. Bullo, "Breaking the hierarchy: Distributed control and economic optimality in microgrids," *IEEE Transactions on Control of Network Systems*, vol. 3, no. 3, pp. 241–253, Sept 2016.
- [42] M. Jin, W. Feng, C. Marnay, and C. Spanos, "Microgrid to enable optimal distributed energy retail and end-user demand response," *Applied Energy*, vol. 210, pp. 1321–1335, 2018.

- [43] P. D. Antunez, D. M. Bishop, Y. Luo, and R. Haight, “Efficient kesterite solar cells with high open-circuit voltage for applications in powering distributed devices,” *Nature Energy*, pp. 1–7, 2017.
- [44] C. Bhowmik, S. Bhowmik, A. Ray, and K. M. Pandey, “Optimal green energy planning for sustainable development: A review,” *Renewable and Sustainable Energy Reviews*, vol. 71, pp. 796–813, 2017.
- [45] N. Mohan and T. M. Undeland, *Power electronics: converters, applications, and design*. John Wiley & Sons, pp. 250-263, 2007.
- [46] Z. Ivanovic, B. Blanusa, and M. Knezic, “Power loss model for efficiency improvement of boost converter,” in *Information, Communication and Automation Technologies (ICAT), 2011 XXIII International Symposium on*. IEEE, 2011, pp. 1–6.
- [47] H. Lotfi and A. Khodaei, “Ac versus dc microgrid planning,” *IEEE Transactions on Smart Grid*, vol. 8, no. 1, pp. 296–304, 2017.
- [48] T. Dragicevic, J. C. Vasquez, J. M. Guerrero, and D. Skrlec, “Advanced lvdc electrical power architectures and microgrids: A step toward a new generation of power distribution networks.” *IEEE Electrification Magazine*, vol. 2, no. 1, pp. 54–65, March 2014.
- [49] C. Wang, J. Duan, B. Fan, Q. Yang, and W. Liu, “Decentralized high-performance control of dc microgrids,” *IEEE Transactions on Smart Grid*, vol. 10, no. 3, pp. 3355–3363, 2018.
- [50] P. Cairoli and R. A. Dougal, “Fault detection and isolation in medium-voltage dc microgrids: Coordination between supply power converters and bus contactors,” *IEEE Transactions on Power Electronics*, vol. 33, no. 5, pp. 4535–4546, 2018.
- [51] M. Saleh, Y. Esa, and A. A. Mohamed, “Communication-based control for dc microgrids,” *IEEE Transactions on Smart Grid*, vol. 10, no. 2, pp. 2180–2195, 2018.

- 
- [52] N. M. Dehkordi, H. R. Baghaee, N. Sadati, and J. M. Guerrero, "Distributed noise-resilient secondary voltage and frequency control for islanded microgrids," *IEEE Transactions on Smart Grid*, vol. 20, no. 6, pp. 1620–1633, 2018.
- [53] S. Y. M. Mousavi, A. Jalilian, M. Savaghebi, and J. M. Guerrero, "Coordinated control of multifunctional inverters for voltage support and harmonic compensation in a grid-connected microgrid," *Electric Power Systems Research*, vol. 155, pp. 254–264, 2018.
- [54] K. Sun, L. Zhang, Y. Xing, and J. M. Guerrero, "A distributed control strategy based on dc bus signaling for modular photovoltaic generation systems with battery energy storage," *IEEE Transactions on Power Electronics*, vol. 26, no. 10, pp. 3032–3045, Oct 2011.
- [55] J. Schonbergerschonberger, R. Duke, and S. D. Round, "Dc-bus signaling: A distributed control strategy for a hybrid renewable nanogrid," *IEEE Transactions on Industrial Electronics*, vol. 53, no. 5, pp. 1453–1460, Oct 2006.
- [56] E. Alizadeh, A. M. Birjandi, and M. Hamzeh, "Decentralised power sharing control strategy in lv microgrids under unbalanced load conditions," *IET Generation, Transmission & Distribution*, vol. 11, no. 7, pp. 1613–1623, 2017.
- [57] S. V. Kulkarni and S. Khaparde, *Transformer engineering*. Marcel Dekker, pp. 27-28, 2004, vol. 1.
- [58] X. Liu, P. Wang, and P. C. Loh, "A hybrid ac/dc microgrid and its coordination control," *IEEE Transactions on smart grid*, vol. 2, no. 2, pp. 278–286, 2011.
- [59] H. Kakigano, Y. Miura, and T. Ise, "Low-voltage bipolar-type dc microgrid for super high quality distribution," *IEEE transactions on power electronics*, vol. 25, no. 12, pp. 3066–3075, 2010.

- 
- [60] M. Amin, Y. Arafat, S. Lundberg, and S. Mangold, "Low voltage dc distribution system compared with 230 v ac," in *2011 IEEE Electrical Power and Energy Conference*. IEEE, 2011, pp. 340–345.
- [61] W. Li, X. Mou, Y. Zhou, and C. Marnay, "On voltage standards for dc home microgrids energized by distributed sources," in *Proceedings of The 7th International Power Electronics and Motion Control Conference*, vol. 3. IEEE, 2012, pp. 2282–2286.
- [62] L. Herrera, W. Zhang, and J. Wang, "Stability analysis and controller design of dc microgrids with constant power loads." *IEEE Trans. Smart Grid*, vol. 8, no. 2, pp. 881–888, 2017.
- [63] C. Li, F. De Bosio, F. Chen, S. K. Chaudhary, J. C. Vasquez, and J. M. Guerrero, "Economic dispatch for operating cost minimization under real-time pricing in droop-controlled dc microgrid," *IEEE Journal of Emerging and Selected Topics in Power Electronics*, vol. 5, no. 1, pp. 587–595, 2017.
- [64] A. Bonfiglio, M. Brignone, F. Delfino, and R. Procopio, "Optimal control and operation of grid-connected photovoltaic production units for voltage support in medium-voltage networks," *IEEE Transactions on Sustainable Energy*, vol. 5, no. 1, pp. 254–263, 2014.
- [65] M. Su, Z. Liu, Y. Sun, H. Han, and X. Hou, "Stability analysis and stabilization methods of dc microgrid with multiple parallel-connected dc-dc converters loaded by cpls," *IEEE Transactions on Smart Grid*, vol. 9, no. 1, pp. 132–142, 2018.
- [66] Y. Li, L. He, F. Liu, C. Li, Y. Cao, and M. Shahidehpour, "Flexible voltage control strategy considering distributed energy storages for dc distribution network," *IEEE Transactions on Smart Grid*, vol. 10, no. 1, pp. 163–172, 2017.
- [67] S. Augustine, M. K. Mishra, and N. Lakshminarasamma, "Adaptive droop control strategy for load sharing and circulating current minimization in

- low-voltage standalone dc microgrid,” *IEEE Transactions on Sustainable Energy*, vol. 6, no. 1, pp. 132–141, 2015.
- [68] S. Anand, B. G. Fernandes, and M. Guerrero, “Distributed control to ensure proportional load sharing and improve voltage regulation in low-voltage dc microgrids,” *Power Electronics, IEEE Transactions on*, vol. 28, no. 4, pp. 1900–1913, 2013.
- [69] A. Yahya, H. El Fadil, M. Oulcaid, L. Ammeh, F. Giri, and J. M. Guerrero, “Control of grid connected photovoltaic systems with microinverters: New theoretical design and numerical evaluation,” *Asian Journal of Control*, vol. 20, no. 2, pp. 906–918, 2018.
- [70] Y. P. Hsieh, J. F. Chen, T. J. Liang, and L. S. Yang, “A novel high step-up dc-dc converter for a microgrid system,” *IEEE Transactions on Power Electronics*, vol. 26, no. 4, pp. 1127–1136, April 2011.
- [71] C. D. Lute, M. G. Simoes, D. I. Brandao, A. Al Durra, and S. Muyeen, “Development of a four phase floating interleaved boost converter for photovoltaic systems,” in *Energy Conversion Congress and Exposition (ECCE), 2014 IEEE*. IEEE, 2014, pp. 1895–1902.
- [72] M. Kabalo, D. Paire, B. Blunier, D. Bouquain, M. G. Simões, and A. Miraoui, “Experimental evaluation of four-phase floating interleaved boost converter design and control for fuel cell applications,” *IET power electronics*, vol. 6, no. 2, pp. 215–226, 2013.
- [73] J. Liu, S. Vazquez, L. Wu, A. Marquez, H. Gao, and L. G. Franquelo, “Extended state observer-based sliding-mode control for three-phase power converters,” *IEEE Transactions on Industrial Electronics*, vol. 64, no. 1, pp. 22–31, 2017.
- [74] C. Bruni, G. Dipillo, and G. Koch, “Bilinear systems: An appealing class of “nearly linear” systems in theory and applications,” *IEEE Transactions on automatic control*, vol. 19, no. 4, pp. 334–348, 1974.

- [75] Y. M. Roshan and M. Moallem, "Control of nonminimum phase load current in a boost converter using output redefinition," *IEEE Transactions on Power Electronics*, vol. 29, no. 9, pp. 5054–5062, 2014.
- [76] Y. Massaoudi, E. Dorsaf, J.-P. Gaubert, D. Mehdi, and T. Damak, "Experimental implementation of new sliding mode control law applied to a dc–dc boost converter," *Asian Journal of Control*, vol. 18, no. 6, pp. 2221–2233, 2016.
- [77] H. Sira-Ramírez and R. Silva-Ortigoza, "Sliding mode- $\delta$  modulation control of the boost converter," *Asian Journal of Control*, vol. 7, no. 4, pp. 349–355, 2005.
- [78] R. Ashok and Y. Shtessel, "Control of fuel cell-based electric power system using adaptive sliding mode control and observation techniques," *Journal of the Franklin Institute*, vol. 352, no. 11, pp. 4911–4934, 2015.
- [79] G. Escobar, R. Ortega, H. Sira-Ramirez, J. Vilain, and I. Zein, "An experimental comparison of several nonlinear controllers for power converters," *Control Systems, IEEE*, vol. 19, no. 1, pp. 66–82, Feb 1999.
- [80] Y. Huangfu, S. Zhuo, F. Chen, and S. Pang, "Evaluation and fault tolerant control of a floating interleaved boost converter for fuel cell systems," in *Industry Applications Society Annual Meeting, 2016 IEEE*. IEEE, 2016, pp. 1–7.
- [81] T. Morstyn, B. Hredzak, and V. G. Agelidis, "Control strategies for microgrids with distributed energy storage systems: An overview," *IEEE Transactions on Smart Grid*, vol. 9, no. 4, pp. 3652–3666, 2018.
- [82] M. Armin, P. N. Roy, S. K. Sarkar, and S. K. Das, "Lmi-based robust pid controller design for voltage control of islanded microgrid," *Asian Journal of Control*, vol. 20, no. 5, pp. 2014–2025, 2018.
- [83] G. G. Talapur, H. M. Suryawanshi, L. Xu, and A. B. Shitole, "A reliable microgrid with seamless transition between grid connected and islanded mode

- for residential community with enhanced power quality,” *IEEE Transactions on Industry Applications*, vol. 54, no. 5, pp. 5246–5255, 2018.
- [84] K. E. Antoniadou-Plytaria, I. N. Kouveliotis-Lysikatos, P. S. Georgilakis, and N. D. Hatziargyriou, “Distributed and decentralized voltage control of smart distribution networks: models, methods, and future research,” *IEEE Transactions on Smart Grid*, vol. 8, no. 6, pp. 2999–3008, 2017.
- [85] X. Wang, L. Harnefors, and F. Blaabjerg, “Unified impedance model of grid-connected voltage-source converters,” *IEEE Transactions on Power Electronics*, vol. 33, no. 2, pp. 1775–1787, 2018.
- [86] Y. Guan, L. Meng, C. Li, J. C. Vasquez, and J. M. Guerrero, “A dynamic consensus algorithm to adjust virtual impedance loops for discharge rate balancing of ac microgrid energy storage units,” *IEEE Transactions on Smart Grid*, vol. 9, no. 5, pp. 4847–4860, 2018.
- [87] M. Cucuzzella, S. Trip, C. De Persis, X. Cheng, A. Ferrara, and A. van der Schaft, “A robust consensus algorithm for current sharing and voltage regulation in dc microgrids,” *IEEE Transactions on Control Systems Technology*, vol. 27, no. 4, pp. 1583–1595, 2018.
- [88] H. Kakigano, Y. Miura, T. Ise, and R. Uchida, “Dc voltage control of the dc micro-grid for super high quality electric power distribution,” *IEEE Transactions on Industry Applications*, vol. 127, pp. 890–897, 2007.
- [89] R. Han, L. Meng, J. M. Guerrero, and J. C. Vasquez, “Distributed nonlinear control with event-triggered communication to achieve current-sharing and voltage regulation in dc microgrids,” *IEEE Transactions on Power Electronics*, vol. 33, no. 7, pp. 6416–6433, 2018.
- [90] J. M. Guerrero, J. C. Vasquez, J. Matas, L. G. de Vicuna, and M. Castilla, “Hierarchical control of droop-controlled ac and dc microgrids 2014; a general approach toward standardization,” *IEEE Transactions on Industrial Electronics*, vol. 58, no. 1, pp. 158–172, Jan 2011.

- [91] M. Shirazi, R. Zane, and D. Maksimovic, "An autotuning digital controller for dc–dc power converters based on online frequency-response measurement," *IEEE transactions on power electronics*, vol. 24, no. 11, pp. 2578–2588, 2009.
- [92] L. Guo, J. Y. Hung, and R. M. Nelms, "Evaluation of dsp-based pid and fuzzy controllers for dc 2013;dc converters," *IEEE Transactions on Industrial Electronics*, vol. 56, no. 6, pp. 2237–2248, June 2009.
- [93] M. Lee, D. Chen, K. Huang, C. W. Liu, and B. Tai, "Modeling and design for a novel adaptive voltage positioning (avp) scheme for multiphase vrms," *IEEE Transactions on Power Electronics*, vol. 23, no. 4, pp. 1733–1742, July 2008.
- [94] C. N. Onwuchekwa and A. Kwasinski, "Analysis of boundary control for buck converters with instantaneous constant-power loads," *IEEE Transactions on Power Electronics*, vol. 25, no. 8, pp. 2018–2032, Aug 2010.
- [95] J. M. Galvez, M. Ordonez, F. Luchino, and J. E. Quaicoe, "Improvements in boundary control of boost converters using the natural switching surface," *IEEE Transactions on Power Electronics*, vol. 26, no. 11, pp. 3367–3376, Nov 2011.
- [96] O. Kirshenboim and M. M. Peretz, "Stability analysis of boundary and hybrid controllers for indirect energy transfer converters," *IEEE Transactions on Power Electronics*, vol. 31, no. 4, pp. 3360–3371, April 2016.
- [97] J. Linares-Flores, A. H. Mndez, C. Garca-Rodrguez, and H. Sira-Ramrez, "Robust nonlinear adaptive control of a boost converter via algebraic parameter identification," *IEEE Transactions on Industrial Electronics*, vol. 61, no. 8, pp. 4105–4114, Aug 2014.
- [98] L. Cavanini, G. Cimini, G. Ippoliti, and A. Bemporad, "Model predictive control for pre-compensated voltage mode controlled dc–dc converters," *IET Control Theory & Applications*, vol. 11, no. 15, pp. 2514–2520, 2017.



- 
- [99] S.-K. Kim, C. R. Park, J.-S. Kim, and Y. I. Lee, “A stabilizing model predictive controller for voltage regulation of a dc/dc boost converter,” *IEEE Transactions on Control Systems Technology*, vol. 22, no. 5, pp. 2016–2023, 2014.
- [100] P. Karamanakos, T. Geyer, and S. Manias, “Direct voltage control of dc–dc boost converters using enumeration-based model predictive control,” *IEEE Transactions on Power Electronics*, vol. 29, no. 2, pp. 968–978, 2014.
- [101] Y.-X. Wang, D.-H. Yu, and Y.-B. Kim, “Robust time-delay control for the dc-dc boost converter.” *IEEE Trans. Industrial Electronics*, vol. 61, no. 9, pp. 4829–4837, 2014.
- [102] V. I. Utkin, “Sliding mode control design principles and applications to electric drives,” *IEEE transactions on industrial electronics*, vol. 40, no. 1, pp. 23–36, 1993.
- [103] J. Calvente, A. El Aroudi, R. Giral, A. Cid-Pastor, E. Vidal-Idiarte, L. Martínez-Salamero *et al.*, “Design of current programmed switching converters using sliding-mode control theory,” *Energies*, vol. 11, no. 8, pp. 1–20, 2018.
- [104] M. B. Delghavi and A. Yazdani, “Sliding-mode control of ac voltages and currents of dispatchable distributed energy resources in master-slave-organized inverter-based microgrids,” *IEEE Transactions on Smart Grid*, vol. 10, no. 1, pp. 980–991, 2017.
- [105] A. Pilloni, A. Pisano, and E. Usai, “Robust finite-time frequency and voltage restoration of inverter-based microgrids via sliding-mode cooperative control,” *IEEE Transactions on Industrial Electronics*, vol. 65, no. 1, pp. 907–917, Jan 2018.
- [106] C. Dou, B. Zhang, D. Yue, Z. Zhang, S. Xu, T. Hayat, and A. Alsaedi, “A novel hierarchical control strategy combined with sliding mode control and consensus control for islanded micro-grid,” *IET Renewable Power Generation*, vol. 12, no. 9, pp. 1012–1024, 2018.

- [107] Y. Fu, H. Zhang, Y. Mi, L. Huang, Z. Li, and J. Wang, "Control strategy of dfig in hybrid micro-grid using sliding mode frequency controller and observer," *IET Generation, Transmission & Distribution*, vol. 12, no. 11, pp. 2662–2669, 2018.
- [108] U. K. Shinde, S. G. Kadwane, S. P. Gawande, M. J. B. Reddy, and D. K. Mohanta, "Sliding mode control of single-phase grid-connected quasi-z-source inverter," *IEEE Access*, vol. 5, pp. 10 232–10 240, 2017.
- [109] Y. Zhu and J. Fei, "Adaptive global fast terminal sliding mode control of grid-connected photovoltaic system using fuzzy neural network approach," *IEEE Access*, vol. 5, pp. 9476–9484, 2017.
- [110] M. I. Ghiasi, M. A. Golkar, and A. Hajizadeh, "Lyapunov based-distributed fuzzy-sliding mode control for building integrated-dc microgrid with plug-in electric vehicle," *IEEE Access*, vol. 5, pp. 7746–7752, 2017.
- [111] A. R. Teja, C. Chakraborty, and B. C. Pal, "Disturbance rejection analysis and fpga-based implementation of a second-order sliding mode controller fed induction motor drive," *IEEE Transactions on Energy Conversion*, vol. 33, no. 3, pp. 1453–1462, 2018.
- [112] B. Yang, T. Yu, H. Shu, J. Dong, and L. Jiang, "Robust sliding-mode control of wind energy conversion systems for optimal power extraction via nonlinear perturbation observers," *Applied Energy*, vol. 210, pp. 711–723, 2018.
- [113] S.-C. Tan, Y. M. Lai, M. K. H. Cheung, and C. K. Tse, "On the practical design of a sliding mode voltage controlled buck converter," *IEEE Transactions on Power Electronics*, vol. 20, no. 2, pp. 425–437, March 2005.
- [114] H. Sira-Ramirez, "Sliding-mode control on slow manifolds of dc-to-dc power converters," *International Journal of Control*, vol. 47, no. 5, pp. 1323–1340, 1988.

- [115] F. M. Shahir, E. Babaei, and M. Farsadi, "Extended topology for a boost dc–dc converter," *IEEE Transactions on Power Electronics*, vol. 34, no. 3, pp. 2375–2384, 2018.
- [116] Y. M. Alsmadi, V. Utkin, M. A. Haj-ahmed, and L. Xu, "Sliding mode control of power converters: Dc/dc converters," *International Journal of Control*, pp. 1–22, 2017.
- [117] P. V. Kokotovic, R. E. O'Malley Jr, and P. Sannuti, "Singular perturbations and order reduction in control theory an overview," *Automatica*, vol. 12, no. 2, pp. 123–132, 1976.
- [118] P. V. Kokotović, "Applications of singular perturbation techniques to control problems," *SIAM review*, vol. 26, no. 4, pp. 501–550, 1984.
- [119] S.-C. Tan, Y. Lai, C. K. Tse *et al.*, "Indirect sliding mode control of power converters via double integral sliding surface," *IEEE Transactions on Power Electronics*, vol. 23, no. 2, pp. 600–615, 2008.
- [120] H. J. Sira-Ramirez and M. Ilic, "A geometric approach to the feedback control of switch mode dc-to-dc power supplies," *IEEE Transactions on Circuits and Systems*, vol. 35, no. 10, pp. 1291–1298, 1988.
- [121] V. Utkin, J. Guldner, and M. Shijun, *Sliding Mode Control in Electromechanical Systems*, ser. Automation and Control Engineering. Taylor & Francis, pp. 250-260, 1999.
- [122] C. Edwards and S. Spurgeon, *Sliding mode control: theory and applications*. Crc Press, pp. 160-175, 1998.
- [123] A. R. Yasin, M. Ashraf, and A. I. Bhatti, "Fixed frequency sliding mode control of power converters for improved dynamic response in dc micro-grids," *Energies*, vol. 11, no. 10, pp. 2799–2814, 2018.
- [124] H. Du, X. Chen, G. Wen, X. Yu, and J. Lü, "Discrete-time fast terminal sliding mode control for permanent magnet linear motor," *IEEE Transactions on Industrial Electronics*, vol. 65, no. 12, pp. 9916–9927, 2018.

- [125] J. Liu, S. Vazquez, L. Wu, A. Marquez, H. Gao, and L. G. Franquelo, "Extended state observer-based sliding-mode control for three-phase power converters," *IEEE Transactions on Industrial Electronics*, vol. 64, no. 1, pp. 22–31, 2017.
- [126] A. Riani, T. Madani, A. Benallegue, and K. Djouani, "Adaptive integral terminal sliding mode control for upper-limb rehabilitation exoskeleton," *Control Engineering Practice*, vol. 75, pp. 108–117, 2018.
- [127] A. Merabet, "Adaptive sliding mode speed control for wind energy experimental system," *Energies*, vol. 11, no. 9, pp. 2238–2246, 2018.
- [128] S. Benhalima, R. Miloud, and A. Chandra, "Real-time implementation of robust control strategies based on sliding mode control for standalone microgrids supplying non-linear loads," *Energies*, vol. 11, no. 10, pp. 2590–2606, 2018.
- [129] H. Wang, L. Shi, Z. Man, J. Zheng, S. Li, M. Yu, C. Jiang, H. Kong, and Z. Cao, "Continuous fast nonsingular terminal sliding mode control of automotive electronic throttle systems using finite-time exact observer," *IEEE Transactions on Industrial Electronics*, vol. 65, no. 9, pp. 7160–7172, 2018.
- [130] C. Chiarelli, L. Malesani, S. Pirondini, and P. Tomasin, "Single-phase, three-level, constant frequency current hysteresis control for ups applications," in *Power Electronics and Applications, 1993., Fifth European Conference on. IET*, 1993, pp. 180–185.
- [131] D. G. Holmes, R. Davoodnezhad, and B. P. McGrath, "An improved three-phase variable-band hysteresis current regulator," *IEEE Transactions on Power Electronics*, vol. 28, no. 1, pp. 441–450, 2013.
- [132] R. Guzman, L. G. de Vicuna, J. Morales, M. Castilla, and J. Matas, "Sliding-mode control for a three-phase unity power factor rectifier operating at fixed switching frequency," *IEEE Transactions on Power Electronics*, vol. 31, no. 1, pp. 758–769, 2016.

- [133] S. C. Huerta, P. Alou, J. Á. Oliver, O. Garcia, J. A. Cobos, and A. M. Abou-Alfotouh, “Nonlinear control for dc–dc converters based on hysteresis of the  $i_{crmsOUT}$  current with a frequency loop to operate at constant frequency,” *IEEE Transactions on Industrial Electronics*, vol. 58, no. 3, pp. 1036–1043, 2011.
- [134] S. C. Huerta, P. Alou, O. Garcia, J. A. Oliver, R. Prieto, and J. Cobos, “Hysteretic mixed-signal controller for high-frequency dc-dc converters operating at constant switching frequency,” *IEEE Transactions on Power Electronics*, vol. 27, no. 6, pp. 2690–2696, 2012.
- [135] W.-T. Yan, C. N. M. Ho, H. S.-H. Chung, and K. T. Au, “Fixed-frequency boundary control of buck converter with second-order switching surface,” *IEEE Transactions on Power Electronics*, vol. 24, no. 9, pp. 2193–2201, 2009.
- [136] L. Malesani, P. Mattavelli, and P. Tomasin, “Improved constant-frequency hysteresis current control of vsi inverters with simple feedforward bandwidth prediction,” *IEEE Transactions on industry applications*, vol. 33, no. 5, pp. 1194–1202, 1997.
- [137] V. Repecho, D. Biel, J. M. Olm, and E. F. Colet, “Switching frequency regulation in sliding mode control by a hysteresis band controller,” *IEEE Transactions on Power Electronics*, vol. 32, no. 2, pp. 1557–1569, 2017.
- [138] J. F. Silva and S. S. Paulo, “Fixed frequency sliding mode modulator for current mode pwm inverters,” in *Power Electronics Specialists Conference, 1993. PESC’93 Record., 24th Annual IEEE*. IEEE, 1993, pp. 623–629.
- [139] P. Mattavelli, L. Rossetto, G. Spiazzi, and P. Tenti, “General-purpose sliding-mode controller for dc/dc converter applications,” in *Power Electronics Specialists Conference, 1993. PESC’93 Record., 24th Annual IEEE*. IEEE, 1993, pp. 609–615.
- [140] E. Fossas, R. Grinó, and D. Biel, “Quasi-sliding control based on pulse width modulation, zero averaged dynamics and the  $l_2$  norm,” in *Advances In*

- Variable Structure Systems: Analysis, Integration and Applications*. World Scientific, 2000, pp. 335–344.
- [141] R. R. Ramos, D. Biel, E. Fossas, and F. Guinjoan, “A fixed-frequency quasi-sliding control algorithm: application to power inverters design by means of fpga implementation,” *IEEE Transactions on Power Electronics*, vol. 18, no. 1, pp. 344–355, 2003.
- [142] A. Abrishamifar, A. Ahmad, and M. Mohamadian, “Fixed switching frequency sliding mode control for single-phase unipolar inverters,” *IEEE Transactions on Power Electronics*, vol. 27, no. 5, pp. 2507–2514, 2012.
- [143] S.-C. Tan, Y. Lai, C. K. Tse, and M. K. Cheung, “A fixed-frequency pulsewidth modulation based quasi-sliding-mode controller for buck converters,” *Power Electronics, IEEE Transactions on*, vol. 20, no. 6, pp. 1379–1392, 2005.
- [144] H. N. Jazi, A. Goudarzian, R. Pourbagher, and S. Y. Derakhshandeh, “Pi and pwm sliding mode control of boost converter,” *IEEE Transactions on Aerospace and Electronic Systems*, vol. 53, no. 5, pp. 2167–2177, 2017.
- [145] H. Al-Baidhani and M. K. Kazimierczuk, “Pwm-based proportional-integral sliding-mode current control of dc-dc boost converter,” in *Texas Power and Energy Conference (TPEC), 2018 IEEE*. IEEE, 2018, pp. 1–6.
- [146] R. Pradhan and B. Subudhi, “Double integral sliding mode mppt control of a photovoltaic system,” *IEEE Transactions on Control Systems Technology*, vol. 24, no. 1, pp. 285–292, 2016.
- [147] S. C. Tan, Y. M. Lai, and C. K. Tse, “Indirect sliding mode control of power converters via double integral sliding surface,” *IEEE Transactions on Power Electronics*, vol. 23, no. 2, pp. 600–611, March 2008.
- [148] S.-C. Tan, Y.-M. Lai, and K. T. Chi, “General design issues of sliding-mode controllers in dc–dc converters,” *IEEE Transactions on Industrial Electronics*, vol. 55, no. 3, pp. 1160–1174, 2008.

- 
- [149] M. Teodorescu and D. Stanciu, "Sliding coefficients estimation for fixed frequency sliding mode control of boost converter," in *Advanced Topics in Electrical Engineering (ATEE), 2015 9th International Symposium on*. IEEE, 2015, pp. 698–703.
- [150] V. I. Utkin and H. Lee, "The chattering analysis," in *Power Electronics and Motion Control Conference, 2006. EPE-PEMC 2006. 12th International*. IEEE, 2006, pp. 2014–2019.
- [151] V. I. Utkin, *Sliding modes in control and optimization*. Springer Science & Business Media, pp. 283-292, 2013.
- [152] C. Morel, J.-C. Guignard, and M. Guillet, "Sliding mode control of dc-to-dc power converters," in *Electronics, Circuits and Systems, 2002. 9th International Conference on*, vol. 3. IEEE, 2002, pp. 971–974.
- [153] S.-C. Tan, Y. Lai, C. Tse, and M. Cheung, "A fixed-frequency pulsewidth modulation based quasi-sliding-mode controller for buck converters," *Power Electronics, IEEE Transactions on*, vol. 20, no. 6, pp. 1379–1392, Nov 2005.